LENSE-THIRRING PRECESSION IN STRONG GRAVITATIONAL FIELDS

By

CHANDRACHUR CHAKRABORTY

(PHYS05201004002)

Saha Institute of Nuclear Physics, Kolkata
India

A thesis submitted to the
Board of Studies in Physical Sciences
In partial fulfillment of requirements
for the Degree of

DOCTOR OF PHILOSOPHY

of

HOMI BHABHA NATIONAL INSTITUTE

January, 2015

Homi Bhabha National Institute

Recommendations of the Viva Voce Committee

As members of the Viva Voce Board, we certify that we have read the dissertation prepared by Chandrachur Chakraborty entitled "Lense-Thirring Precession in Strong Gravitational Fields" and recommend that it may be accepted as fulfilling the thesis requirement for the Degree of Doctor of Philosophy.

Date:

_____

Chairman -

Date:

_____

Convener -

Date:

_____

Member 1 -

Date:

_____

Member 2 -

Date:

_____

Member 3 -

Date:

_____

Member 4 -

Final approval and acceptance of this dissertation is contingent upon the candidates submission of the final copies of the thesis to HBNI.

I hereby certify that I have read this thesis prepared under my direction and recommend that it may be accepted as fulfilling the thesis requirement.

Date:
Place: **Guide**

STATEMENT BY AUTHOR

This dissertation has been submitted in partial fulfillment of requirements for an advanced degree at Homi Bhabha National Institute (HBNI) and is deposited in the Library to be made available to borrowers under rules of the HBNI.

Brief quotations from this dissertation are allowable without special permission, provided that accurate acknowledgement of source is made. Requests for permission for extended quotation from or reproduction of this manuscript in whole or in part may be granted by the Competent Authority of HBNI when in his or her judgment the proposed use of the material is in the interests of scholarship. In all other instances, however, permission must be obtained from the author.

Chandrachur Chakraborty

DECLARATION

I, hereby declare that the investigation presented in the thesis has been carried out by me. The work is original and has not been submitted earlier as a whole or in part for a degree / diploma at this or any other Institution / University.

Chandrachur Chakraborty

List of Publications arising from the thesis

Journal

1. **Dragging of inertial frames inside the rotating neutron stars**

   C. Chakraborty, K.P. Modak, D. Bandyopadhyay, *Astrophys. J.* **790**, 2 (2014)

2. **Inner-most stable circular orbits in extremal and non-extremal Kerr-Taub-NUT spacetimes**

   C. Chakraborty, *Eur. Phys. J.* **C 74**, 2759 (2014)

3. **Strong gravity Lense-Thirring Precession in Kerr and Kerr-Taub-NUT spacetimes**

   C. Chakraborty, P. Majumdar, *Class. Quantum Grav.* **31**, 075006 (2014)

4. **Lense-Thirring Precession in Plebański-Demiański spacetimes**

   C. Chakraborty, P. Pradhan, *Eur. Phys. J.* **C 73**, 2536 (2013)

5. **Anomalous Lense-Thirring precession in Kerr-Taub-NUT spacetimes**

   C. Chakraborty, arXiv:1407.6294v2 [gr-qc]

Chandrachur Chakraborty

"जननी जन्मभूमिश्च स्वर्गादपि गरीयसी...."

(Mother and Motherland are greater than even 'Heaven')

Dedicated To

My Mother and Motherland

ACKNOWLEDGEMENTS

"Comrade of the road,

Here are my traveller's greetings to thee..."

— Rabindranath Tagore

My sincere gratitude and indebtedness to my thesis supervisors Prof. Dr. Debades Bandyopadhyay and Prof. Dr. Parthasarathi Majumdar for providing their sincere help and guidance during the entire period of my research. They have always motivated me and incessantly encouraged me to pursue my own line of thinking. I am grateful to them for their patience and boosting my confidence from time to time. Academic and non-academic discussions with them also help to boost up my mental strength and to grow up my knowledge in General Relativity as well as in Astrophysics.

I wish to express my warm and sincere thanks to Prof. Dr. Parthasartahi Mitra, Prof. Dr. Pijushpani Bhattacharjee, Prof. Dr. Debasish Majumdar and Prof. Dr. Ambar Ghosal for extending all kinds of help and support throughout my thesis work.

Immediate next name that comes to my mind is my friend, Kamakshya P. Modak who helped me all through my research days at SINP. I am grateful to him for collaborating with me in a project which constituted my thesis in turn and also for helping me to acquire programming skills. I am also grateful to Dr. P. P. Pradhan for collaborating with me in an another project which is also a part of my thesis.

Thanks to all of my seniors; Rana, Srijit, Pritibhajan, Abhishek (Majhi), Lab, Tapan, Niladri, Abhishek (Chowdhury), Swapan for helping me through various ways in my research career. Special thanks due to Parijat, Chiranjib, Amit, Prasanta, Satyajit, Abhik, Goutam, Kuntal, Apurba, Aminul, Anshu, Mithun, Palash, Biswarup, Tanmay, Uttam, Kalyanmoy, Atanu, Rajani, Souvik for their constant support and encouragements by maintaining an ambient atmosphere around my workplace. Thanks also to Bijoy and Nilanjan for their help and support in official purposes. I express my indebtedness to

my very special friends Sutapa, Moumita, Kamakshya and Tapas for their love, youthful company and real friendship. I also want to thank all the members (teaching, non-teaching, JRFs, SRFs, RAs of Physics and Bio-physics divisions) of SINP to maintain the pleasant atmosphere at the institute. I am grateful to Dept. of Atomic Energy (DAE, Govt. of India) for the financial assistance in my Ph.D career.

My sincere gratitude and indebtedness to Dr. Mani Bhaumik with whom I discuss many important academic and non-academic things. His valuable suggestions and advices help me a lot. I am also influenced by his life history which boosts up my mental strength. My sincere gratitude also to Dr. A. L. Bhaumik, Bhabes Pan, Debasis Bhattacharyya, Goutam Bhattacherjee, Indrani Chattopadhyay, Samit De and Sikha Roychoudhury for their various help and constant encouragement in my Ph.D life.

I wish to express my deep sense of gratitude to my parents and my brother (Indranil) for their immense patience, love, affection, encouragements and support. I am indebted to my parents for giving me the freedom to choose my own career and for constantly providing me the moral and emotional support at every stage of my life. I am also indebted to my uncle (Snehasis) and aunt (Aparajita) due to their valuable suggestions, advices and constant supports in the various stages of my life. Their appreciation of my works have boosted up my mental strength. Immense respect and best regards to my Grand Mother, maternal Grand Father and maternal Grand Mother whom I will never forget in my whole life. They were my primary 'guides' and they always used to inspire me to gain more and more knowledge. It is only because of their kind blessings that I could complete this work.

Finally, I bow down to Ishwarchandra Vidyasagar, Rabindranath Tagore, Swami Vivekananda and S. C. Bose whose lives and teachings have inspired me tremendously since my childhood and built up my character for which I could able to achieve this goal.

Chandrachur Chakraborty

Contents

1 Introduction **15**
- 1.1 General Introduction . . . 15
- 1.2 Spin precession in curved spacetimes . . . 16
- 1.3 Geodetic precession . . . 18
- 1.4 Lense-Thirring precession . . . 19
  - 1.4.1 Lense-Thirring precession outside of a slowly rotating body . . . 19
  - 1.4.2 Measurement of LT precession: Gravity Probe B . . . 22
- 1.5 Summary . . . 22

2 General formulation of Lense-Thirring effect and its application to Kerr spacetime **27**
- 2.1 Introduction . . . 27
- 2.2 Derivation of Lense-Thirring precession frequency . . . 28
- 2.3 Lense-Thirring precession in Kerr spacetime . . . 34
  - 2.3.1 Weak field limit . . . 36
  - 2.3.2 Preliminary comparison with observational data . . . 38
- 2.4 Summary . . . 41

3 Lense-Thirring precession in Plebański-Demiański spacetime **44**
- 3.1 Introduction . . . 44
- 3.2 Non-extremal case . . . 46
  - 3.2.1 Plebański-Demiański (PD) spacetimes . . . 46
  - 3.2.2 Special cases . . . 48
  - 3.2.3 Non-vanishing Lense-Thirring precession in 'zero angular momentum' Plebański-Demiański spacetimes . . . 50
- 3.3 Extremal case . . . 53
  - 3.3.1 Extremal Plebański-Demiański Spacetime . . . 53
  - 3.3.2 Extremal Kerr Spacetime . . . 57
  - 3.3.3 Extremal Kerr-Newman Spacetime . . . 58
  - 3.3.4 Extremal Kerr-de Sitter Spacetime . . . 59
  - 3.3.5 Extremal Kerr-Taub-NUT spacetime . . . 60
- 3.4 Summary . . . 60

4 Anomalous Lense-Thirring precession in Kerr-Taub-NUT and Taub-NUT spacetimes **62**
4.1 Introduction . . . 62
4.2 Lense-Thirring precession in Kerr-Taub-NUT spacetime . . . 65
4.3 Results & Discussion . . . 69
4.4 Lense-Thirring precession in Taub-NUT spacetime . . . 76
4.4.1 Analytic extension of Taub-NUT spacetime . . . 78
4.5 Digression : ISCOs in KTN spacetimes . . . 80
4.5.1 Motivation . . . 80
4.5.2 ISCOs for the null geodesics in Kerr-Taub-NUT spacetimes . . . 84
4.5.3 ISCOs for the timelike geodesics in Kerr-Taub-NUT spacetimes . . . 93
4.6 Summary . . . 108

5 Dragging of inertial frames inside the rotating neutron stars **111**
5.1 Introduction . . . 111
5.2 Basic equations of frame-dragging effect inside rotating neutron stars . . . 114
5.3 Numerical method . . . 118
5.3.1 Equation of state (EoS) of dense matter . . . 120
5.4 Results and Discussion . . . 121
5.4.1 Pulsars rotating with their Kepler frequencies $\Omega = \Omega_K$ . . . 121
5.4.2 Pulsars rotating with their frequencies $\Omega < \Omega_K$ . . . 127
5.5 Summary . . . 129

6 Conclusion & Outlook **131**

Bibliography **136**

List of Figures

2.1 *Observer moves in a stationary spacetime [14].* 29
2.2 *Plot of* Ω_{LT} *(in* m^{-1}*) vs* r *(in* m*) at* $\theta = 0$ *for* $a = 0.7\ m$ *&* $M = 1\ m$ *[28].* 38

4.1 *Plot of* Ω_{LT} *(in* m^{-1}*) vs* r *(in* m*) in the KTN spacetime for* $a = 0.1\ m$, $n = 1\ m$ *&* $M = 1\ m$ *[45].* 66
4.2 *Plot of* Ω_{LT} *(in* m^{-1}*) vs* r *(in* m*) in the KTN spacetime for* $a = 0.7\ m$, $n = 0.3\ m$ *&* $M = 1\ m$ *[45].* 67
4.3 *Plot of* Ω_{LT} *(in* m^{-1}*) vs* r *(in* m*) in the KTN spacetime for* $a = n = 1\ m$ *&* $M = 1\ m$ *[45].* 69
4.4 *Plot of strong gravity* Ω_{LT} *(in* m^{-1}*) vs* r *(in* m*) in the Kerr spacetime for* $a = M = 1\ m$ *[45].* 70
4.5 *Plot of* η *vs* r *(in* m*) in the Kerr and Kerr-Taub-NUT spacetimes for* $a = n = 1\ m$ *&* $M = 1\ m$ *[45].* 71
4.6 *3-D plot of* $\Omega_{LT}(r, \theta)$ *in the KTN spacetime for* $a = n = 1\ m$ *&* $M = 1\ m$ *[45].* 72
4.7 *3-D plot of* $\Omega_{LT}(r, \theta)$ *in the KTN spacetime for* $a = 0.7\ m$, $n = 0.3\ m$ *&* $M = 1\ m$ *[45].* 73
4.8 *3-D plot of* $\Omega_{LT}(r, \theta)$ *in the KTN spacetime for* $a = 0.1\ m$, $n = 1\ m$ *&* $M = 1\ m$ *[45].* 73
4.9 *3-D plot of* $\Omega_{LT}(r, \theta)$ *in the Kerr spacetime for* $a = 1\ m$ *&* $M = 1\ m$ *[45].* . 74
4.10 *Plot of* Ω_{LT} *in the Taub-NUT spacetime for* $n = 1\ m$ *&* $M = 1\ m$ *(basically, the expression of* Ω_{LT} *(see Eq. (25) of Ref. [28]) is independent of* θ*, thus the value (colour) of* Ω_{LT} *does not change with* $\cos\theta$ *in panel(b)) [45].* . . . 74
4.11 *Plot of* Ω_{LT} *(in* m^{-1}*) vs* r *(in* m*) for* $n = 3\ m$ *&* $M = 1\ m$ *and* Ω_{LT} *vs* r *for* $n = 3\ m$ *&* $M = 0$ *[28].* 78
4.12 *Plot of* r_{Mcn} *(green) and* r_{+M} *(red) vs* n_M *[41].* 91
4.13 *Plot of radius of direct ISCO (*r_{MISCO}*) along* y *axis vs NUT charge* n_M *along* x *axis [41].* 104

5.1 *Frame-dragging effect inside the rotating neutron stars from the origin to the surface, calculated for the APR EoS.* Ω_K *and* ε_c *denote the Kepler frequency and the central energy density, respectively. Surface of the neutron star along the pole located around* $0.6r_e$ *but the plot is still valid beyond the surface of the pole as our formalism is applicable for regions outside the pulsar [43].* 124
5.2 *Same as Fig. 5.1, but calculated for the DD2 EoS [43].* 125
5.3 *Same as Fig. 5.1, but calculated for the Chiral EoS [43].* 125

5.4 *3-D plots of Ω_{LT} of the pulsar which is rotating with $\Omega_K = 5000\,s^{-1}$* as a function of s and $\cos\theta$ for (a) DD2 EoS and (b) APR EoS [43]. 127
5.5 *Frame-dragging effect inside the rotating neutron star from the origin to the surface, calculated for J1807-2500B ($M = 1.366M_\odot, \Omega = 1500.935\,s^{-1}$) [43].* 128
5.6 *Frame-dragging effect inside the rotating neutron star from the origin to the surface, calculated for J0737-3039A ($M = 1.337M_\odot, \Omega = 276.8\,s^{-1}$) [43].* 129
5.7 *Frame-dragging effect inside the rotating neutron star from the origin to the surface, calculated for B1257+12 ($M = 1.5M_\odot, \Omega = 1010.321\,s^{-1}$) [43].* 129
5.8 *3-D plots of Ω_{LT} of the pulsar J0737-3039A as a function of s and* $\cos\theta$ *for DD2 (panel (a)) and APR (panel (b)) EoSs [43].* 130

List of Tables

2.1 Comparison between strong gravity and weak gravity LT precession (all these values are calculated at the pole ($\theta = 0$) and near the surface ($r \to R$) of that massive object). 39

4.1 Comparison between the radius of the horizon (r_{Mhor}) and the radius of the ISCO (r_{MISCO}) at Taub-NUT spacetimes [41]. 105

5.1 Maximum gravitational masses ($M_G/M_\odot$), equatorial radii (R), and their corresponding central energy densities (ε_c) for static ($\Omega = 0$) and Keplerian limit ($P = P_K = 2\pi/\Omega_K$) with different EoS, where P_K is the Kepler period in millisecond [43]. 121

5.2 Normalised angular velocities of the local inertial frame-dragging at the surface $\tilde{\Omega}_s$ and centre $\tilde{\Omega}_c$ of the neutron stars which are rotating at their respective Kepler periods ($P_K \equiv 2\pi/\Omega_K$) as measured by a distant observer [43]. 126

5.3 Normalised angular velocities of the local inertial frame-dragging at the surface $\tilde{\Omega}_s$ and centre $\tilde{\Omega}_c$ of some known rotating neutron stars [43]. 128

Synopsis

Earlier analyses of the Lense-Thirring effect assume large distances and slow rotation for the test gyroscope. Further, the rotating spacetime solution is usually approximated as a Schwarzschild spacetime, and the effect of rotation is confined to a perturbative term added on to the Schwarzschild metric. This leads to the standard result for LT precession frequency in the weak field approximation. Most textbook calculations as well as almost in all the research articles of the LT precession rate focus usually on the weak-field approximation.

We derive the exact LT precession formula for full Kerr spacetime without invoking either the weak gravity approximation or an approximation involving the Kerr parameter (slow rotation limit). The weak-field approximation is then shown to emerge straightforwardly from our general formulation. We also derive the exact LT precession rates in the non-extremal and extremal Plebański-Demiański (PD) spacetimes. For the extremal PD spacetimes we first derive the general extremal condition for PD spacetimes. This general result could be applied to obtain the extremal limit in any stationary and axisymmetric spacetimes. Next, we derive the exact LT precession rate in Kerr-Taub-NUT (KTN) spacetimes which include the Kerr parameter and NUT parameter or (gravito)magnetic monopoles. Interestingly, in the *non-rotating* (when Kerr parameter vanishes) and *spherically symmetric* Taub-NUT spacetime the LT precession does not vanish. We also study the causal geodesics in the equatorial plane of the extremal Kerr-Taub-NUT spacetime, focusing on the Innermost Stable Circular Orbit (ISCO), and compare its behaviour with extant results for the ISCO in the extremal Kerr spacetime.

Later, we derive the exact frame-dragging rate inside rotating neutron stars. This formula is applied to show that the frame-dragging rate monotonically decreases from the centre to the surface of the neutron star along the pole. In case of frame-dragging rate along the equatorial distance, it decreases initially away from the centre, become negligibly

small well before the surface of the neutron star, rises again and finally approaches to a small value at the surface. The appearance of local maximum and minimum in this case is the result of the dependence of frame-dragging frequency on the distance and angle. Moving from the equator to the pole, it is observed that this local maximum and minimum in the frame-dragging rate along the equator disappears after crossing a critical angle.

Currently the accretion mechanism of black holes and pulsars is not properly studied with the exact formulation of strong gravity frame-dragging effect. It would be worth to investigate the accretion disk theory to model the QPOs and jets using the strong gravity LT precession formula in the astrophysicaly relevant important spacetimes. The relation between mass and angular momentum of the black holes and pulsars could also be studied in the light of strong gravity frame-dragging effect.

Chapter 1

Introduction

1.1 General Introduction

Though we know that no astrophysical object in nature is exactly nonrotating, yet many astrophysical phenomena are explained by Schwarzschild geometry as it is the simplest metric by which the curvature of the spacetime is described easily. The another advantage is that it is a spherically symmetric spacetime and also an excellent approximation to the outside of nonrotating stars and black holes. There is also no star which is perfectly spherically symmetric. Generally, the star like Sun is also slightly squeezed along the rotation axis. However, the Schwarzschild geometry is a good approximation for the *very* slowly rotating astrophysical objects.

If any stellar body rotates with a significant angular velocity the Schwarzschild geometry is failed to describe the curvature of the spacetime produced by the rotating object. The curved spacetime produced by a rotating object has a complex structure than the Schwarzschild geometry. General relativity predicts that the curvature of spacetime is produced not only by the distribution of mass-energy but also by its motion. In electromagnetism, the fields are produced not only by charge distributions but also by currents. Considering this analogy, this effect can be called as *gravitomagnetic effect*. An important

gravitomagnetic effect will be explored in this thesis- the dragging of inertial frames. If a small part of the matter starts to rotate, the inertial frame must be dragged along slightly. The small rotation of the earth also drags the local inertial frame along it. The dragging rate is very small in the case of earth. It is around $\sim 0.3''$/year on the surface of the earth. The frame-dragging effect was first derived [1] in 1918 by Austrian physicists Josef Lense and Hans Thirring and is also known as the Lense-Thirring (LT) precession. They showed that the rotation of a massive body could distort the spacetimes, making the spin of nearby test gyroscope precesses [2]. This does not happen in Newtonian gravity for which the gravitational field of a body depends only on its mass, not on its rotation.

A gyroscope is a natural test body to observe the frame-dragging effect as the spin of a gyro points in a fixed direction in an inertial frame [3]. Thus, we should begin our study of frame-dragging effect with a discussion of gyroscopes in curved spacetimes.

1.2 Spin precession in curved spacetimes

To explore the geometry of curved spacetime we can study the behaviour of a small test body with spin which could be called as test gyro or test spin. *Spin* means either the polarization vector of a particle (i.e., the expectation value of the spin operator for a particle in a particular quantum mechanical state) or an intrinsic angular momentum of a rigid body (such as a gyroscope). As in classical mechanics, the angular motion of a constant magnitude angular momentum is called *precession*. In curved spacetimes, a freely falling test gyro which moves along a timelike geodesic with its four velocity $u(\tau)$ obeys the geodesic equation:

$$\nabla_u u = 0 \ . \tag{1.1}$$

The gyro is described by the spacelike spin four vector $S(\tau)$. S could be expressed as $S = (0, s)$ in a local inertial frame in which the gyro is at rest. As the gyro is at rest in

that frame the four velocity u could be expressed as $u = (1, \vec{0})$. Thus,

$$< S, u >= 0 \ . \tag{1.2}$$

$<, >$ implies the scalar product. In the absence of external forces, the equivalence principle implies that in the local rest frame

$$\frac{ds(t)}{dt} = 0 \ , \tag{1.3}$$

for a gyroscope or a elementary particle. In the local rest frame we can write it in a covariant form:

$$(\nabla_u S)_{rest} = \left(\frac{ds^0}{dt}, \frac{ds}{dt}\right) = \left(\frac{ds^0}{dt}, 0\right) \ . \tag{1.4}$$

We obtain from Eq. (1.2)

$$< \nabla_u S, u >= - < S, f > \ , \tag{1.5}$$

if the test gyro does not move along the geodesic (where $f = \nabla_u u$ is the acceleration). Hence,

$$< \nabla_u S, u >= -\frac{ds^0}{dt}|_{rest} = - < S, f > \ . \tag{1.6}$$

From Eq. (1.4) and Eq. (1.6) we get

$$(\nabla_u S)_{rest} = (< S, f >, 0) = (< S, f > u)|_{rest} \ . \tag{1.7}$$

Thus the covariant equation is

$$\nabla_u S =< S, f > u \ . \tag{1.8}$$

From Eq. (1.8), we obtain

$$< u, \nabla_u S >=< S, f >< u, u >= - < S, f >= - < S, \nabla_u u > \ . \tag{1.9}$$

Thus

$$\nabla_u < u, S >= 0 \ , \tag{1.10}$$

which is consistent with Eq. (1.2). If the gyroscope moves along its geodesics ($f = 0$) the Eq. (1.8) reduces to

$$\nabla_u S = 0 \ ,$$

or

$$\frac{dS^\beta}{d\tau} + \Gamma^\beta_{\delta\lambda} S^\delta u^\lambda = 0 \ . \tag{1.11}$$

We call Eq. (1.8) (when gyroscope does not move along its geodesic) and Eq. (1.11) (when gyroscope moves along its geodesic) the gyroscope equation.

General Relativity predicts that the spin of a gyro will precess with respect to infinity due to the (i) curvature of the spacetime produced by a body (called Geodetic precession) and also due to the (ii) rotation of the body (called the Lense-Thirring precession). We discuss both precessions in the next two sections.

1.3 Geodetic precession

What would be the behaviour of a gyroscope in orbit around a nonrotating spherically symmetric spacetime? An observer riding with the gyro will see the spin of the gyro to precess. The spin remains fixed in a local inertial frame falling with the gyro but precesses with respect to infinity due to the curvature of spacetime produced by the spherical body.

Suppose, an observer orients the gyro in the direction of a distant star in the equatorial plane of an orbit. General Relativity predicts that, after completion of an orbit, the gyro will point in a different direction making an angle $\Delta\phi_{gd}$ with the starting one. The change in the direction is called geodetic precession. In the case of *static* and *spherically symmetric* Schwarzschild geometry, the spin in an *equatorial* ($\theta = \pi/2$) orbit is rotated by an angle

$$\Delta\phi_{gd} = 2\pi \left[1 - \left(1 - \frac{3M}{R}\right)^{\frac{1}{2}}\right] , \tag{1.12}$$

in the direction of motion (where M is the mass of the spacetime and R is the distance of the gyro from the center of the spacetime).

1.4 Lense-Thirring precession

Formally, stationary spacetimes with angular momentum are known to exhibit an effect called the LT precession whereby locally inertial frames are dragged along the rotating spacetime, making any test gyroscope in such spacetimes *precess* with a certain frequency called the LT precession frequency. Thus, the frame-dragging effect is absent in the nonrotating spacetime, i.e., Schwarzschild spacetime.

1.4.1 Lense-Thirring precession outside of a slowly rotating body

If a spherical body set into slow rotation with a uniform angular velocity about its own axis, the body will change from the spherically symmetric Schwarzschild geometry. This change arises due to the rotational distortion of the body. This will also bring the change of the first order in J ($\sim I\Omega$, angular momentum of the rotating body) in the metric. For $J = 0$, it reduces to the Schwarzschild metric and the polar axis coincides with the rotation axis. Thus, we can express the slowly rotating metric (neglecting higher order

term of J) in the following form:

$$ds^2 = ds^2_{Sch} - \frac{4J\sin^2\theta}{r^2} r d\phi dt + O(J^2) \ , \tag{1.13}$$

where ds^2_{Sch} represents the Schwarzschild line element. According to Hartle's prescription [3] of the frame-dragging effect along the pole, one must transform the polar coordinates (r, θ, ϕ) into Cartesian coordinates (x, y, z) as polar coordinates are singular along the axis in which the gyro falls. After the transformations, the metric of Eq. (1.13) is reduced to

$$ds^2 = ds^2_{Sch-Car} - \frac{4J}{r^2}\left(\frac{xdy - ydx}{r}\right) dt + O(J^2) \ , \tag{1.14}$$

where $ds^2_{Sch-Car}$ is the Schwarzschild metric in Cartesian coordinates (the explicit form is not needed). According to Hartle [3], the gyroscope equation is solved to obtain the LT precession rate; the term M/r of the Schwarzschild metric does not contribute to the final result because it would give rise to the term MJ/r^3 in the precession rate. That implies that the leading order precession rate calculation could be carried out taking $M = 0$. Thus, the $ds^2_{Sch-Car}$ of the Schwarzschild metric in Cartesian coordinates could be taken as the flat metric (Minkowski spacetime)

$$ds^2_{Mink} = -dt^2 + dx^2 + dy^2 + dz^2 \ . \tag{1.15}$$

It has also been taken that the gyro is falling along the z-axis to simplify the calculation. So, the four-velocity could be presented as

$$u^\beta = (u^t, 0, 0, u^z) \ , \tag{1.16}$$

$$S^\beta = (0, s^x, s^y, 0) \ . \tag{1.17}$$

Spin is taken to lie in the xy plane and the Eq. (1.2) is satisfied automatically on the z-axis. Replacing $ds^2_{Sch-Car}$ of Eq. (1.13) with the flat metric and calculating the non-vanishing Christoffel symbols in the gyroscope Eq. (1.11) for s^x and s^y it is obtained

$$\Gamma^x_{ty} = \frac{2J}{z^3} \ , \tag{1.18}$$

$$\Gamma^y_{tx} = -\frac{2J}{z^3} \ . \tag{1.19}$$

Thus,

$$\frac{ds^x}{dt} = -\frac{2J}{z^3}s^y \ , \tag{1.20}$$

$$\frac{ds^y}{dt} = \frac{2J}{z^3}s^x \ . \tag{1.21}$$

The above equations describe that a gyroscope precesses with respect to coordinate axes (x, y, z) in the same direction, along which the spacetime is rotating. This is called the LT precession [3]. Thus, the LT precession rate at the distance z from the center of the rotating body is

$$\Omega_{LT} = \frac{2J}{z^3} \ . \tag{1.22}$$

This precession rate is calculated in the frame in which the center of the body is at rest and the gyroscope is falling.

A gyroscope in a realistic orbit about the slowly rotating body would experience the LT precession which depends on the colatitude as [3, 4]

$$\vec{\Omega}_{LT} = \frac{1}{r^3}[3(\vec{J}.\hat{r})\hat{r} - \vec{J}] \ , \tag{1.23}$$

where, $\hat{r}$ is the unit vector along r direction. The above expression reduces to Eq. (1.22) for $\theta = 0$. This expression of the LT has a similarity with that of the magnetic/electric

field where $\vec{J}$ plays the role of dipole moment.

1.4.2 Measurement of LT precession: Gravity Probe B

On 20th April, 2004 NASA launched the Grvity Probe B satellite to measure the Geodetic and LT precession due to the rotation of Earth. The satellite carried four precession gyroscopes which were spheres of fused quartz 1.5 inch in diameter. Each gyroscope was eletrostatically suspended by the saucer-shaped electrodes in the two-halves of the housing. One of the gyroscopes was used as the 'test mass'. Other three gyroscopes were operating in an ideal free-fall conditions. The whole system was kept in superfluid helium (temperature 2K). The GPB satellite was flown in 642 km polar orbit and a reference telescope enabled the satellite to be looked onto HR8703 (also known as IM Pegasi), a binary star in the constellation Pegasus. The gyro spin was initially pointed to the guide star and analysing the data from all four gyroscopes it was reported that the geodetic precession rate was $6,601.8 \pm 18.3$ milliarcsecond/year (mas/yr) and the LT precession rate of 37.2 ± 7.2 mas/yr [5]. The theoretical predictions of general relativity were of $6,606.1$ mas/yr and 39.2 mas/yr, respectively. The GPB spacecraft decommissioned on 8th December, 2010.

1.5 Summary

We have already discussed that the LT precession frequency has been discovered by Lense and Thirring and it has also been shown to decay as the inverse cube of the distance of the test gyroscope from the source [1] for large enough distances where curvature effects are small, and known to be proportional to the angular momentum of the source. The largest precession frequencies (Ω_{LT}) are thus expected to be seen very close to the source (like the surface of a pulsar, or the horizon of a black hole), as well as for spacetimes rotating very fast with large angular momenta.

Most of earlier analyses of the LT effect assumed large distances ($r >> M$, M is the mass of the rotating spacetime due to a compact object like a pulsar) for the test gyroscope. In a recent work reported in ref. [6], an alternative approach based on solving the geodesic equations of the test gyroscope numerically, *once again* within the weak gravitational field approximation, was used to compute the frame-dragging effect for galactic-centre black holes. In another related work [7], Hackman and Lämmerzahl had given an expression of the LT precession valid up to *first order* in the Kerr parameter a for a general axisymmetric Plebański-Demiański spacetime. This is obviously a good approximation for slowly-rotating compact objects. The LT precession rate has also been derived [8, 9] by solving the geodesic equations for both Kerr and Kerr-de-Sitter spacetimes at the *polar orbit*. These results are not applicable for orbits which lie in orbital planes other than the polar plane. We understand that observations of precession due to locally inertial frame-dragging have so far been possible only for spacetimes whose curvatures are small enough; e.g., the LT precession in the earth's gravitational field which was probed recently by the LAGEOS experiment [10] and also by Gravity Probe B [5]. Though there has been so far no attempt to measure the LT precession effects due to the frame-dragging in *strong gravity regimes* [11] but Stella and Possenti [12] had given some important discussions regarding the LT precession in the astrophysical context in strong gravity regimes.

The physics of accretion disc regions not too far from the outer layer of rotating neutron stars or the horizons of black holes emitting X-rays ought to entail nontrivial LT precession of local inertial frames in their vicinity. Most extant treatments of accretion disc physics appear to ignore these effects, even though there is not much in the way of a computation to theoretically justify this viewpoint. Precision estimates of strong gravity LT precession thus appear essential to ensure that errors stemming from ignoring this are within acceptable limits. Further, upcoming X-ray observatories, as well as multi-wavelength strong gravity space probes currently under construction, which envisage to make observations of possible frame-dragging effects in strong gravity situations in the

near future, make it necessary to go beyond the weak field approximation paramount. A recent work by Stone and Loeb [13] estimated the effect of weak-field LT precession on accreting matter close to compact accreting objects. While there are claims what has been estimated in this work pertains more to orbital precession, rather than precession of a test gyroscope, it is obvious that in the vicinity of the spacetime near the surface of pulsars (respectively, the horizons of black holes), the large LT precession of test gyroscopes ought to manifest in changes in the predicted X-ray emission behaviour originating from modifications in the behaviour of infalling timelike geodesics of accreting matter particles due to the LT precession. It also stands to reason that pulsar emission mechanisms may need to be corrected due to frame dragging effects in the strong gravity regime. As a precursor to precise estimation of these effects, a theoretical understanding of the LT precession in strongly curved spacetimes (as near compact systems like black holes and pulsars) is in order.

In the next chapter, we review in detail the LT precession rate [14, 15] in a strong gravity regime in a 'Copernican' frame, examining its domain of validity. Recall that a Copernican frame is a local orthonormal tetrad at rest (so moving only in the "time" direction determined by the timelike Killing vector of the spacetime) and "locked" to the spatial part of whatever such coordinate system is chosen, so that it is "at rest" with respect to the local inertial frames at infinity. Within this frame, an untorqued gyro in a stationary but not static spacetime held fixed by a support force applied to its center of mass precesses. Since the Copernican frame does not rotate (by construction) relative to the inertial frames at asymptotic infinity ("fixed stars"), the observed precession rate in the Copernican frame also gives the precession rate of the gyro relative to the fixed stars. We argue that the LT precession rate is applicable to all stationary spacetimes, irrespective of whether they are axisymmetric or not. This result is also applicable for all orbits (not only for polar and equatorial orbits), located at various distances and different angles. In this sense, it is rather more general than the result of [16], whose approach was

discussed for comparison at the end. Also, the oft-quoted weak-field result in Eq. (1.23) (in a 'Copernican' frame) for the LT precession rate is readily obtained from this general result, inserting the metric for the desired spacetime.

Armed with this general formula for inertial frame dragging, we explore its ramifications for axisymmetric spacetimes like the Kerr-Taub-NUT, mainly for its intrinsic general relativistic merits, especially in the limit of vanishing angular momentum. To forge some link with actual astrophysical processes, we briefly consider the LT precession in Kerr spacetime for possible phenomenological application to actual compact bodies like pulsars. We emphasize here that though this thesis focuses on the general relativistic aspects of the LT precession in strongly curved domains, rather than on its applications to actual astrophysical processes, we expect that our work will eventually relate to those very interesting aspects in the near future.

The thesis is organized in the following way. In Chapter 2, we study the general formulation of the LT effect in any stationary spacetime and applying this general result we derive the exact LT precession rate in Kerr spacetime. We derive the exact LT precession rates in non-extremal and extremal Plebański-Demiański spacetimes in Chapter 3. Chapter 4 is devoted to computation of the anomalous LT precession rates in Kerr-Taub-NUT and Taub-NUT spacetimes. We also derive the radii of the Inner-most Stable Circular Orbits (ISCOs) for non-extremal and extremal Kerr-Taub-NUT spacetimes and discuss about the LT precession frequencies in these ISCOs. This chapter is basically for future applications of the strong gravity LT effect in accretion disk theory in which ISCO plays a very important role. Dragging of inertial frames inside the rotating neutron stars are derived in Chapter 5. In this chapter, we show that the general formulation of the LT precession is also applicable for realistic stellar bodies which are described by stationary and axisymmetric metrics. Here, we have applied it for pulsars only but it could be applicable for other astronomical bodies as well. These applications would be helpful to describe the other astronomical processes which have explicit or implicit dependency on

the LT precession. Finally we conclude in Chapter 6 with an overview and our future outlook.

Chapter 2

General formulation of Lense-Thirring effect and its application to Kerr spacetime

2.1 Introduction

At first, our aim was to obtain the LT precession rate in such a manner so that we can use it to get the exact LT precession rate in Kerr spacetime as Kerr spacetime is very useful in astrophysics. In this chapter we are going to derive the LT precession rate in a more general sense. Kerr spacetime is an axisymmetric spacetime but we have to remember that the LT precession rate is not a property only of an axisymmetric spacetime rather it is a property of every stationary spacetime whether it is axisymmetric or not. There are exceptions also in some special cases. However, we can easily say that *every stationary spacetime shows the LT precession and static spacetime is unable to do so in any circumstances.* This is due a basic difference between the stationary and static spacetimes. It will be cleared in the following paragraph.

A spacetime is said to be stationary if it possesses a timelike Killing vector field ξ^a;

further, a stationary spacetime is said to be static if there exists a spacelike hypersurface Σ which is orthogonal to the orbits of the timelike isometry. By Frobenius's theorem of hypersurface orthogonality, we can write for a static spacetime

$$\xi_{[a}\nabla_b\xi_{c]} = 0 \ . \tag{2.1}$$

If $\xi^a \neq 0$ everywhere on Σ, then in a neighbourhood of Σ, every point will lie on a unique orbit of ξ^a which passes through Σ. From the explicit form of a static metric, it can be seen that the diffeomorphism defined by $t \to -t$ (the map which takes each point on each Σ_t to the point with the same spatial coordinates on Σ_{-t}), is an isometry. The "time translation" symmetry, $t \to t + constant$ is possessed by all stationary spacetimes. Static spacetimes on the other hand, possess an additional symmetry, "time reflection" symmetry over and above the "time translation symmetry". Physically, the fields which are time translationally invariant can fail to be time reflection invariant if any type of "rotational motion" is involved, since the time reflection will change the direction of rotation. For example, a rotating fluid ball may have a time-independent matter and velocity distribution, but is unable to possess a time reflection symmetry [17]. In the case of stationary spacetimes, the failure of the hypersurface orthogonality condition Eq. (2.1) implies that neighbouring orbits of ξ^a "twist" around each other. The twisting of the orbits of ξ^a is the cause of that *extra precession* in stationary non-static spacetimes. This *extra precession* for any stationary spacetime is now being presented in the next section.

2.2 Derivation of Lense-Thirring precession frequency

Let us consider that an observer is at rest in a stationary spacetime with a timelike Killing field K. The observer moves along an integral curve $\gamma(\tau)$ of K and his 4-velocity can be written as

$$u = (-K^2)^{-\frac{1}{2}}K \ . \tag{2.2}$$

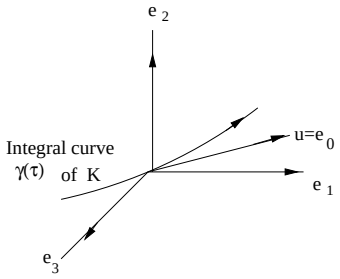

Figure 2.1: *Observer moves in a stationary spacetime [14].*

We can now choose an orthonormal tetrad e_α along γ which is Lie-transported.

$$L_K e_\alpha = 0 \ , \tag{2.3}$$

where $\alpha = 0, 1, 2, 3$. As e_0 is just $u = \dot{\gamma}$ (where,'dot' denotes the differentiation with respect to τ), u is perpendicular to e_1, e_2, e_3 axes. We also have

$$< e_\alpha, e_\beta >= \eta_{\alpha\beta} \ , \tag{2.4}$$

where, $\eta_{\alpha\beta} = diag(-1, 1, 1, 1)$.

We can interpret e_α as axes at rest. We know that the spin of the gyroscope precesses with respect to those axes of rest and we are interested in the change of the spin relative to this system. We know that torsion

$$T(K, e_i) = \nabla_K e_i - \nabla_{e_i} K - [K, e_i] = 0 \ . \tag{2.5}$$

The rotation coefficient can be defined as

$$\omega_{ij} =< \nabla_u e_i, e_j > \ \ . \tag{2.6}$$

Now, using Eq. (2.6) and Eq. (2.2) we get,

$$\omega_{ij} = (-K^2)^{-\frac{1}{2}} < e_j, \nabla_K e_i > \ , \tag{2.7}$$

where ω_{ij} is related with the angular velocity Ω^l as

$$\omega_{ij} = \epsilon_{ijl}\Omega^l \ . \tag{2.8}$$

The gyroscope precesses with the angular velocity Ω relative to the tetrad frame e_α, Ω is considered as the angular velocity or the precession rate of the LT precession. As $[K, e_i] = L_K e_i = 0$, we get from Eq. (2.5)

$$\nabla_K e_i = \nabla_{e_i} K \ . \tag{2.9}$$

Substituting this result in Eq. (2.7) we get,

$$\omega_{ij} = (-K^2)^{-\frac{1}{2}} < e_j, \nabla_{e_i} K >= (-K^2)^{-\frac{1}{2}} \nabla \tilde{K}(e_j, e_i) \ , \tag{2.10}$$

where, $\tilde{K}$ is the one-form of K. Now, Eq. (2.10) reduces to (as ω_{ij} is anti-symmetric)

$$\omega_{ij} = -(-K^2)^{-\frac{1}{2}} \frac{1}{2} [\nabla \tilde{K}(e_i, e_j) - \nabla \tilde{K}(e_j, e_i)] \ . \tag{2.11}$$

As $\tilde{K}$ is one-form, we can write Eq. (2.11) as

$$\omega_{ij} = \frac{1}{2}(-K^2)^{-\frac{1}{2}} d\tilde{K}(e_i, e_j) \ . \tag{2.12}$$

Let $\{e^\delta\}$ be the dual basis of $\{e_\delta\}$. In this basis

$$\tilde{K} = (-K^2)^{\frac{1}{2}} e^0 \ , \tag{2.13}$$

and

$$d\tilde{K} = (-K^2)^{\frac{1}{2}}\omega_{ij}e^i \wedge e^j \ . \tag{2.14}$$

We get the above expression for $d\tilde{K}$ from Eq. (2.12). We refer to the differential geometric result (see section 12.6 of [14] for a derivation)

$$e^\delta \wedge (\tilde{K} \wedge d\tilde{K}) = \eta < e^\delta, *(\tilde{K} \wedge d\tilde{K}) > \ , \tag{2.15}$$

where, η is the volume form and '*' represents the hodge dual operator. For $\delta = 0$, the left hand side of Eq. (2.15) would be,

$$e^0 \wedge (\tilde{K} \wedge d\tilde{K}) = (-K^2)\omega_{ij}e^0 \wedge e^0 \wedge e^i \wedge e^j = 0 \ . \tag{2.16}$$

It means that the time component of Ω is zero. For the spatial component we can take $\delta = k$. So,

$$e^k \wedge (\tilde{K} \wedge d\tilde{K}) = -K^2\epsilon_{ijl}\Omega^l e^k \wedge e^0 \wedge e^i \wedge e^j \ . \tag{2.17}$$

As $e^k \wedge e^0 \wedge e^i \wedge e^j = -\eta\epsilon^{ijk}$, the above equation reduces to

$$e^k \wedge (\tilde{K} \wedge d\tilde{K}) = 2K^2\eta\Omega^k \ . \tag{2.18}$$

Substituting this result in Eq. (2.15), we get

$$2K^2\Omega^k =< e^k, *(\tilde{K} \wedge d\tilde{K}) > \ . \tag{2.19}$$

So, the exact LT frequency of precession of test gyroscopes in strongly curved stationary spacetimes analyzed within a Copernican frame, is expressed as a co-vector given in terms of the timelike Killing vector fields K of the stationary spacetime as (in the notation of

Ref. [14, 15])

$$\tilde{\Omega} = \frac{1}{2K^2} * (\tilde{K} \wedge d\tilde{K}) \ , \tag{2.20}$$

or,

$$\Omega_\mu = \frac{1}{2K^2} \eta_\mu{}^{\nu\rho\sigma} K_\nu \partial_\rho K_\sigma \ , \tag{2.21}$$

where, $\eta^{\mu\nu\rho\sigma}$ represents the components of the volume-form in spacetime and $\tilde{K}$ & $\tilde{\Omega}$ denote the one-form of K & Ω, respectively. $\tilde{\Omega}$ will vanish if and only if $(\tilde{K} \wedge d\tilde{K})$ does. This happens only in a static spacetime. Using the coordinate basis form of $K = \partial_0$, the co-vector components are easily seen to be $K_\mu = g_{\mu 0}$. This co-vector could also be written in the following form

$$\tilde{K} = g_{00} dx^0 + g_{0i} dx^i \ . \tag{2.22}$$

Now,

$$d\tilde{K} = g_{00,k} dx^k \wedge dx^0 + g_{0i,k} dx^k \wedge dx^i \ , \tag{2.23}$$

$$(\tilde{K} \wedge d\tilde{K}) = (g_{00} g_{0i,j} - g_{0i} g_{00,j}) dx^0 \wedge dx^j \wedge dx^i + g_{0k} g_{0i,j} dx^k \wedge dx^j \wedge dx^i \ , \tag{2.24}$$

$$*(\tilde{K} \wedge d\tilde{K}) = (g_{00} g_{0i,j} - g_{0i} g_{00,j}) * (dx^0 \wedge dx^j \wedge dx^i) + g_{0k} g_{0i,j} * (dx^k \wedge dx^j \wedge dx^i) \ . \tag{2.25}$$

It can be shown that

$$\begin{aligned} * (dx^0 \wedge dx^j \wedge dx^i) &= \eta^{0jil} g_{l\mu} dx^\mu = -\frac{1}{\sqrt{-g}} \epsilon_{jil} g_{l\mu} dx^\mu \ , \\ *(dx^k \wedge dx^j \wedge dx^i) &= \eta^{kji0} g_{0\mu} dx^\mu = -\frac{1}{\sqrt{-g}} \epsilon_{kji} g_{0\mu} dx^\mu \ . \end{aligned} \tag{2.26}$$

Now, from Eq. (2.25) we get,

$$*\,(\tilde{K}\wedge d\tilde{K}) = \frac{\epsilon_{ijl}}{\sqrt{-g}}[(g_{00}g_{0i,j}-g_{0i}g_{00,j})(g_{l0}dx^0+g_{lk}dx^k)-g_{0l}g_{0i,j}(g_{00}dx^0+g_{0k}dx^k)]\ . \tag{2.27}$$

Simplifying the above equation we get,

$$*\,(\tilde{K}\wedge d\tilde{K}) = \frac{\epsilon_{ijl}}{\sqrt{-g}}[g_{0i,j}\,(g_{00}g_{kl}-g_{0k}g_{0l})-g_{0i}g_{kl}g_{00,j}]dx^k\ . \tag{2.28}$$

Now, using Eq. (2.21) we find that the spatial components of the precession rate (in the chosen frame) is

$$\Omega_k = \frac{1}{2}\frac{\epsilon_{ijl}}{g_{00}\sqrt{-g}}\left[g_{0i,j}\,(g_{00}g_{kl}-g_{0k}g_{0l})-g_{0i}g_{kl}g_{00,j}\right]\ . \tag{2.29}$$

[using $K^2 = g_{00}$]

The vector field corresponding to the LT precession co-vector in Eq. (2.29) can be expressed as

$$\begin{aligned}\Omega &= \Omega^\mu\partial_\mu = g^{\mu\nu}\Omega_\nu\partial_\mu \\ &= g^{\mu k}\Omega_k\partial_\mu\ [\text{as }\Omega_0=0] \\ &= g^{0k}\Omega_k\partial_0 + g^{nk}\Omega_k\partial_n \\ &= \frac{1}{2}\frac{\epsilon_{ijl}}{\sqrt{-g}}\left[g_{0i,j}\left(\partial_l-\frac{g_{0l}}{g_{00}}\partial_0\right)-\frac{g_{0i}}{g_{00}}g_{00,j}\partial_l\right]\ .\end{aligned} \tag{2.30}$$

The remarkable feature of Eq. (2.30) is that it is applicable to any arbitrary stationary spacetime (irrespective of whether it is axisymmetric or not); it gives us the exact rate of the LT precession in such a spacetime. For instance, a Newman-Unti-Tamburino (NUT) spacetime with vanishing ADM mass is known to be spherically symmetric, but still has an angular momentum (dual or 'magnetic' mass [18]); we will use Eq. (2.30) to compute

the LT precession frequency in this case as well (see subsection 4.4.1). This result is rather general, because, there is only one constraint on the spacetime : that it must be stationary, which is the only necessary condition for the LT precession. The utility of this equation is that; if any metric ($g_{\mu\nu}$) contains all 10 (4×4) elements non-vanishing, it can be used to calculate the LT precession in that spacetime. In this case, the precession rate depends only on non-zero $g_{0i}(i = 1, 2, 3)$ components, not on any other non-zero off-diagonal components of the metric. So, this equation also reveals that the LT precession rate is completely determined by the metric components $g_{0\mu}(\mu = 0, i)$, and is quite independent of the other components (in co-ordinate basis).

2.3 Lense-Thirring precession in Kerr spacetime

One can now use Eq. (2.30) to calculate the angular momentum of a test gyroscope in a Kerr spacetime to get the LT precession in a strong gravitational field. In Boyer-Lindquist coordinates, the Kerr metric is written as,

$$ds^2 = -\left(1 - \frac{2Mr}{\rho^2}\right) dt^2 - \frac{4Mar\sin^2\theta}{\rho^2} d\phi dt + \frac{\rho^2}{\Delta} dr^2 + \rho^2 d\theta^2 + \left(r^2 + a^2 + \frac{2Mra^2\sin^2\theta}{\rho^2}\right) \sin^2\theta d\phi^2 \ , \tag{2.31}$$

where, a is Kerr parameter, defined as $a = \frac{J}{M}$, the angular momentum per unit mass and

$$\rho^2 = r^2 + a^2\cos^2\theta \ , \Delta = r^2 - 2Mr + a^2 \ . \tag{2.32}$$

For the Kerr spacetime, the only nonvanishing $g_{0i} = g_{0\phi}$, $i = \phi$ and $j, l = r, \theta$; substituting these in Eq. (2.30), the precession frequency vector is given by

$$\Omega_{LT} = \frac{1}{2\sqrt{-g}} \left[\left(g_{0\phi,r} - \frac{g_{0\phi}}{g_{00}} g_{00,r} \right) \partial_\theta - \left(g_{0\phi,\theta} - \frac{g_{0\phi}}{g_{00}} g_{00,\theta} \right) \partial_r \right] \ , \tag{2.33}$$

where, the various metric components can be read off from Eq. (2.31). Likewise,

$$\sqrt{-g} = \rho^2 \sin\theta \ . \tag{2.34}$$

In order to make numerical predictions for the LT precession frequency in a strong gravity domain, we need to transform the precession frequency formula from the coordinate basis to the orthonormal 'Copernican' basis: first note that

$$\Omega_{LT} = \Omega^\theta \partial_\theta + \Omega^r \partial_r, \tag{2.35}$$

$$\Omega^2_{LT} = g_{rr}(\Omega^r)^2 + g_{\theta\theta}(\Omega^\theta)^2 \ . \tag{2.36}$$

Next, in the orthonormal 'Copernican' basis at rest in the rotating spacetime, the tetrad vector $e_0 = u$ is basically the tangent vector along the integral curve of the timelike Killing vector K. In this basis, with our choice of polar coordinates, Ω_{LT} can be written as

$$\vec{\Omega}_{LT} = \sqrt{g_{rr}}\Omega^r \hat{r} + \sqrt{g_{\theta\theta}}\Omega^\theta \hat{\theta} \ , \tag{2.37}$$

where, $\hat{r}$ is the unit vector along the direction r and $\hat{\theta}$ is the unit vector along the direction θ. For the Kerr metric,

$$\Omega^\theta = -J \sin\theta \frac{(\rho^2 - 2r^2)}{\rho^4(\rho^2 - 2Mr)} \ , \tag{2.38}$$

$$\Omega^r = 2J \cos\theta \frac{r\Delta}{\rho^4(\rho^2 - 2Mr)} \ . \tag{2.39}$$

Substituting the values of Ω^r and Ω^θ in Eq. (2.37), we get the following expression of LT precession rate in Kerr spacetime

$$\vec{\Omega}_{LT} = 2aM \cos\theta \frac{r\sqrt{\Delta}}{\rho^3(\rho^2 - 2Mr)}\hat{r} - aM \sin\theta \frac{\rho^2 - 2r^2}{\rho^3(\rho^2 - 2Mr)}\hat{\theta} \ . \tag{2.40}$$

The magnitude of this vector is

$$\Omega_{LT}(r,\theta) = \frac{aM}{\rho^3(\rho^2-2Mr)}\left[4\Delta r^2\cos^2\theta + (\rho^2-2r^2)^2\sin^2\theta\right]^{\frac{1}{2}} \ . \tag{2.41}$$

This is the LT precession rate where no weak gravity approximation has been made. It should therefore be applicable to any rotating black hole but it is not applicable in the case of pulsars. This issue has been addressed at the end of this chapter.
In the next two subsections, we discuss the weak field limit of the above Eq. (2.40) and give the preliminary comparison between the strong and weak field LT precession rates with the observational data.

2.3.1 Weak field limit

For large distances, the Kerr metric is approximated as a Schwarzschild metric with the cross term ($g_{\phi t}d\phi dt$), that is

$$ds^2 = ds^2_{Sch} - \frac{4Ma\sin^2\theta}{r}d\phi dt \ , \tag{2.42}$$

and it has been shown that [3]

$$\vec{\Omega}_{LT} = \frac{1}{r^3}[3(\vec{J}.\hat{r})\hat{r} - \vec{J}] \ , \tag{2.43}$$

where, $J = aM$ is the angular momentum of the rotating spacetime. For a rotating compact object J could be determined by $J \simeq I\omega \simeq MR^2\omega$ (following Eq. (14.23) of Ref. [3] and for perfect formulation of Moment of inertia I, see Ref. [19]).

For large distances and in weak gravitational fields (where we can take $r > M$ and

$r > a$), the second term of Eq. (2.40) reduces to

$$\begin{aligned}\sqrt{g_{\theta\theta}}\Omega^{\theta}\hat{r} &= -\frac{J\sin\theta}{r^3(1+\frac{a^2}{r^2}\cos^2\theta)^{\frac{3}{2}}}\frac{(-1+\frac{a^2}{r^2}\cos^2\theta)\hat{r}}{(1+\frac{a^2}{r^2}\cos^2\theta-\frac{2M}{r})} \\ &\simeq \frac{J\sin\theta}{r^3}\hat{r}\ . \end{aligned} \tag{2.44}$$

Similarly, from the first term of Eq. (2.40) one obtains the following,

$$\begin{aligned}\sqrt{g_{rr}}\Omega^{r}\hat{r} &= \frac{2J\cos\theta.r^2\sqrt{1+\frac{a^2}{r^2}-\frac{2M}{r}}}{r^5(1+\frac{a^2}{r^2}\cos^2\theta)^{\frac{3}{2}}\big(1+\frac{a^2}{r^2}\cos^2\theta-\frac{2M}{r}\big)}\hat{\theta} \\ &\simeq \frac{2J\cos\theta}{r^3}\hat{\theta}\ . \end{aligned} \tag{2.45}$$

It follows that

$$\vec{\Omega}_{LT}(r,\theta) = \frac{J}{r^3}\left[2\cos\theta\hat{r}+\sin\theta\hat{\theta}\right]\ , \tag{2.46}$$

where, θ is the colatitude. The resemblance of this equation with Eq. (1.23) is unmistakeable.

The LT precession for a general stationary metric in the weak field limit may also be derived from Eq. (2.30). In this approximation,

$$g_{00} \simeq -1, g_{ij} = \delta_{ij}, \frac{g_{0l}}{g_{00}} << 1\ .$$

Under these conditions Eq. (2.30) reduces to,

$$\Omega \simeq -\frac{1}{2}\epsilon_{ijl}g_{0i,j}\partial_l\ . \tag{2.47}$$

As $e_l \simeq \partial_l$, a test gyroscope precesses in such a weak gravitational field with an angular velocity

$$\vec{\Omega} \simeq -\frac{1}{2}\vec{\nabla}\times\vec{g}\ , \tag{2.48}$$

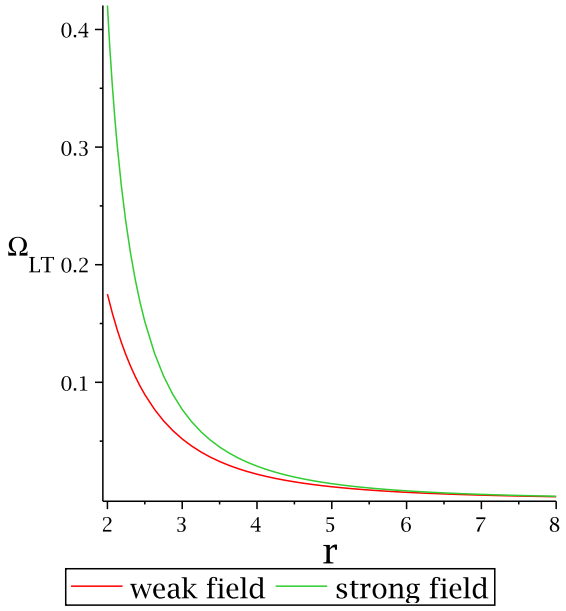

Figure 2.2: *Plot of* Ω_{LT} *(in* m^{-1}*) vs* r *(in* m*) at* $\theta = 0$ *for* $a = 0.7$ m *&* $M = 1$ m *[28].*

where, $\vec{g} \equiv (g_{01}, g_{02}, g_{03})$. Here, 1,2,3 indicate the space components in that spacetime.

We can visualize the difference between strong and weak gravity LT precession through a graphical representation. In Fig. (2.2), we draw two graphs, the red straight line is for $\Omega_{weakLT} = \frac{2aM}{r^3}$ and the green curve is for $\Omega_{strongLT} = \frac{2aMr}{(r^2+a^2)^{\frac{3}{2}}\sqrt{r^2-2Mr+a^2}}$ at $\theta = 0$. We see that $\Omega_{strongLT}$ is much much greater than Ω_{weakLT} for small r, i.e., near the compact body. As r increases, the red and the green lines overlap with each other, i.e., the linear approximation (weak gravity) emerges as a reasonable approximation.

2.3.2 Preliminary comparison with observational data

Let us take, as an example for the LT precession in strong gravitational field, the case of the Hulse-Taylor binary pulsar (also called PSR B1913+16) in the constellation of Aquila, located roughly at 21,000 light-years from the earth. Its mass, radius and rotational time

Massive objects	$\Omega_{strongLT}(\mathrm{s}^{-1})$	$\Omega_{weakLT}(\mathrm{s}^{-1})$
Earth	4.02×10^{-14}	4.02×10^{-14}
Sun	4.56×10^{-12}	4.56×10^{-12}
PSR B1257+12	238	178
PSR B1913+16	24	18
PSR J1614-2230	712	463
PSR J1748-2021B	274	121

Table 2.1: Comparison between strong gravity and weak gravity LT precession (all these values are calculated at the pole ($\theta = 0$) and near the surface ($r \to R$) of that massive object).

period (T) are, respectively,

$$\begin{aligned} M &= 1.44 M_{\odot} = 2120.95 \text{ m} , \\ R &\approx 10 \text{ km(assuming)} , \\ T &= 59.03 \times 10^{-3} \text{ s} , \end{aligned} \tag{2.49}$$

respectively. Using these numerical values, we can easily calculate the angular velocity (ω) of the pulsar

$$\begin{aligned} \omega = \frac{2\pi}{59.03 \times 10^{-3}} &= 105.96 \text{ s}^{-1} \\ &= 3.53 \times 10^{-7} \text{ m}^{-1} , \end{aligned} \tag{2.50}$$

and Kerr parameter (taking moment of inertia $I \approx 0.4MR^2$)

$$a \approx 14.13 \text{ m} . \tag{2.51}$$

All numerical values are in gravitational units with $G = c = 1$.

Now, let us imagine a test gyroscope very close to the surface of the pulsar such that we may capture the strong gravitational effects for LT precession. So, we take $r \to R$.

Substituting the above values in Eq. (2.41) for $\theta = 0$ (which indicates that we are

measuring the LT precession at the pole of the pulsar), we get

$$\begin{aligned} \Omega_{strongLT} &= \frac{2JRc}{(R^2+a^2)^{\frac{3}{2}}\sqrt{R^2-2MR+a^2}} \\ &\approx 24 \text{ s}^{-1} , \end{aligned} \tag{2.52}$$

or,

$$\frac{\Omega_{strongLT}}{\omega} \approx 0.22 . \tag{2.53}$$

On the other hand, if we use our well known weak field approximation (Eq. (2.46)) for the LT precession rate, we get

$$\Omega_{weakLT} = \frac{2Jc}{R^3} \approx 18 \text{ s}^{-1} , \tag{2.54}$$

or,

$$\frac{\Omega_{weakLT}}{\omega} \approx 0.17 . \tag{2.55}$$

So, we can easily see that there is really a substantial (~ 30 %) difference between the *weak* and *strong* gravity LT precession rates in this case. But, the precession rate for a gyroscope or a satellite due to the rotation of the earth or the sun, the numerical results from the *weak* and *strong* gravity LT precession rate formulas appear to be the same. So, for the earth or the sun, it does not matter whether one takes the strong gravity Eq. (2.40) or the weak gravity LT Eq. (2.46).

In Table 2.1, we offer a comparative numerical study between calculated values of $\Omega_{strongLT}$ and Ω_{weakLT} for a few recently discovered pulsars, with those of the sun and the earth. The effect of strong gravity is as high as above 100 % in one particular example, and certainly above 30 % in general for all pulsars.

During the $\Omega_{strongLT}$ calculations, the backreaction effects of the binary companion of a particular pulsar can be usually neglected, because, the distance of this companion is $\sim$ 1 lt-sec(10^5 km) or more than that and Ω_{LT} is inversely proportional to ρ^3. The

strong gravity LT effect computed which we focus on, is significant near the surface of pulsars and near black hole event horizons. If the binary system under consideration has a non-compact companion of the pulsar which is reasonably distant, backreaction effects of this companion on the LT precession of test gyroscopes may be safely ignored.

We should be careful in pointing out, however, that the table of comparisons above is merely to convey the importance of strong gravity effects in the rate of dragging of inertial frames in the case of compact gravitating objects; the actual numbers may have errors, both theoretical and observational, which have not been fully analysed yet.

2.4 Summary

The analyses presented above has two important features : (a) the LT precision frequency of a gyroscope in a 'Copernican' frame within a Kerr spacetime is computed without any assumption on the angular momentum parameter or indeed the curvature of spacetime. The only comparable attempt in the literature is that in Ref. [16], which however is not the same computation as ours, and the result is not the same in terms of metric coefficients. (b) The result derived in Eq. (2.30) is in fact valid, not just for axisymmetric spacetimes, but also for general non-static stationary spacetimes, once again without any assumptions about the curvatures involved. This result, we believe is applicable to a very large class of strong gravity systems.

Majority of the textbook calculations of the LT precession rate focus on the weak-field approximation. Only in the book of Misner-Thorne-Wheeler [16], the orbital angular velocity for *locally non-rotating* observers in a Kerr-Newman spacetime is given by Eq. (33.24) as an exercise. This formula does not appear to be restricted to the weak-field approximation. However, from an astrophysical standpoint, it is not clear that the computed angular frequency corresponds to what might be measured as the LT precession in a strong gravity situation, because it has been derived in a locally non-rotating frame

which the authors amply clarify is *not* a *Copernican frame*. A naive limiting procedure does not appear to reduce this frequency to the standard weak-field result of Eq. (2.43) in 'Copernican' frames quoted in most other textbooks for the LT precession rate in a weak gravitational field.

The substantial difference between the LT precession frequency arising in strong gravity regime and the standard weak field precession rate for inertial frame dragging ought to provide a strong motivation for their measurement in space probes planned for the near future. The fascinating world of gravitational effects associated with strongly gravitating compact objects may provide the best yet dynamical observational signatures of general relativity.

We may reiterate that the preliminary numerical results on LT precession rates for various systems is intended to serve as motivation for prospective measurements in strong gravity situations, as also for further theoretical work towards understanding the emission mechanism of pulsars and x-ray emission from black holes and neutron stars. We expect nontrivial modifications to arise from incorporation of frame-dragging effects in the theoretical analyses of these phenomena. We hope to report on this in the near future.

There are issues related to the use of the Kerr metric for the external spacetime due to a rotating neutron star, as pointed out in Ref. [20,21]. We note that spacetime outside a rapidly rotating neutron star has been described in *section 3* of Ref. [22] in terms of a metric which differs from the Kerr metric and thus Eq. (2.41) should not be exactly applicable to the pulsars. The spacetime in the vicinity of a neutron star is described by a Kerr metric *only if* the angular velocity is 'small'; otherwise, the metric receives corrections from higher gravitational multipole moments [20]. However, there does not appear to be a consensus in the literature as to how small the angular speed must be at the neutron star surface, for the use of the Kerr metric as a reasonable description just outside the region. According to Ref. [21], the product $\omega \cdot R << c$ where, R is the radial size of the neutron star. Now, in the case of the millisecond pulsars PSR B1257+12,

PSR B1913+16, PSR J1614-2230, PSR J1748-2021B this product is still $< c$; so the use of the Kerr metric is perhaps not totally unjustified, although perhaps not adequately accurate for observational purposes. But then, we reiterate our disclaimer above that the numerical results in the table above are not meant to be taken as 'predictions' for upcoming measurements. Rather, they are given merely to underline the importance of the exact formula for the strong gravity regime, as opposed to the oft-used weak-field-approximation. Generally, the LT precession rate could deviate by $\sim 40\%$ from its original value at the strong gravity regime if we use the Kerr metric instead of the general metrics which are basically used to describe the exterior spacetimes of the pulsars. This issue has also been addressed in Ref. [23] that due to the higher order in angular momentum, the exterior spacetimes of the rotating neutron stars deviate from the Kerr geometry. Clearly, results discussed in Table. 2.1 must be embellished by a more precise and careful numerical analysis to reach observational viability.

In the next chapter (Chapter 3), we discuss the most general axisymmetric and stationary solution of Einstein's equation given by the Plebański-Demiański metric for an understanding of the LT precession in this spacetime [24].

Chapter 3

Lense-Thirring precession in Plebański-Demiański spacetime

3.1 Introduction

The axisymmetric vacuum solutions of the Einstein equations are used to describe the various characteristics of different spacetimes. The most important and physical spacetime is the Kerr spacetime [25], describes the rotating black hole which possesses a finite angular momentum J. The Kerr spacetime with a finite charge Q is expressed as Kerr-Newman black hole. Actually the inclusion of Cosmological constant in these spacetimes may arise some complexity in calculations. Without this particular constant the spacetimes possess two horizons, such as, event horizon and Cauchy horizon. But, the presence of the cosmological constant leads to an extra horizon - the cosmological horizon. All these spacetimes can be taken as the special cases of the most general axisymmetric spacetime of Petrov type D which was first discovered by Plebański and Demiański (PD) [26]. This spacetime contains the seven parameters - acceleration, mass (M), Kerr parameter (a, angular momentum per unit mass), electric charge (Q_c), magnetic charge (Q_m), NUT parameter (n) and Cosmological constant. At present, this is the most general axially symmetric

vacuum solution of Einstein field equation. This solution is important at the present time because it is now being used in many ways. People working in semi-classical quantum gravity have used this type of metric to investigate the pair production of black holes in cosmological backgrounds [27]. Some people are working to extend this type of solution to higher dimensions. But this spacetime is still not well understood at the classical level of general relativity. In particular, the physical significance of the parameters employed in the original forms are only properly identified in the most simplified special cases and the most general PD metric covers all spacetimes which are well known to us till now.

It is already well known that any axisymmetric and stationary spacetime with angular momentum (rotation) are known to exhibit an effect called the LT precession whereby locally inertial frames are dragged along the rotating spacetime, making any test gyroscope in such spacetimes *precess* with a certain frequency called the LT precession frequency [1]. More generally, we can say that the frame-dragging effect is the property of all stationary spacetimes which may or may not be axisymmetric [14]. We have also discussed this special feature in detail in our paper [28]. In that paper, we showed that only the Kerr parameter was not responsible for the LT precession, NUT parameter is equally important for the frame-dragging effect [28]. It was shown by Hackmann and Lämmerzahl that the LT precession vanishes (Eq. (45) of Ref. [7]) in PD spacetimes (with vanishing acceleration of the gravitating source), if the Kerr parameter $a = 0$. But, it is not the actual case. As we showed in our paper [28], the same thing also happened in the PD spacetimes with *zero angular momentum* ($J = a = 0$), the LT precession did not vanish due to the presence of NUT charge n (*angular momentum monopole* [18]).

It may be noted that our LT precession formulas for different spacetimes are valid in strong as well as weak gravitational field as we do not make any approximation to derive the LT precession rate. We also note that the earth's gravitational field may be described by Kerr geometry which is physically reliable. But the most general axisymmetric PD spacetime is not physically reliable till now because the existence of some parameters

(e.g., NUT parameter (n), Q_c, Q_m) of PD spacetimes are not yet proved.

In this chapter, our aim is to derive the exact LT precession rates in non-extremal and extremal Plebański-Demiański spacetimes without invoking the weak field approximation. So, we organize this chapter as follows. In section 3.2, we review the general LT precession formula in stationary and axisymmetric spacetimes and derive the exact LT precession rate in Plebański-Demiański(PD) spacetimes with vanishing acceleration of the gravitating source and discuss the exact LT precession rates in some other stationary and axisymmetric spacetimes as the special cases of PD spacetimes. If the Kerr parameter vanishes in PD spacetimes, the frame-dragging effect does not vanish due to the existence of NUT charge. It is shown in subsection 3.2.3, as a special case of the LT precession in PD spacetimes. In section 3.3, we derive the more general extremal condition for PD spacetimes and discuss about the exact LT precession rates in PD spacetimes and also other various extremal axisymmetric spacetimes as the special cases of PD spacetimes. We summarize this chapter in section 3.4.

3.2 Non-extremal case

3.2.1 Plebański-Demiański (PD) spacetimes

The PD spacetime is the most general axially symmetric vacuum solution of Einstein equation, at present. The line element of six parameters PD spacetimes taking vanishing acceleration can be written as (taking, $G = c = 1$) [7],

$$ds^2 = -\frac{\Delta}{p^2}(dt - Ad\phi)^2 + \frac{p^2}{\Delta}dr^2 + \frac{p^2}{\Xi}d\theta^2 + \frac{\Xi}{p^2}\sin^2\theta(adt - Bd\phi)^2 \ , \tag{3.1}$$

where,

$$
\begin{aligned}
p^2 &= r^2 + (n - a\cos\theta)^2 \ , \\
A &= a\sin^2\theta + 2n\cos\theta \ , B = r^2 + a^2 + n^2 \ , \\
\Delta &= (r^2 + a^2 - n^2)\left(1 - \frac{1}{\ell^2}(r^2 + 3n^2)\right) - 2Mr + Q_c^2 + Q_m^2 - \frac{4n^2r^2}{\ell^2} \ , \\
\Xi &= 1 + \frac{a^2\cos^2\theta}{\ell^2} - \frac{4an\cos\theta}{\ell^2} \ .
\end{aligned} \tag{3.2}
$$

$\frac{1}{\ell^2} = \lambda$ denoting the Cosmological constant divided by three, represents the Plebański-Demiański-de-Sitter (PD-dS) spacetimes and if ℓ^2 is replaced by $-\ell^2$, it represents the PD-AdS spacetimes. So, our metric $g_{\mu\nu}$ is thus following

$$
g_{\mu\nu} = \begin{pmatrix}
-\frac{1}{p^2}(\Delta - a^2\Xi\sin^2\theta) & 0 & 0 & \frac{1}{p^2}(A\Delta - aB\Xi\sin^2\theta) \\
0 & \frac{p^2}{\Delta} & 0 & 0 \\
0 & 0 & \frac{p^2}{\Xi} & 0 \\
\frac{1}{p^2}(A\Delta - aB\Xi\sin^2\theta) & 0 & 0 & \frac{1}{p^2}(-A^2\Delta + B^2\Xi\sin^2\theta)
\end{pmatrix} . \tag{3.3}
$$

In the Chapter 2, we have already discussed about the exact expression of the LT precession rate. This is applicable for any non-accelerating stationary spacetimes. In this chapter, we are going to derive the exact LT precession rate for non-accelerating PD spacetimes and also some others axially symmetric spacetimes like this. The expression for the LT precession rate in non-accelerating, stationary and axisymmetric spacetime can be written as,

$$
\Omega_{LT} = \frac{1}{2\sqrt{-g}}\left[\left(g_{0\phi,r} - \frac{g_{0\phi}}{g_{00}}g_{00,r}\right)\partial_\theta - \left(g_{0\phi,\theta} - \frac{g_{0\phi}}{g_{00}}g_{00,\theta}\right)\partial_r\right] \ , \tag{3.4}
$$

which is same as Eq. (35) of Ref. [28]. The various metric components can be read off

from the above metric (3.3). Likewise,

$$\sqrt{-g} = p^2 \sin\theta. \tag{3.5}$$

Substituting the metric components into Eq. (3.4) we can easily get the LT precession rate in PD spacetimes. But, there is a problem in that formulation as the precession formula is in co-ordinate basis. So, we should transform the precession frequency formula from the coordinate basis to the orthonormal 'Copernican' basis: first we note that

$$\Omega_{LT} = \Omega^\theta \partial_\theta + \Omega^r \partial_r \ , \tag{3.6}$$

$$\Omega^2_{LT} = g_{rr}(\Omega^r)^2 + g_{\theta\theta}(\Omega^\theta)^2 \ . \tag{3.7}$$

Next, in the orthonormal 'Copernican' basis at rest in the rotating spacetime, with our choice of polar coordinates, Ω_{LT} can be written as

$$\vec{\Omega}_{LT} = \sqrt{g_{rr}}\Omega^r \hat{r} + \sqrt{g_{\theta\theta}}\Omega^\theta \hat{\theta} \ , \tag{3.8}$$

where, $\hat{\theta}$ is the unit vector along the direction θ. Our final result of the LT precession in the non-accelerating PD spacetime is then,

$$\begin{aligned} \vec{\Omega}^{PD}_{LT} &= \frac{\sqrt{\Delta}}{p}\left[\frac{a(\Xi\cos\theta + (2n - a\cos\theta)\frac{a}{\ell^2}\sin^2\theta)}{\Delta - a^2\Xi\sin^2\theta} - \frac{a\cos\theta - n}{p^2}\right]\hat{r} \\ &+ \frac{\sqrt{\Xi}}{p}a\sin\theta\left[\frac{r - M - \frac{r}{\ell^2}(a^2 + 2r^2 + 6n^2)}{\Delta - a^2\Xi\sin^2\theta} - \frac{r}{p^2}\right]\hat{\theta} \ . \end{aligned} \tag{3.9}$$

Now, from the above expression we can easily derive the LT precession rates for various axisymmetric stationary spacetimes as the special cases of the PD spacetime.

3.2.2 Special cases

(a) Schwarzschild and Schwarzschild-de-Sitter spacetimes : As the Schwarzschild

and Schwarzschild-de-Sitter spacetimes both are static and $a = \lambda = Q_c = Q_m = n = 0$, the inertial frames are not dragged along it. So, we can't see any LT effect in these spacetimes. This is very well known feature of static spacetime.

(b) Kerr spacetimes : The LT precession rate for non-extremal Kerr spacetimes is already discussed in Chapter 2. Setting $\lambda = Q_c = Q_m = n = 0$ in Eq. (3.9) we can recover our result (Eq. (42) of Ref. [28]) which is applicable for Kerr spacetimes.

(c) Kerr-Newman spacetime : Rotating black hole spacetimes with electric charge Q_c and magnetic charge Q_m is described by Kerr-Newman metric, which is quite important in General Relativity. Setting $\lambda = n = 0$ in Eq. (3.9), we can easily get the LT precession in Kerr-Newman spacetime. It has the following form (taking $Q_c^2 + Q_m^2 = Q^2$),

$$\vec{\Omega}_{LT}^{KN} = \frac{a}{\rho^3(\rho^2 - 2Mr + Q^2)} \left[\sqrt{\Delta}(2Mr - Q^2)\cos\theta\hat{r} + (M(2r^2 - \rho^2) + rQ^2)\sin\theta\hat{\theta}\right] . \tag{3.10}$$

In the Kerr-Newman spacetime,

$$\Delta = r^2 - 2Mr + a^2 + Q^2 \text{ , and } \rho^2 = r^2 + a^2\cos^2\theta . \tag{3.11}$$

From the expression (3.10) of the LT precession in Kerr-Newman spacetime we can see that at the polar plane, **the LT precession vanishes for the orbit $r = \frac{Q^2}{2M}$, though the spacetime is rotating** ($a \neq 0$). So, if a gyroscope rotates in the polar orbit of radius $r = \frac{Q^2}{2M}$ in this spacetime, the gyroscope does not experience any frame-dragging effect. So, if any experiment is performed in future by which we can't see any LT precession in that spacetime, it may happen that the specified spacetime is the Kerr-Newman black

hole and the gyroscope is rotating at the polar orbit whose radius is $r = \frac{Q^2}{2M}$. This is a very interesting feature of the Kerr-Newman geometry. Though the spacetime is rotating with the angular momentum J, the nearby frames are not dragged along it. Except this particular orbit, the LT precession is found everywhere in this spacetimes.

(d) Kerr-de-Sitter spacetimes : The Kerr-de-Sitter spacetime is more realistic, when we do not neglect the Cosmological constant parameter (though its value is very small, it may be very useful in some cases, where we need very precise calculation). Setting $n = Q_c = Q_m = 0$, we get the following expression for the Kerr-de-Sitter spacetime

$$\begin{aligned}\vec{\Omega}_{LT}^{KdS} &= \frac{a}{\rho^3(\rho^2 - 2Mr - \frac{1}{\ell^2}(a^4 + a^2r^2 - a^4\sin^2\theta\cos^2\theta))}\left[\sqrt{\Delta}\left(2Mr + \frac{1}{\ell^2}\rho^4\right)\cos\theta\hat{r}\right. \\ &\left. +\sqrt{\Xi}\left[M(2r^2 - \rho^2) + \frac{r}{\ell^2}\{a^4 + a^2r^2 - a^4\sin^2\theta\cos^2\theta - \rho^2(a^2 + 2r^2)\}\right]\sin\theta\hat{\theta}\right] ,\end{aligned} \tag{3.12}$$

where,

$$\Delta = (r^2 + a^2)\left(1 - \frac{r^2}{\ell^2}\right) - 2Mr \text{ , and } \Xi = 1 + \frac{a^2}{\ell^2}\cos^2\theta \ . \tag{3.13}$$

3.2.3 Non-vanishing Lense-Thirring precession in 'zero angular momentum' Plebański-Demiański spacetimes

This subsection can be regarded as a special case of non-accelerating Plebański-Demiański spacetime in where we take that PD spacetime is not rotating, we mean the Kerr parameter $a = 0$. In a very recent paper, Hackmann and Lämmerzahl showed that the LT effect vanished (Eq. (45) of Ref. [7]) due to the vanishing Kerr parameter. But, we can find easily from the Eq. (3.9) that if a vanishes in PD spacetime, the LT precession rate will

be

$$\vec{\Omega}^{PD}_{LT}|_{a=0} = \frac{n\sqrt{\Delta|_{a=0}}}{p^3}\hat{r} \ , \tag{3.14}$$

where,

$$\begin{aligned} \Delta|_{a=0} = (r^2 - n^2)\left(1 - \frac{1}{\ell^2}(r^2 + 3n^2)\right) \ &- \ 2Mr + Q_c^2 + Q_m^2 - \frac{4n^2r^2}{\ell^2} \ , \\ \text{and,} \quad p^2 = r^2 \ &+ \ n^2 \ . \end{aligned} \tag{3.15}$$

So, it is evident that the LT precession does not vanish when the Kerr parameter is zero. The above expression reveals that NUT charge n is responsible for the LT precession in 'zero angular momentum' PD spacetimes. Here, M represents the "gravitoelectric mass" or 'mass' and n represents the "gravitomagnetic mass" or 'dual' (or 'magnetic') mass [29] of this spacetime. It is obvious that the spacetime is not invariant under time reversal $t \to -t$, signifying that it must have a sort of 'rotational sense' which is analogous to a magnetic monopole in electrodynamics. One is thus led to the conclusion that the source of the nonvanishing LT precession is this "rotational sense" arising from a nonvanishing NUT charge. Without the NUT charge, the spacetime is clearly hypersurface orthogonal and frame-dragging effects vanish, as already mentioned in detail in our paper (section 3 of Ref. [28]). This *'dual' mass* has been investigated in details in Ref. [30, 31] and it is also referred as an *'angular momentum monopole* [18] in the Taub-NUT spacetime. This implies that the inertial frame dragging seen here in such a spacetime can be identified as a *gravitomagnetic* effect.

In Ref. [7] and Ref. [32], the authors investigated the timelike geodesic equations in the PD spacetime and Taub-NUT spacetime, respectively. The *orbital plane precession frequencies* $(\Omega_\phi - \Omega_\theta)$ were computed, following the earlier works of Ref. [33] and Ref. [34],

and the vanishing result ensued. Both of these results were then interpreted as the signature for the null LT precession in the 'zero angular momentum' PD spacetime as well as in the Taub-NUT spacetime.

We would like to say that what we have focused on in this thesis is quite different from the 'orbital plane precession' considered in Ref. [7] and Ref. [32]. Using a 'Copernican' frame, we calculate the precession of a gyroscope which is moving in an arbitrary integral curve (not necessarily geodesic). Within this frame, an untorqued gyro in a stationary but not static spacetime held fixed by a support force applied to its center of mass, undergoes the LT precession. Since the Copernican frame does not rotate (by construction) relative to the inertial frames at asymptotic infinity ("fixed stars"), the observed precession rate in the Copernican frame also gives the precession rate of the gyro relative to the fixed stars. It is thus, more an intrinsic property of the classical *spin* of the spacetime (as an untorqued gyro must necessarily possess), in the sense of a dual mass, rather than an *orbital* plane precession effect for timelike geodesics in a 'zero angular momentum' PD spacetime and a Taub-NUT spacetime. The dual mass is like the *Saha spin* of a magnetic monopole in electrodynamics [29], which may have a vanishing orbital angular momentum, but to which a spinning electron must respond so that its wavefunction acquires a geometric phase.

More specifically, in our case, we consider the gyroscope equation [14] in an arbitrary integral curve

$$\nabla_u S =< S, f > u \ , \tag{3.16}$$

where, $f = \nabla_u u$ is the acceleration, u is the four velocity and S indicates the spacelike classical spin four vector $S^\alpha = (0, \vec{S})$ of the gyroscope. For geodesics $f = 0 \Rightarrow \nabla_u S = 0$.

In contrast, Hackmann and Lämmerzahl [7] and Kagramanova et al. [32] considered the behaviour of massive test particles with *vanishing spin* $S = 0$ [35], and computed the orbital plane precession rate for such particles, obtaining a vanishing result. We are thus

led to conclude that because of two different situations are being considered, there is no inconsistency between our results and theirs.

It is important to mention here that the detailed analyses on the LT precession in Kerr-Taub-NUT [36], Taub-NUT [37,38] and massless Taub-NUT spacetimes will be discussed in the next chapter (Chapter 4).

3.3 Extremal case

3.3.1 Extremal Plebański-Demiański Spacetime

In this section, we would like to describe the LT precession in extremal Plebański-Demiański spacetime, whose non-extremal case is already described in the previous section. To get the extremal limit in PD spacetimes we should first determine the radius of the horizons r_h which can be determined by setting $\Delta|_{r=r_h} = 0$. We can make a comparison of coefficients in

$$\begin{aligned}\Delta &= -\frac{1}{\ell^2}r^4 + \left(1 - \frac{a^2}{\ell^2} - \frac{6n^2}{\ell^2}\right)r^2 - 2Mr + \left[(a^2 - n^2)\left(1 - \frac{3n^2}{\ell^2}\right) + Q_c^2 + Q_m^2\right] \\ &= -\frac{1}{\ell^2}[r^4 + (a^2 + 6n^2 - \ell^2)r^2 + 2M\ell^2 r + b] \\ &= -\frac{1}{\ell^2}\Pi_{i=1}^4(r - r_{hi}) \ , \end{aligned} \tag{3.17}$$

where,

$$b = (a^2 - n^2)(3n^2 - \ell^2) - \ell^2(Q_c^2 + Q_m^2) \ , \tag{3.18}$$

and r_{hi}(i = 1, 2, 3, 4) denotes the zeros of Δ. From this comparison we can conclude that for the PD-AdS (when λ is negative) black hole, there are two separated positive horizons at most, and Δ is positive outside the outer horizon of the PD black hole. In the same way, we can conclude for the PD-dS (when λ is positive) black hole that there are three separated positive horizons at most, and Δ is negative outside the outer horizon

of the black hole. When two horizons of the PD black hole coincide, the black hole is extremal [39].

If we consider the extremal PD black hole, we have to make a comparison of coefficients in

$$\begin{aligned} \Delta &= (r-x)^2(a_2 r^2 + a_1 r + a_0) \qquad (3.19) \\ &= -\frac{1}{\ell^2}[r^4 + (a^2 + 6n^2 - \ell^2)r^2 + 2Mr\ell^2 + b] \ , \end{aligned}$$

with a_0, a_1, a_2 being real [7]. From this comparison we can get the following for PD ("AdS") spacetime,

$$\frac{b_A}{x^2} - 3x^2 = a^2 + 6n^2 + \ell^2 \ , \qquad (3.20)$$

$$x^3 - \frac{b_A}{x} = -M\ell^2 \ , \qquad (3.21)$$

where, b_A represents the value of b at PD ("AdS") spacetimes.

$$b_A = (a^2 - n^2)(3n^2 + \ell^2) + \ell^2(Q_c^2 + Q_m^2) \ . \qquad (3.22)$$

Solving equation (3.20) for x, we get

$$x = \sqrt{\frac{1}{6}\left[-(\ell^2 + a^2 + 6n^2) + \sqrt{(\ell^2 + a^2 + 6n^2)^2 + 12b_A}\right]} \ . \qquad (3.23)$$

Similarly, we can obtain for PD("dS") black hole ,

$$\frac{b}{x^2} - 3x^2 = a^2 + 6n^2 - \ell^2 \ , \qquad (3.24)$$

$$x^3 - \frac{b}{x} = M\ell^2 \ . \qquad (3.25)$$

In these equation x is positive and related to the coincided horizon of the extremal

PD (for "dS") black hole.

Solving equation (3.24) for x, we get

$$x_+ = \sqrt{\frac{1}{6}\left[\ell^2 - a^2 - 6n^2 + \sqrt{(\ell^2 - a^2 - 6n^2)^2 + 12b}\right]}\,, \tag{3.26}$$

$$x_- = \sqrt{\frac{1}{6}\left[\ell^2 - a^2 - 6n^2 - \sqrt{(\ell^2 - a^2 - 6n^2)^2 + 12b}\right]}\,, \tag{3.27}$$

where, x_+ and x_- indicate the outer horizon and inner horizon, respectively. This can be seen by calculating

$$\frac{d^2\Delta}{dr^2}|_{r=x_+} = -\frac{2}{\ell^2}\sqrt{(\ell^2 - a^2 - 6n^2)^2 + 12b}\,, \tag{3.28}$$

and

$$\frac{d^2\Delta}{dr^2}|_{r=x_-} = \frac{2}{\ell^2}\sqrt{(\ell^2 - a^2 - 6n^2)^2 + 12b}\,. \tag{3.29}$$

For the PD("dS") black hole, on the outer extremal horizon, $\frac{d\Delta}{dr} = 0$ and $\frac{d^2\Delta}{dr^2} < 0$ and on the inner extremal horizon $\frac{d^2\Delta}{dr^2} > 0$. Now, we can solve M and a from the two Eqs. (3.24) and (3.25).

$$M = \frac{x\left[x^4 + 2x^2(3n^2 - \ell^2) + (3n^2 - \ell^2)(7n^2 - \ell^2) + \ell^2(Q_c^2 + Q_m^2)\right]}{\ell^2(\ell^2 + x^2 - 3n^2)}\,, \tag{3.30}$$

$$a_e^2 = \frac{3x^4 + (6n^2 - \ell^2)x^2 + n^2(3n^2 - \ell^2) + \ell^2(Q_c^2 + Q_m^2)}{(3n^2 - \ell^2 - x^2)}\,. \tag{3.31}$$

From the above values of a_e^2 and M, we get

$$a_e^2 = -M\ell^2\frac{[3x^4 + (6n^2 - \ell^2)x^2 + n^2(3n^2 - \ell^2) + \ell^2(Q_c^2 + Q_m^2)]}{x\left[x^4 + 2x^2(3n^2 - \ell^2) + (3n^2 - \ell^2)(7n^2 - \ell^2) + \ell^2(Q_c^2 + Q_m^2)\right]}\,. \tag{3.32}$$

The ranges of x and a_e are determined from the following expressions

$$x^2 < \left(\frac{\ell^2+\ell\sqrt{\ell^2-12Q^2}}{6}-n^2\right) , \tag{3.33}$$

$$0<a_e^2 < \left[(7\ell^2-24n^2)-\sqrt{(7\ell^2-24n^2)^2-(\ell^4-12\ell^2(Q_c^2+Q_m^2))}\right] . \tag{3.34}$$

Due to the presence of Cosmological constant, there exist four roots of x in Eq. (3.31). When Cosmological constant $\frac{1}{l^2}\to 0$, Eq. (3.30) and Eq. (3.31) reduce to

$$x = M , \tag{3.35}$$

and,

$$a_e^2 = x^2+n^2-Q_c^2-Q_m^2 , \tag{3.36}$$

or,

$$a_e^2 = M^2+n^2-Q_c^2-Q_m^2 , \tag{3.37}$$

respectively.

Now, the line element of extremal PD spacetimes can be written as,

$$ds^2 = -\frac{\Delta_e}{p_e^2}(dt-A_e d\phi)^2+\frac{p_e^2}{\Delta_e}dr^2+\frac{p_e^2}{\Xi_e}d\theta^2+\frac{\Xi_e}{p_e^2}\sin^2\theta(a_e dt-B_e d\phi)^2 , \tag{3.38}$$

and, the final LT precession rate in extremal PD spacetime is,

$$\begin{aligned}\vec{\Omega}_{LT}^{ePD} &= \frac{\sqrt{\Delta_e}}{p_e}\left[\frac{a_e(\Xi_e\cos\theta+(2n-a_e\cos\theta)\frac{a_e}{\ell^2}\sin^2\theta)}{\Delta_e-a_e^2\Xi_e\sin^2\theta}-\frac{a_e\cos\theta-n}{p_e^2}\right]\hat{r}\\ &+ \frac{\sqrt{\Xi_e}}{p_e}a_e\sin\theta\left[\frac{r-M-\frac{r}{\ell^2}(a_e^2+2r^2+6n^2)}{\Delta_e-a_e^2\Xi_e\sin^2\theta}-\frac{r}{p_e^2}\right]\hat{\theta} ,\end{aligned} \tag{3.39}$$

where,

$$\Delta_e = -\frac{1}{\ell^2}(r-x)^2\left(r^2+2rx+\frac{b}{x^2}\right)\ , \Xi_e = 1+\frac{a_e^2}{\ell^2}\cos^2\theta - \frac{4a_e n}{\ell^2}\cos\theta\ ,$$
$$p_e = r^2+(n-a_e\cos\theta)^2\ ,\quad A_e = a_e\sin^2\theta+2n\cos\theta\ ,\quad B_e = r^2+a_e^2+n^2\ , \tag{3.40}$$

and, the value of a_e is determined from the Eq. (3.31) and the range of x and a_e ('e' stands for the *extremal* case) are determined from the Eqs. (3.33) and (3.34), respectively. It could be noted that, for the extremal PD("dS"), spacetimes, *there are upper limiting values for angular momentum and extremal horizon of the black hole.* Substituting all the above mentioned values and ranges in Eq. (3.39), we get the exact LT precession rate in extremal PD spacetimes.

3.3.2 Extremal Kerr Spacetime

Substituting $a_e = M$ in Eq. (42) of Ref. [28] or substituting $a = M$ and $\lambda = Q_c = Q_m = n = 0$ in Eq. (3.39) we can easily get the LT precession rate in the extremal Kerr spacetime,

$$\vec{\Omega}_{LT}^{eK} = \frac{M^2[2r(r-M)\cos\theta\hat{r}+(r^2-M^2\cos^2\theta)\sin\theta\hat{\theta}]}{(r^2+M^2\cos^2\theta)^{\frac{3}{2}}(r^2-2Mr+M^2\cos^2\theta)}\ . \tag{3.41}$$

We consider two cases here.

Case I: On the polar region i.e. $\theta = 0$, the Ω_{LT} becomes

$$\Omega_{LT}^{eK} = \frac{2M^2 r}{(r^2+M^2)^{3/2}(r-M)}\ . \tag{3.42}$$

Case II: On the equator i.e. $\theta = \pi/2$, the Ω_{LT} becomes

$$\Omega_{LT}^{eK} = \frac{M^2}{r^2(r-2M)}\ . \tag{3.43}$$

It could be easily seen that Ω_{LT} diverges at $r = M$. Since $r = M$ is the only direct ISCO in extremal Kerr geometry which coincides with the principal null geodesic generator of the horizon [40] and it is also the radius of the horizon which is a null surface. The general LT precession formula is derived only considering that the observer is rest in a timelike Killing vector field. We have not incorporated the LT effect for any null geodesic. So, our formula is valid only in timelike region.

3.3.3 Extremal Kerr-Newman Spacetime

Substituting $a^2 = M^2 - (Q_c^2 + Q_m^2) = M^2 - Q^2$ and $\lambda = n = 0$ in Eq. (3.10), we can obtain the following LT precession rate for the extremal Kerr-Newman black hole

$$\vec{\Omega}_{LT}^{eKN} = \frac{\sqrt{M^2 - Q^2}}{\rho^3(\rho^2 - 2Mr + Q^2)} \left[(r - M)(2Mr - Q^2)\cos\theta\hat{r} + (M(2r^2 - \rho^2) + rQ^2)\sin\theta\hat{\theta}\right] , \tag{3.44}$$

where,

$$\rho^2 = r^2 + (M^2 - Q^2)\cos^2\theta \ . \tag{3.45}$$

From the above expression (Eq. (3.44)), we can make a similar comment again, like the extremal Kerr-Newman black hole that the gyroscope which is rotating in a polar orbit of radius $r = \frac{Q^2}{2M}$, cannot experience any frame-dragging effect. Apparently, it seems that this argument is also true for the gyroscope which is rotating at $r = M$ orbit. But, this is not true. Because, this is the horizon of the extremal Kerr-Newman spacetime. So, $r = M$ is a null surface. The general formula which we have considered in this thesis, is valid only in timelike spacetimes (outside the horizon), but not in any null or spacelike regions.

3.3.4 Extremal Kerr-de Sitter Spacetime

The extremal Kerr-de Sitter spacetime is interesting because it involves the Cosmological constant. Setting $n = Q_c = Q_m = 0$ in Eq. (3.9), we can find the following expression of the LT precession at extremal Kerr-de Sitter spacetimes

$$\begin{aligned}\vec{\Omega}_{LT}^{eKdS} &= \frac{a_e}{\rho^3(\rho^2 - 2Mr - \frac{1}{\ell^2}(a_e^4 + a_e^2 r^2 - a_e^4 \sin^2\theta\cos^2\theta))}\left[\sqrt{\Delta_e}\left(2Mr + \frac{\rho^4}{\ell^2}\right)\cos\theta\hat{r}\right. \\ &\left. + \sqrt{\Xi_e}\left[M(2r^2 - \rho^2) + \frac{r}{\ell^2}\{a_e^4 + a_e^2 r^2 - a_e^4\sin^2\theta\cos^2\theta - \rho^2(a_e^2 + 2r^2)\}\right]\sin\theta\hat{\theta}\right] ,\end{aligned} \tag{3.46}$$

where,

$$\rho^2 = r^2 + a_e^2\cos^2\theta \ , \quad \Xi_e = 1 + \frac{a_e^2}{\ell^2}\cos^2\theta \ , \tag{3.47}$$

and

$$\Delta_e = -\frac{1}{\ell^2}(r - x)^2\left(r^2 + 2xr - \frac{a^2\ell^2}{x^2}\right) \ .$$

Using Eqs. (3.30) and (3.31), we obtain the value for a and M are

$$\begin{aligned} a_e^2 &= \frac{(\ell^2 - 3x^2)x^2}{(\ell^2 + x^2)} \ , \\ M &= \frac{x(\ell^2 - x^2)^2}{\ell^2(\ell^2 + x^2)} \ , \end{aligned} \tag{3.48}$$

where the horizons are at

$$\begin{aligned} x_+ &= \sqrt{\frac{1}{6}\left[\ell^2 - a^2 + \sqrt{(\ell^2 - a^2)^2 - 12a^2\ell^2}\right]} \ , \\ x_- &= \sqrt{\frac{1}{6}\left[\ell^2 - a^2 - \sqrt{(\ell^2 - a^2)^2 - 12a^2\ell^2}\right]} \ , \end{aligned} \tag{3.49}$$

where, x_+ and x_- indicate the outer horizon and inner horizon. The range of a_e^2 and x

are the following,

$$0 < a_e^2 < (7 - 4\sqrt{3})\ell^2 \quad \text{, and,} \quad x^2 < \ell^2/3 \ , \tag{3.50}$$

which is already discussed in Ref. [39]. Substituting all the above values in Eq. (3.46) and taking the ranges of a_e and x, we get the exact LT precession rate in extremal Kerr-dS spacetimes.

3.3.5 Extremal Kerr-Taub-NUT spacetime

To derive the extremal limit in the Kerr-Taub-NUT spacetime we set,

$$\Delta = r^2 - 2Mr + a^2 - n^2 = 0 \ . \tag{3.51}$$

Solving for r, we get two horizons which are located at $r_\pm = M \pm \sqrt{M^2 + n^2 - a^2}$. So, the extremal condition ($r_+ = r_-$) for Kerr-Taub-NUT spacetimes is $a_e^2 = M^2 + n^2$. If we set $Q_c = Q_m = \lambda = 0$ and $M^2 + n^2 = a_e^2$ in Eq. (3.9), we get the following exact LT precession rate at the extremal Kerr-Taub-NUT spacetime,

$$\begin{aligned} \vec{\Omega}_{LT}^{eKTN} &= \frac{(r-M)}{p}\left[\frac{\sqrt{M^2+n^2}\cos\theta}{p^2 - 2Mr - n^2} - \frac{\sqrt{M^2+n^2}\cos\theta - n}{p^2}\right]\hat{r} \\ &+ \frac{\sqrt{M^2+n^2}\sin\theta}{p}\left[\frac{r-M}{p^2-2Mr-n^2} - \frac{r}{p^2}\right]\hat{\theta} \ , \end{aligned} \tag{3.52}$$

where $p^2 = r^2 + (n \mp \sqrt{M^2+n^2}\cos\theta)^2$.

3.4 Summary

In this work we have explicitly derived the LT precession frequencies for extremal and non- extremal Plebański-Demiański(PD) spacetime. The PD family of solutions are the solutions of Einstein field equations which contain a number of well known black hole solu-

tions. These solutions are Schwarzschild, Schwarzschild-de-Sitter, Kerr, Kerr- ads, Kerr-Newman, Kerr-Taub-NUT etc. We observe that the LT precession frequency strongly depends upon the different parameters like mass M, spin a, Cosmological constant λ, NUT charge n, electric charge Q_c and magnetic charge Q_m. An interesting point is that the LT precession occurs solely due to the "dual mass". This "dual mass" is equivalent to angular momentum monopole (n) of NUT spacetime. For the completeness we have also deduced the LT precession for the extremal PD spacetime and also for others axisymmetric PD-like spacetimes. To get the LT precession rate in the extremal Kerr-Taub-NUT-de-Sitter spacetime, the basic procedure is same as PD spacetimes with the additional requirement $Q_c^2 + Q_m^2 = 0$ in Eqs. (3.30) and (3.31) and the range of $x^2 < (\frac{\ell^2}{3} - n^2)$ and a_e^2 has a range of $0 < a_e^2 < (7\ell^2 - 24n^2) - 4\sqrt{3(\ell^2 - 3n^2)(\ell^2 - 4n^2)}$. As there is no valid extremal condition at the NUT spacetime (with M or without M), we could not get any *real* LT precession rate due to the frame-dragging effect. Since, the direct ISCO coincides with the principal null geodesic generator [40] in extremal Kerr spacetimes and Kerr-Newman spacetimes, we are unable to discuss the LT precession at that particular geodesic. So this formula is not valid for the domain of $r \leq M$ for the extremal Kerr and Kerr-Newman spacetimes. Here, our formula is valid only for $r > M$. The general formula for the LT precession in stationary spacetime is valid only outside the horizon, as the observer is in timelike Killing vector field. The formula is not valid on the horizon and inside the horizon. We will discuss about this problem in near future.

Chapter 4

Anomalous Lense-Thirring precession in Kerr-Taub-NUT and Taub-NUT spacetimes

4.1 Introduction

We have already obtained the exact LT precession rate in Kerr spacetime in Chapter 2. Now, in this present chapter we are going to derive the exact LT precession rate in Kerr-Taub-NUT and Taub-NUT spacetimes. Kerr and KTN spacetimes both are the vacuum solutions of Einstein equation. Kerr spacetime has two parameters: mass and Kerr parameter (angular momentum per unit mass) but these are three parameters to describe the KTN spacetime. The parameters are: mass, Kerr parameter and NUT parameter. If the NUT parameter vanishes the KTN spacetime reduces to the Kerr spacetime and if the Kerr parameter vanishes the KTN spacetime reduces to the Taub-NUT spacetime. In the absence of the NUT parameter, the Taub-NUT spacetime reduces to pure Schwarzschild spacetime which is non-rotating. The Kerr spacetime is very well known to us and it is also physically reliable. We can easily describe the exterior geometry

of many rotating astrophysical objects by the Kerr spacetime. So, the Kerr spacetime is astrophysically relevant. But, the KTN spacetime is quite different than the Kerr geometry. As it holds an additional parameter (NUT), this spacetime is not physically relevant till now.

Lynden-Bell and Nouri-Zonoz [29] are the first to motivate investigation on the observational possibilities for NUT charges or (gravito)magnetic monopoles. They have claimed that the signatures of such spacetime might be found in the spectra of supernovae, quasars, or active galactic nuclei. It has been recently brought into focus by Kagramanova et. al [32] by a detail and careful analysis of geodesics in the Taub-NUT spacetime. A rigorous analysis in extremal and non-extremal KTN spacetimes for timelike and spacelike geodesics has already been done by myself [41]. It should be noted that the (gravito)magnetic monopole spacetime with angular momentum (basically the KTN spacetime) admits relativistic thin accretion disks of a black hole in a galaxy or quasars [42]. The accretion disks are basically formed just near the above mentioned astrophysical objects. In this sense the accretion phenomena takes place in a very strong gravity regime where the frame-dragging effect is expected to be very high. Thus the frame-dragging effect should have greater impact on accretion disk phenomena. This provides us a strong motivation for studying the LT precession or frame-dragging effect in the KTN spacetime in more detail because it will affect the accretion in such spacetimes from massive stars, and might offer novel observational prospects.

The Kerr-Taub-NUT (KTN) spacetime is a stationary and axisymmetric vacuum solution of Einstein equation. This spacetime consists of the Kerr and NUT parameters. The Kerr parameter is responsible for the rotation of the spacetime. In general sense the NUT charge should not be responsible explicitly for the rotation of the spacetime but implicitly this NUT charge can add a "rotational sense" in a non-rotating spacetime. The NUT charge is also called as 'dual mass' whose properties have been investigated in detail by Ramaswamy and Sen [30]. They also called the NUT parameter as the "angular

momentum monopole" [18] which is quite sound in this sense that it can give a "rotational sense" of the Taub-NUT spacetime even when the Kerr parameter vanishes (see 3.2.3). In this regards, though the Kerr parameter vanishes in the Kerr-Taub-NUT spacetime, the Taub-NUT spacetime retains the rotational sense due to the NUT parameter. Due to the presence of the NUT parameter the spacetime still remains stationary and violates the time reflection symmetry. Time reflection changes the direction of rotation and thus does not restore one to the original configuration [17]. Thus, the failure of the hypersurface orthogonality (it also means that the spacetime preserves the time translation symmetry but violates the time reflection symmetry) condition implies that the neighbouring orbits of ξ^a (the timelike Killing vector which must exist in any stationary spacetime) "twist" around each other. In the Kerr spacetime, the presence of the Kerr parameter makes the spacetime stationary instead of static (this has been clearly stated at section 2.1). Similarly, in the case of the Taub-NUT spacetime the NUT parameter compels the spacetime stationary instead of static. So, the Kerr and NUT parameters both are responsible to make the spacetime in rotation. Thus, it is needless to say that the KTN spacetime must be stationary.

Modak, Bandyopadhyay and myself [43] recently have discovered that frame-dragging curves are not smooth along the equator and its surroundings inside a rotating neutron star (it will be discussed in Chapter 5). Rather, the frame-dragging effect shows an interesting *anomaly* along the equator inside the pulsars. The frame-dragging rate is maximum at the center and decreases initially away from the center, tends to zero (not exactly zero but very small) before the surface of the neutron star, rises again and finally approaches small value on the surface as well as outside of the pulsars. We think that this may not be the only case where we see this *anomaly*. After that we start to hunt for this type of feature in other spacetimes which are the vacuum solutions of Einstein equation and we get the almost similar *anomaly* in the KTN spacetime (we note that there are many differences between the KTN spacetime and the spacetime of a rotating neutron star;

they are not same). Previously, the strong gravity LT precession in Plebański-Demiański (PD) spacetimes (most general axisymmetric and stationary spacetime till now) has been investigated by Pradhan and myself [24]. But our close observation says that due to the presence of the NUT charge this anomaly in the frame-dragging can also arise in the PD spacetime. In this present chapter, we are investigating the LT precession in the KTN (sections 4.2 & 4.3) and Taub-NUT (section 4.4) spacetimes as both of these spacetimes could be astrophysically relevant in future. In section 4.5, we would like to discuss the geodesics of the KTN metric on the equatorial plane of precisely extremal spacetime. In the two subsections 4.5.2 and 4.5.3, we derive the radii of ISCOs for the KTN spacetime and also for the Taub-NUT and massless Taub-NUT spacetimes as the special cases of KTN spacetimes for the nulllike and timelike geodesics, respectively. We conclude in section 4.6 with a summary.

4.2 Lense-Thirring precession in Kerr-Taub-NUT spacetime

The KTN spacetime is a geometrically stationary and axisymmetric vacuum solution of Einstein equation. This spacetime consists mainly three parameters: mass (M), angular momentum (J) per unit mass or Kerr parameter ($a = J/M$) and NUT charge (n) or dual mass. The metric of the KTN spacetime can be written as [44]

$$ds^2 = -\frac{\Delta}{p^2}(dt - Ad\phi)^2 + \frac{p^2}{\Delta}dr^2 + p^2 d\theta^2 + \frac{1}{p^2}\sin^2\theta(adt - Bd\phi)^2 \ , \tag{4.1}$$

with

$$\begin{aligned} \Delta &= r^2 - 2Mr + a^2 - n^2 \ , p^2 = r^2 + (n + a\cos\theta)^2 \ , \\ A &= a\sin^2\theta - 2n\cos\theta \ , B = r^2 + a^2 + n^2 \ . \end{aligned} \tag{4.2}$$

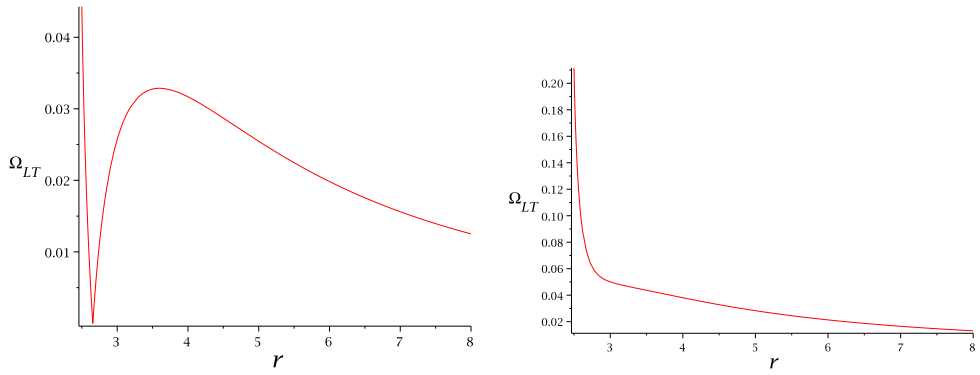

(a) along the pole (b) along the equator

Figure 4.1: *Plot of Ω_{LT} (in m^{-1}) vs r (in m) in the KTN spacetime for $a = 0.1\ m$, $n = 1\ m$ & $M = 1\ m$ [45].*

The exact LT precession rate in the Kerr-Taub-NUT spacetime is (Eq. (20) of [28])

$$\vec{\Omega}_{LT} = \frac{\sqrt{\Delta}}{p}\left[\frac{a\cos\theta}{\rho^2 - 2Mr - n^2} - \frac{a\cos\theta + n}{p^2}\right]\hat{r} + \frac{a\sin\theta}{p}\left[\frac{r - M}{\rho^2 - 2Mr - n^2} - \frac{r}{p^2}\right]\hat{\theta}\ , \quad (4.3)$$

where, $\rho^2 = r^2 + a^2\cos^2\theta$. The modulus of the above LT precession rate is

$$\begin{aligned}\Omega_{LT} = |\vec{\Omega}_{LT}| &= \frac{1}{p}\left[\Delta\left(\frac{a\cos\theta}{\rho^2 - 2Mr - n^2} - \frac{a\cos\theta + n}{p^2}\right)^2\right. \\ &+ \left. a^2\sin^2\theta\left(\frac{r - M}{\rho^2 - 2Mr - n^2} - \frac{r}{p^2}\right)^2\right]^{\frac{1}{2}}\ . \end{aligned} \quad (4.4)$$

It could be easily seen that the above equation is valid only in timelike region, we mean, outside the ergosphere which is located at $r_+ = M + \sqrt{M^2 + n^2 - a^2\cos^2\theta}$.

We plot r vs Ω_{LT} for $a < n$ (Fig. 4.1) and $a > n$ (Fig. 4.2). We see that the LT precession rate curve is smooth along the equator (panel (b)) but it is not smooth along the pole (panel (a)). The LT precession rate along the pole is very high just outside the ergosphere and falls sharply and becomes zero, rises again and finally approaches to a small value after crossing the very strong gravity regime. We will now discuss an interesting situation in which the Kerr parameter a is equal to the NUT parameter n.

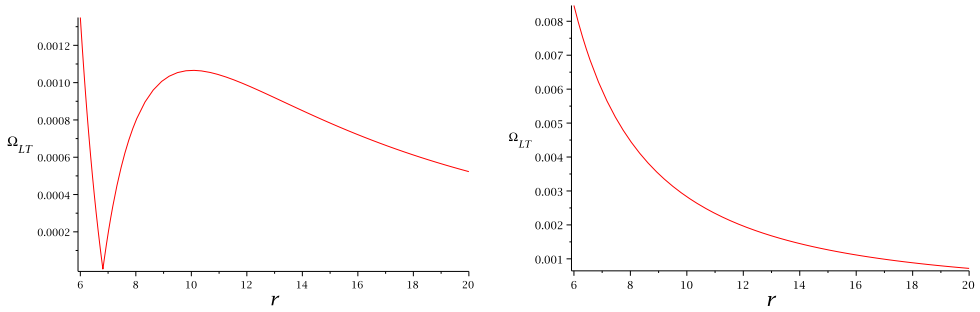

(a) along the pole (b) along the equator

Figure 4.2: *Plot of* Ω_{LT} *(in* m^{-1}*) vs* r *(in* m*) in the KTN spacetime for* $a = 0.7\ m$, $n = 0.3\ m$ *&* $M = 1\ m$ *[45].*

Special case: $a = n$

The horizons of the KTN spacetime are located at $r_{\pm} = M \pm \sqrt{M^2 + n^2 - a^2}$ [41]. One horizon is located at $r_+ > 0$ and another is located at $r_- < 0$ (if $n > a$) [32]. The Kerr parameter a takes any value but less than or equal to $\sqrt{M^2 + n^2}$ in case of the KTN spacetime whereas a takes its highest value as M in case of the Kerr spacetime. Without this restriction (if $a^2 > M^2 + n^2$) the both spacetimes lead to show the naked singularities. There are two special cases in KTN spacetimes for which a can take the value M only and for the second case a can take the value n. For the first case the angular momentum of the KTN spacetime would be $J = M^2$ which is similar to the case of extremal Kerr spacetime. In this case the horizons will be located at the distances $r_+ = M + n$ and $r_- = M - n$. If the mass of the spacetime is greater than the dual mass of the spacetime ($M > n$), the both horizons could be located at the positive distances ($r_{\pm} > 0$) but if the dual mass is greater than the mass of the spacetime ($M < n$) r_- will be located at the negative distance ($r_- < 0$).

For the second case ($a = n$) the angular momentum of the KTN spacetime would be $J = Mn$. It is a very interesting situation. In this case the line element of the KTN

spacetime would be

$$ds_n^2 = -\frac{\Delta_n}{p_n^2}(dt - A_n d\phi)^2 + \frac{p_n^2}{\Delta_n}dr^2 + p_n^2 d\theta^2 + \frac{1}{p_n^2}\sin^2\theta(ndt - B_n d\phi)^2 \ , \qquad (4.5)$$

with

$$\begin{aligned} \Delta_n &= r(r-2M) \ , p_n^2 = r^2 + n^2(1+\cos\theta)^2 \ , \\ A_n &= n(\sin^2\theta - 2\cos\theta) \ , B_n = r^2 + 2n^2 \ . \end{aligned} \qquad (4.6)$$

It could be easily seen that this special rotating spacetime has outer horizon at the distance $r_+ = 2M$ and inner horizon at $r_- = 0$. Outer horizon at the distance $r_+ = 2M$ is just similar to the Schwarzschild spacetime where the event horizon is located at $r = 2M$. This spacetime can be treated as the rotating spacetime with the *event horizon* at $r = 2M$ and its angular momentum will be

$$J = Mn \ . \qquad (4.7)$$

In other words, it could be said that *the KTN spacetime rotating with the angular momentum $J = Mn$, possessed an outer horizon at $r = 2M$ and an inner horizon at $r = 0$.* There is an apparent similarity between Eq. (40) of Ref. [46] with our results but it is a completely different situation. Furthermore, there should be an ergoregion in this special KTN spacetime. For this special case ($a = n$), the radius of the ergosphere for the KTN spacetime will be $M + \sqrt{M^2 + n^2\sin^2\theta}$. The LT precession rate in this special spacetime will be

$$\Omega_{LT}|_{a=n} = \frac{n}{p_n}\left[\Delta_n\left(\frac{\cos\theta}{r^2 - 2Mr - n^2\sin^2\theta} - \frac{1+\cos\theta}{p_n^2}\right)^2 + \sin^2\theta\left(\frac{r-M}{r^2 - 2Mr - n^2\sin^2\theta} - \frac{r}{p_n^2}\right)^2\right]^{\frac{1}{2}} \ . \qquad (4.8$$

The above expression is valid outside the ergosphere as it diverges on the ergosphere and

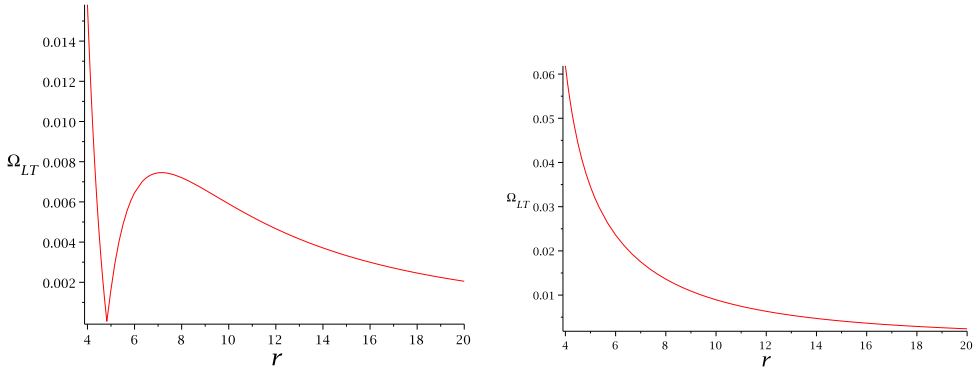

(a) along the pole (b) along the equator

Figure 4.3: *Plot of Ω_{LT} (in m^{-1}) vs r (in m) in the KTN spacetime for $a = n = 1$ m & $M = 1$ m [45].*

we also know that the LT precession is not defined in the spacelike surface. In Fig. 4.3, we plot r vs Ω_{LT} for $a = n = 1$. We see that the curve falls smoothly with increasing distance along the equator but it is not smooth along the pole. Similar behaviour is noticed in Fig. 4.1 and Fig. 4.2. The LT precession rate along the pole is very high just outside the ergosphere and falls sharply and becomes zero, rises again and finally approaches to a small value after crossing the strong gravity regime. This is really very peculiar and this was not observed in any other spacetimes which are the vacuum solution of Einstein equation, previously.

4.3 Results & Discussion

We know that the LT precession varies as $1/r^3$ in the weak gravity regime ('weak' Kerr metric) by the famous relation (Eq. 14.34 of Ref. [3])

$$\vec{\Omega}_{LT} = \frac{1}{r^3}[3(\vec{J}.\hat{r})\hat{r} - \vec{J}] \ , \tag{4.9}$$

where, $\hat{r}$ is the unit vector along r direction. We plot Ω_{LT} vs r in the strong gravity situation (see Eq. (42) of Ref. [28]) for maximally rotated Kerr spacetime along the pole

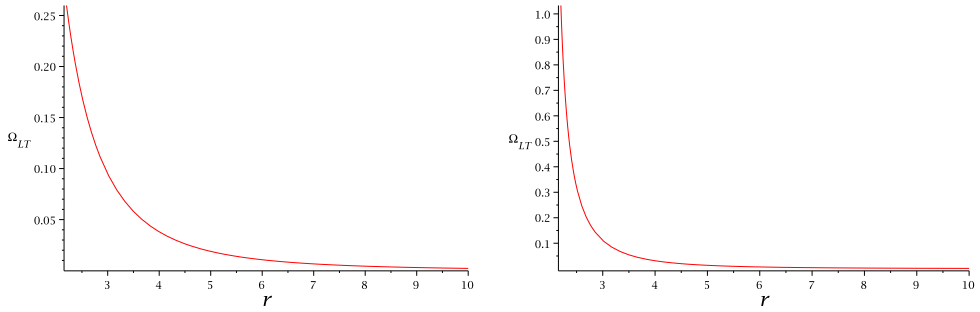

(a) along the pole (b) along the equator

Figure 4.4: *Plot of strong gravity Ω_{LT} (in m^{-1}) vs r (in m) in the Kerr spacetime for $a = M = 1$ m [45].*

(panel(a)) and the equator (panel(b)) in Fig. 4.4. Close observation reveals that the LT precession rates at the same distances (for a fixed r) along the equator and the pole are not the same. In the strong gravity regime Ω^e_{LT} is higher than Ω^p_{LT} as the ratio (η) of the LT precession rate along the pole (Ω^p_{LT}) to the equator (Ω^e_{LT}) in the strong gravity regime is

$$\eta_K^{strong} = \frac{\Omega^p_{LT}}{\Omega^e_{LT}} = \frac{2r^3(r-2M)}{(r^2+a^2)^{\frac{3}{2}}(r^2-2Mr+a^2)^{\frac{1}{2}}} \ , \tag{4.10}$$

but in the weak gravity regime it follows from Eq. (1.23)

$$\eta_K^{weak} = \frac{\Omega^p_{LT}}{\Omega^e_{LT}} = \frac{\frac{2J}{r^3}}{\frac{J}{r^3}} = 2 \ , \tag{4.11}$$

which is a constant. If we look for this ratio in the case of the KTN spacetime we find that

$$\eta_{KTN}^{strong} = \frac{\Omega^p_{LT}}{\Omega^e_{LT}} < 1 \ . \tag{4.12}$$

It holds for ever i.e. the LT precession rate along the equator (Ω^e_{LT}) is always higher than the LT precession rate along the pole (Ω^p_{LT}). In the weak gravity regime the ratio is only

$$\eta_{KTN}^{weak} = 1 \ . \tag{4.13}$$

We can plot the ratio for the clear scenario. The plot in Fig. 4.5 for the Kerr spacetime

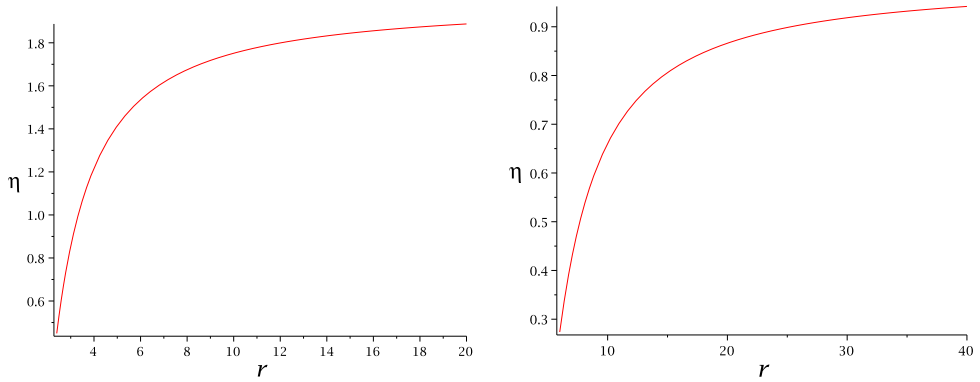

(a) Kerr spacetime (b) Kerr-Taub-NUT spacetime

Figure 4.5: *Plot of η vs r (in m) in the Kerr and Kerr-Taub-NUT spacetimes for $a = n = 1\ m$ & $M = 1\ m$ [45].*

shows that Ω^p_{LT} and Ω^e_{LT} are the same at a distance $r_0 = 3.324$ m. For $r < r_0$, $\Omega^p_{LT} < \Omega^e_{LT}$ and for $r > r_0$, $\Omega^p_{LT} > \Omega^e_{LT}$.

We have already seen that the plots of Ω_{LT} vs r along the pole and along the equator both are smooth for the Kerr spacetime but this is not the same for the KTN spacetime. In the KTN spacetime though the curve of Ω_{LT} vs r along the the equator is smooth, it is not smooth along the pole. We have studied here basically three cases. These are the following:

(i) $a = n$ **:** In this case shown in Fig. 4.3, we take the Kerr parameter a is equal to the NUT parameter n ($a = n = 1$ m) and mass of the spacetime M is unity. Thus, the radius of horizon is $r_h \sim 2$ m. The LT precession rate along the pole (panel (a)) is tremendously high just outside the horizon. Then it falls sharply and becomes zero (local minima) at $r_{min} \sim 4.8$ m. It rises again and gives a local maxima at $r_{max} \sim 7$ m. After that the curve of the LT precession rate follows the general inverse cube law and falls accordingly. We cannot see the same feature along the equator. We plot a 3-D picture of the LT precession rate in Fig. 4.6 where the Y axis represents the cosine of colatitude

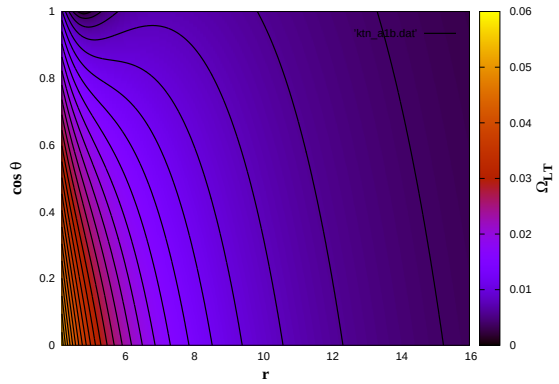

Figure 4.6: *3-D plot of* $\Omega_{LT}(r, \theta)$ *in the KTN spacetime for* $a = n = 1$ *m &* $M = 1$ *m [45].*

$(\cos\theta)$ and X axis represents the distance (r) from the centre of the spacetime. The colors represent the value of the LT precession rate and the values of the same precession rates are also separated by the isocurves. It shows that there is a local maximum and local minimum along the pole but it disappears after crossing a certain 'critical' angle. Here, it is around $\cos\theta \sim 0.6$.

(ii) $a > n$ **:** In the second case shown in Fig. 4.7, the Kerr parameter $a = 0.7$ m and NUT parameter $n = 0.3$ m. Mass of the spacetime is $M = 1$ m. Radius of the horizon $r_h \sim 1.8$ m, distance of local minimum is $r_{min} \sim 7$ m and distance of local maximum is $r_{max} \sim 10$ m . The 'critical' angle is around $\cos\theta \sim 0.8$.

(iii) $a < n$ **:** For the third case exhibited in Fig. 4.8, the Kerr parameter $a = 0.1$ m and NUT parameter $n = 1$ m. Mass of the spacetime is $M = 1$ m. Radius of the horizon $r_h \sim 2.4$ m, distance of local minimum is $r_{min} \sim 2.6$ m and distance of local maximum is $r_{max} \sim 3.5$ m . The 'critical' angle is around $\cos\theta \sim 0.4$.

In all three cases, plots show the same feature but the numerical values are different depending on the values of a and n. For a fixed value of n, if a decreases the value of the

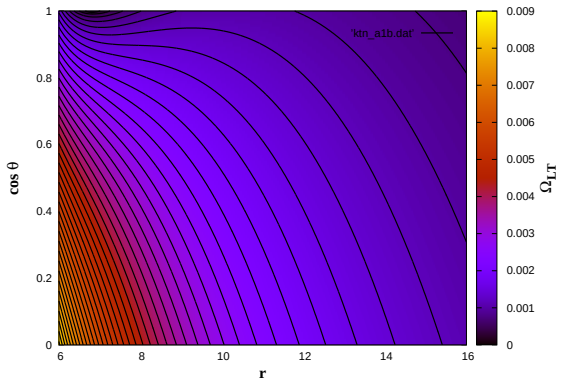

Figure 4.7: *3-D plot of* $\Omega_{LT}(r, \theta)$ *in the KTN spacetime for* $a = 0.7\ m$, $n = 0.3\ m$ *&* $M = 1\ m$ *[45].*

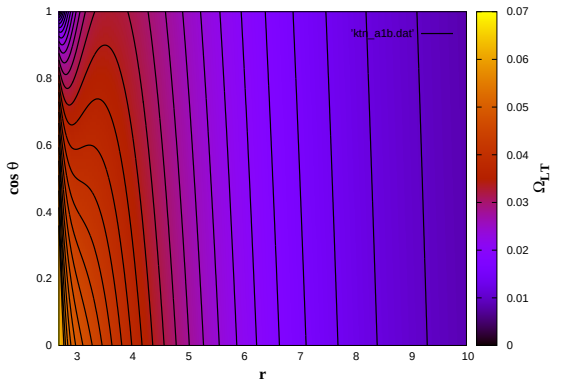

Figure 4.8: *3-D plot of* $\Omega_{LT}(r, \theta)$ *in the KTN spacetime for* $a = 0.1\ m$, $n = 1\ m$ *&* $M = 1\ m$ *[45].*

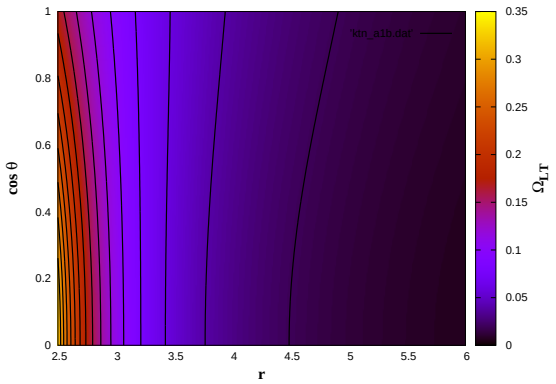

Figure 4.9: *3-D plot of $\Omega_{LT}(r,\theta)$ in the Kerr spacetime for $a = 1\ m$ & $M = 1\ m$ [45].*

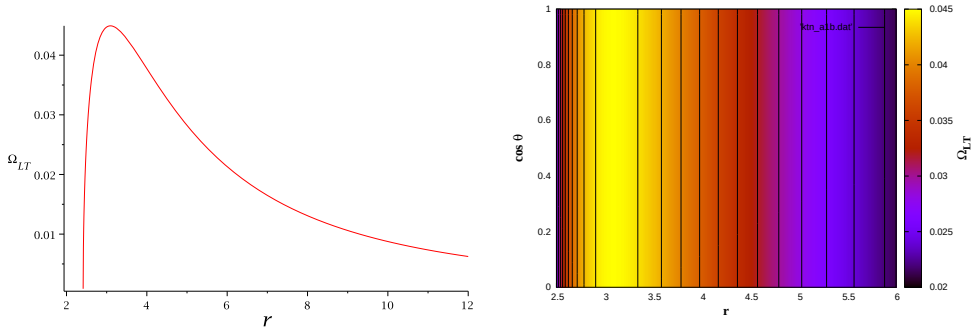

(a) plot of Ω_{LT} (in m^{-1}) vs r (in m) (b) 3-D plot

Figure 4.10: *Plot of Ω_{LT} in the Taub-NUT spacetime for $n = 1\ m$ & $M = 1\ m$ (basically, the expression of Ω_{LT} (see Eq. (25) of Ref. [28]) is independent of θ, thus the value (colour) of Ω_{LT} does not change with $\cos\theta$ in panel(b)) [45].*

LT precession rate at the local maximum increases and also the distance of local minimum and maximum are shifted towards the horizon of the spacetime. If the NUT parameter vanishes (for the Kerr spacetime) there will be no local maximum and minimum as noticed in Fig. 4.4 and Fig. 4.9.

The local maximum along the pole in the KTN spacetime arises due to the NUT parameter and it is clear from Fig. 4.10 (panel(a)) that it is valid only for the Taub-NUT spacetime where the Kerr parameter vanishes but the NUT parameter does not vanish. The local minimum along the pole in KTN spacetime arises due to the Kerr parameter. It could not be seen directly from the Fig. 4.4(panel(a)). If we take Fig. 4.4(panel(a))

of the Kerr spacetime and Fig. 4.10(panel(a)) of the Taub-NUT spacetime and overlap these two figures with each other (as the KTN spacetime includes both the Kerr and NUT parameters) just for our clear understanding, we can easily visualize the nature of the plots of the LT precession (panel(a) of Fig. 4.1-4.3) along the pole in the KTN spacetimes. Thus, the presence of the Kerr parameter is responsible for showing the local minimum along the pole in the KTN spacetime.

Without the Kerr parameter the LT precession rate at a 'local maximum' in the Taub-NUT spacetime is higher than the LT precession rate at a 'local maximum' in the KTN spacetime. The presence of the Kerr parameter (or increasing the value of the Kerr parameter from 0 to a finite number) shifts the 'local maximum' and 'local minimum' away from the horizon and reduces the LT precession rate at the local maximum.

We note that the Taub-NUT spacetime is a stationary and spherically symmetric spacetime and the expression of Ω_{LT} (see Eq. (25) of Ref. [28]) is also independent of θ (the LT precession in the Taub-NUT spacetime has been discussed in detail in the next section 4.4). Thus the value (colour) of Ω_{LT} does not change with $\cos\theta$. It means that the LT precession rate is same everywhere in that spacetime for a fixed distance r (no matter whether it is pole or equator) and the LT precession rate curve always shows a 'peak' as seen in panel(a) of Fig. 4.10 near the horizon. But, if this Taub-NUT spacetime starts to rotate with an angular momentum $J(= aM, a$ is the Kerr parameter), it turns out to be the KTN spacetime. In this case, the LT precession rate curve shows a 'peak' (or 'local maximum') along the pole but disappears after crossing the 'critical' angle and we cannot see any 'peak' in the LT precession rate curve along the equator as discussed earlier. The 'intrinsic' angular momentum of the spacetime (J) is fully responsible for the no-show of 'local maximum' along the equator. The Kerr parameter is also responsible for reducing the LT precession rate at the 'local maximum' which has already been discussed in the previous paragraph. Thus, the 'dual mass' or the 'angular momentum monopole' n is only responsible for the 'anomaly' (appearance of local maximum and local minimum in

the LT precession rate) and the Kerr parameter or the rotation of the spacetime tries to reduce this 'anomaly' as far as possible. The Kerr parameter is fully successful to reduce this effect along the equator but slowly it loses its power of reduction of this anomaly along the pole.

For the consistency check of the appearance of 'local maximum' and 'local minimum' if we take the derivative of Eq. (4.4) with respect to r and plot $\frac{d\Omega_{LT}}{dr}|_{(r=R,\theta=\pi/2)}$ vs r we cannot find any positive real root in the region $r_h < r < \infty$. But the plot of $\frac{d\Omega_{LT}}{dr}|_{(r=R,\theta=0)}$ vs r shows two positive real roots (which are basically local maximum $R_1 = r_{max}$ and local minimum $R_2 = r_{min}$) in the region $r_h < r < \infty$.

4.4 Lense-Thirring precession in Taub-NUT spacetime

Now, we are going to dicuss the frame-dragging effect in the Taub-NUT spacetime separately. The Taub-NUT spacetime is geometrically a stationary, spherically symmetric vacuum solution of Einstein equation with NUT charge (n). The Einstein-Hilbert action requires no modification to accommodate this NUT charge or "dual mass" which is perhaps an intrinsic feature of general relativity, being a gravitational analogue of a magnetic monopole in electrodynamics [29].

Consider the line element (of the NUT spacetime), which is presented by Newman et. al. [36]

$$ds^2 = -f(r)\left[dt + 4n\sin^2\frac{\theta}{2}d\phi\right]^2 + \frac{1}{f(r)}dr^2 + (r^2+n^2)(d\theta^2 + \sin^2\theta d\phi^2)\ , \qquad (4.14)$$

where,

$$f(r) = \frac{r^2 - 2Mr - n^2}{r^2 + n^2}\ . \qquad (4.15)$$

Here, M represents the "gravitoelectric mass" or 'mass' and n represents the "gravitomagnetic mass" or 'dual' (or 'magnetic') mass of this spacetime. It is obvious that the spacetime (4.14) is not invariant under time reversal $t \to -t$, signifying that it must have a sort of 'rotational sense', once again analogous to a magnetic monopole in electrodynamics. One is thus led to the conclusion that the source of the nonvanishing LT precession is this "rotational sense" arising from a nonvanishing NUT charge. Without the NUT charge, the spacetime is clearly hypersurface orthogonal and frame-dragging effects vanish.

In the Schwarzschild coordinate system, $f(r) = 0$ at

$$r = r_{\pm} = M \pm \sqrt{M^2 + n^2} \ . \tag{4.16}$$

$r_{\pm}$ are similar to *horizons* in this geometry in the sense that $f(r)$ changes sign from positive to negative across the horizon and the radial coordinate r changes from spacelike to timelike. But is $r = r_+$ an event horizon in the sense of the event horizon of Schwarzschild spacetime ? We shall focus on this issue momentarily. For the present, we note that the LT precession rate is given by

$$\vec{\Omega}_{LT}^{MTN} = \frac{n(r^2 - 2Mr - n^2)^{\frac{1}{2}}}{(r^2 + n^2)^{\frac{3}{2}}} \hat{r} \ . \tag{4.17}$$

It is clear that $\Omega_{LT}^{MTN} = 0$ on $r = r_{\pm}$, in contrast to the LT precession frequency in the standard Kerr spacetime which is maximum closest to the event horizon ! Further, if we plot the magnitude of the precession rate as a function of the radial coordinate for $r > r_+$, as obtained from (4.17), one obtains the profile as shown in Fig. 4.11.

Thus, the precession rate is maximum very close to the 'horizon' $r = r_+$, but it sharply drops for $r \to r_+$, most likely becoming ill-defined on the 'horizon'.

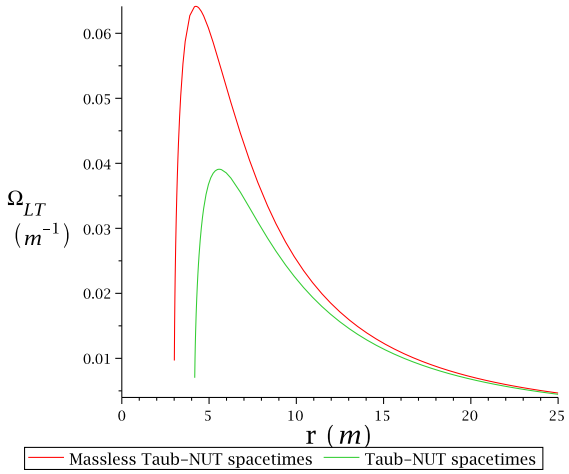

Figure 4.11: *Plot of* Ω_{LT} *(in* m^{-1}*) vs* r *(in* m*) for* $n = 3\ m$ *&* $M = 1\ m$ *and* Ω_{LT} *vs* r *for* $n = 3\ m$ *&* $M = 0$ *[28].*

4.4.1 Analytic extension of Taub-NUT spacetime

As the metric (4.14) blows up at $r = r_{\pm}$, we should perhaps try a different co-ordinate system where it is smooth on the 'horizon'. Following Ref. [47], wherein an analytic extension of the metric (4.14) has been attempted, one obtains the transformed metric

$$\begin{aligned} ds^2 &= (r^2+n^2)(d\theta^2+\sin^2\theta d\phi^2) \\ &+ F^2\left[du_{\pm}^2 - dv_{\pm}^2 - (2n/r_{\pm})(u_{\pm}dv_{\pm} - v_{\pm}du_{\pm})\cos\theta d\phi - (n/r_{\pm})^2(u_{\pm}^2 - v_{\pm}^2)\cos^2\theta d\phi^2\right] , \end{aligned} \tag{4.18}$$

where,

$$F^2 = 4r_{\pm}^4(r^2+n^2)^{-1}\left(\frac{r-r_{\mp}}{r_{\pm}}\right)^{1-\frac{r_{\mp}}{r_{\pm}}}\exp\left(-\frac{r}{r_{\pm}}\right) , \tag{4.19}$$

$$u_{\pm} = \left(\frac{r-r_{\pm}}{r_{\pm}}\right)^{1/2}\left(\frac{r-r_{\mp}}{r_{\pm}}\right)^{\frac{r_{\mp}}{2r_{\pm}}}\exp\left(\frac{r}{2r_{\pm}}\right)\cosh\left(\frac{t}{2r_{\pm}}\right) , \tag{4.20}$$

$$v_{\pm} = \left(\frac{r-r_{\pm}}{r_{\pm}}\right)^{1/2}\left(\frac{r-r_{\mp}}{r_{\pm}}\right)^{\frac{r_{\mp}}{2r_{\pm}}}\exp\left(\frac{r}{2r_{\pm}}\right)\sinh\left(\frac{t}{2r_{\pm}}\right) . \tag{4.21}$$

In u, v co-ordinate system r could be redefined as

$$u_{\pm}^2 - v_{\pm}^2 = \left(\frac{r - r_{\pm}}{r_{\pm}}\right)\left(\frac{r - r_{\mp}}{r_{\pm}}\right)^{\frac{r_{\mp}}{r_{\pm}}} \exp\left(\frac{r}{r_{\pm}}\right) \ . \tag{4.22}$$

Recall that locally every spherically symmetric four dimensional spacetime has the structure $\mathcal{I}_2 \otimes S^2$ where $\mathcal{I}_2$ is a two dimensional Lorentzian spacetime. In this Taub-NUT case, the attempted analytic extension discussed immediately above leads to a *vanishing* of the two dimensional Lorentzian metric on the 'horizon' $r = r_+$, in contrast to the Schwarzschild metric. This might be taken to imply that perhaps the null surface $r = r_+$ is *not quite* an event horizon; rather it is a null surface where ingoing future-directed null geodesics appear to *terminate*, as already noticed in Ref. [32]. So, physical effects on this null hypersurface might not be easy to compute, as a result of which the apparent vanishing of the LT precession on this hypersurface is to be taken with a pinch of salt.

The NUT spacetime, for the mass $M = 0$ is also well defined (see, for example, appendix of Ref. [18]). We can also write down the precession rate only for massless dual mass (NUT charge n can be regarded as dual mass) solutions of the NUT spacetime. This turns out to be

$$\vec{\Omega}_{LT}^{TN} = \frac{n(r^2 - n^2)^{\frac{1}{2}}}{(r^2 + n^2)^{\frac{3}{2}}}\hat{r} \ . \tag{4.23}$$

At, the points $r = \pm n$, the LT precession vanishes akin to the previous case, but the same caveats apply here as well. One may plot the precession frequency as a function of the radial coordinate as earlier.

Here, we observe that for $n = 3$, the LT precession is starting for $r > 3$ and continued to the infinity. Setting $\frac{d\Omega_{LT}^{TN}}{dr} = 0$, we get that Ω_{LT}^{TN} is maximum at $r = \sqrt{2}n$. In the Fig. 4.11, this value is $r = 3\sqrt{2} = 4.24$ m. Now, we are not interested for $r < 3$. Our formulas are not comfortable in that regions and $r < r_{\pm}$ is also not well defined for Taub-NUT spacetimes. From our precession rate formulas (4.17,4.23) at dual mass spacetimes we can see that the precession rate (Ω_{LT}^{TN}) is the same, starting from the polar region to

the equatorial plane for a fixed distance. Ω_{LT}^{TN} depends only on distance (r) of the test gyroscope from the 'dual mass'.

We have noted in this subsection several subtleties of computing the LT precession rate on and near the 'horizon' of a Taub-NUT spacetime, and our results are consistent with earlier literature where geodesic incompleteness on this null hypersurface has been noted.

4.5 Digression : ISCOs in KTN spacetimes

4.5.1 Motivation

Now, we want to calculate the LT precession rates on the Inner-most stable circular orbit (ISCO) in the KTN and Taub-NUT spacetimes. Thus, at first, we have to derive the radii of the ISCOs in these spacetimes. It is already well known to us that the marginally stable orbit (also called ISCO) plays an important role in the accretion disk theory. That fact is important for spectral analysis of X-ray sources [3,48]. The circular orbits with $r > r_{ISCO}$ turn out to be stable, while those with $r < r_{ISCO}$ are not. Basically, accretion flows of almost free matter (stresses are insignificant in comparison with gravity or centrifugal effects), resemble almost circular motion for $r > r_{ISCO}$, and almost radial free-fall for $r < r_{ISCO}$. In case of thin disks, this transition in the character of the flow is expected to produce an effective inner truncation radius in the disk. The exceptional stability of the inner radius of the X-ray binary LMC X-3 [49], provides considerable evidence for such a connection and, hence, for the existence of the ISCO. The transition of the flow at the ISCO may also show up in the observed variability pattern, if variability is modulated by the orbital motion [48]. One may expect that there will be no variability observed with frequencies $\Omega > \Omega_{ISCO}$, i.e., higher than the Keplerian orbital frequency at ISCO, or that the quality factor for variability, $Q \sim \frac{\Omega}{\Delta\Omega}$ will significantly drop at Ω_{ISCO}. Several variants of this idea have been discussed in the following references [50, 51].

The Taub-NUT geometry [37,38] possesses gravitomagnetic monopoles. Basically, this spacetime is a stationary and spherically symmetric vacuum solution of Einstein equation. As already mentioned, the authors of Ref. [32] have made a complete classification of geodesics in Taub-NUT spacetimes and describe elaborately the 'full' set of orbits for massive test particles. However, there is no specific discussion on the various innermost stable orbits in such spacetimes for null as well as timelike geodesics. This is the gap in the literature which we wish to fulfill in this chapter. Our focus here is the the three parameter Taub-NUT version of the Kerr spacetime which has angular momentum, mass and the NUT parameter (n,the gravitomagnetic monopole strength), and is a stationary, axisymmetric vacuum solution of the Einstein equation. The geodesics and the orbits of the charged particles in Kerr-Taub-NUT (KTN) spacetimes have also been discussed by Miller [44]. Abdujabbarov [52] et. al. discuss some aspects of these geodesics in the KTN spacetime, although the black hole solution remains a bit in doubt. Liu et. al. [42] have also obtained the geodesic equations but there are no discussions about the ISCOs in the KTN spacetime. We know that ISCO plays many important roles in astrophysics as well as in gravitational physics, hence the strong physical motivation to study them.

The presence of the NUT parameter lends the Taub-NUT spacetime a peculiar character and makes the NUT charge into a quasi-topological parameter. For example in the case of maximally rotating Kerr spacetime (extremal Kerr) where we can see that the timelike circular geodesics and null circular geodesics coalesce into a zero energy trajectory. This result and also the geodesics of the extremal Kerr spacetime have been elaborately described in Ref. [40]. They show that the ISCOs of the extremal Kerr spacetime for null geodesics and timelike geodesics coincide on the horizon (at $r = M$) which means that the geodesic on the horizon must coincide with the principal null geodesic generator. This is a very peculiar feature of extremal spacetimes.

In the case of the non-extremal Kerr spacetime Chandrasekhar [53] presented complete and detailed discussion on timelike and null geodesics (including ISCOs and other circular

orbits). However, in that reference, subtleties associated with the extremal limit and special features of the precisely extremal Kerr spacetime had not been probed significantly. Likewise, the behaviour of geodesics, especially those close to the horizon (in the equatorial plane, where subtleties regarding geodesic incompleteness [32] can be avoided), had not been considered in any detail.

Here we wish to investigate the differences of ISCOs in KTN spacetimes due to the inclusion of the NUT parameter in the Kerr spacetime. While focusing on the set of ISCOs, we also probe the Keplerian orbital frequencies and other important astronomical observables (namely, angular momentum (L), energy (E), rotational velocity ($v^{(\phi)}$) etc.), relevant for accretion disk physics, in the KTN and Taub-NUT spacetimes; these had not been investigated extensively in the extant literature. The presence of the NUT parameter in the metric always throws up some interesting phenomena in these particulars spacetimes (KTN and Taub-NUT), arising primarily from their topological properties, which we wish to bring out here in the context of our investigation on the ISCOs. e.g., while it had been demonstrated in Ref. [32] that the orbital precession of spinless test particles in Taub-NUT geodesics vanishes, investigation by us has shown that in both the massive and massless Taub-NUT spacetimes spinning gyroscopes exhibit nontrivial frame-dragging (Lense-Thirring) precession [28]. Even though we do not discuss inertial frame-dragging in detail in this section, this does provide a theoretical motivation as well to probe ISCOs in KTN spacetimes, following well established techniques [53].

A word about our rationale for explicitly restricting to causal geodesics on the *equatorial* plane : these geodesics are able to avoid issues involving geodesic incompleteness exhibited in the spacetimes for other polar planes. Since there is a good deal of discussion of these issues elsewhere (see Ref. [32] for a competent review), we prefer to avoid them and concentrate instead on other issues of interest.

At first, we want to study the geodesic motions in the equatorial plane of KTN space-

times. So, the line element of the KTN spacetime (Eq. 4.1) at the equator will be

$$ds_e^2 = -\frac{r^2 - 2Mr - n^2}{p_e^2}dt^2 - \frac{4a(Mr + n^2)}{p_e^2}d\phi dt + \frac{B^2 - a^2\Delta}{p_e^2}d\phi^2 + \frac{p_e^2}{\Delta}dr^2 \ , \qquad (4.24)$$

where,

$$p_e^2 = r^2 + n^2 \ . \qquad (4.25)$$

From the above metric we can easily derive the velocity components (for $\theta = \frac{\pi}{2}$ and $\dot{\theta} = 0$) of the massive test particle [24]

$$\dot{t} = \frac{1}{p^2}\left[\frac{B}{\Delta}P(r) + aO(\theta)\right] \ , \qquad (4.26)$$

$$\dot{\phi} = \frac{1}{p^2}\left[\frac{a}{\Delta}P(r) + O(\theta)\right] \ , \qquad (4.27)$$

$$\dot{r}^2 = \frac{\Delta}{p^2}\left[k + \frac{1}{p^2}\left(\frac{P^2}{\Delta} - O^2\right)\right] \ , \qquad (4.28)$$

where,

$$P(r) = BE - La \ , \qquad (4.29)$$

$$O(\theta) = L - aE = x \ . \qquad (4.30)$$

We may set without loss of generality,

$$\begin{aligned} k &= -1 \text{ for timelike geodesics} \ , \\ &= 0 \text{ for nulllike geodesics} \ . \end{aligned} \qquad (4.31)$$

L is specific angular momentum or angular momentum per unit mass of the test particle and, E is to be interpreted as the specific energy or energy per unit mass of the test particle for the timelike geodesics.

4.5.2 ISCOs for the null geodesics in Kerr-Taub-NUT spacetimes

In this section, we derive the radii of ISCOs and other important astronomical quantities for null geodesics ($k = 0$) in the two spacetimes, one is KTN spacetimes and another is Taub-NUT spacetimes.

As we have noted, $k = 0$ for null geodesics and the radial Eq. (4.28) becomes

$$\dot{r}^2 = E^2 + 2(L - aE)^2 \frac{(Mr + n^2)}{(r^2 + n^2)^2} - \frac{(L^2 - a^2E^2)}{(r^2 + n^2)} \ . \tag{4.32}$$

It will be more convenient to distinguish the geodesics by the impact parameter

$$D = \frac{L}{E} \ , \tag{4.33}$$

rather than L .

We first consider the geodesics with the impact parameter

$$D = a \ \text{ or } \ L = aE \ . \tag{4.34}$$

Thus, in this case, Eqs. (4.26), (4.27) and (4.32) reduce to

$$\dot{r} = \pm E \ , \tag{4.35}$$

$$\dot{t} = \frac{(r^2 + n^2 + a^2)}{\Delta} E \ , \tag{4.36}$$

and,

$$\dot{\phi} = \frac{a}{\Delta} E \ . \tag{4.37}$$

The radial co-ordinate is described uniformly with respect to the affine parameter while

the equations governing t and ϕ are

$$\frac{dt}{dr} = \pm\frac{(r^2+n^2+a^2)}{\Delta} ,$$

and

$$\frac{d\phi}{dr} = \pm\frac{a}{\Delta} . \tag{4.38}$$

The solutions of these equations are

$$\pm t = r + \frac{r_+^2+a^2+n^2}{r_+-r_-}\ln\left(\frac{r}{r_+}-1\right) - \frac{r_-^2+a^2+n^2}{r_+-r_-}\ln\left(\frac{r}{r_-}-1\right) , \tag{4.39}$$

$$\pm\phi = \frac{a}{r_+-r_-}\ln\left(\frac{r}{r_+}-1\right) - \frac{a}{r_+-r_-}\ln\left(\frac{r}{r_-}-1\right) . \tag{4.40}$$

These solutions exhibit the characteristic behaviors of t and ϕ of tending to $\pm\infty$ as the horizons at r_+ and r_- are approached. The coordinate ϕ, like the coordinate t, is not a 'good' coordinate for describing what really happens with respect to a co-moving observer: a trajectory approaching the horizon (at r_+ or r_-) will spiral round the spacetime an infinite number of times even as it will take an infinite coordinate time t to cross the horizon and neither will be the experience of the co-moving observer.

The null geodesics which are described by Eq. (4.38), are the members of the principal null congruences and these are confined to the equatorial plane.

In general it is clear that there is a critical value of the impact parameter $D = D_c$ for which the geodesic equations allow an unstable circular orbit of radius r_c. In case of $D < D_c$, only one kind of orbit is possible: it arrives from infinity and crosses both horizons and terminates at the singularity. For $D > D_c$, we can get two types of orbits:

(a) those arriving from infinity and have perihelion distances greater than r_c, eventually terminating at the singularity at $r = 0$ and $\theta = \frac{\pi}{2}$

(b) those arriving from infinity, have aphelion distances less than r_c, and terminate at

the singularity at $r = 0$ and $\theta = \frac{\pi}{2}$. For $n = 0$, we can recover the results in the case of Kerr geometry (see Eq. (77) of Ref. [53]).

The equations determining the radius (r_c) of the stable circular 'photon orbit' are (Eq. 4.32)

$$E^2 + 2(L - aE)^2 \frac{(Mr_c + n^2)}{(r_c^2 + n^2)^2} - \frac{(L^2 - a^2E^2)}{(r_c^2 + n^2)} = 0 \ , \tag{4.41}$$

and

$$-(L - aE)^2 \frac{(3Mr_c^2 + 4r_c n^2 - Mn^2)}{(r_c^2 + n^2)^3} + \frac{r_c(L^2 - a^2E^2)}{(r_c^2 + n^2)^2} = 0 \ . \tag{4.42}$$

Substituting $D = \frac{L}{E}$ in the above Eqs. (4.41,4.42), we get from Eq. (4.42)

$$\frac{D_c - a}{D_c + a} = \frac{r_c(r_c^2 + n^2)}{r_c(3Mr_c + 4n^2) - Mn^2} \ . \tag{4.43}$$

Letting

$$y = D_c + a \ , \tag{4.44}$$

and substituting it in Eq. (4.43) we get

$$y = 2a \left[1 - \frac{r_c(r_c^2 + n^2)}{r_c(3Mr_c + 4n^2) - Mn^2}\right]^{-1} \ . \tag{4.45}$$

So, the critical value of the impact parameter D_c in the KTN spacetime is

$$D_c = 2a \left[1 - \frac{r_c(r_c^2 + n^2)}{r_c(3Mr_c + 4n^2) - Mn^2}\right]^{-1} - a \ . \tag{4.46}$$

To get the value of r_c we have to take Eq. (4.41) which reduces to

$$1 + 2(D_c - a)^2 \frac{(Mr_c + n^2)}{(r_c^2 + n^2)^2} - \frac{(D_c^2 - a^2)}{(r_c^2 + n^2)} = 0 \ . \tag{4.47}$$

Substituting the value of

$$D_c = y - a = 2a\left[1 + \frac{r_c(r_c^2 + n^2)}{r_c(3Mr_c + 4n^2) - Mn^2}\right] - a \ , \tag{4.48}$$

(neglecting the higher order terms of r_c, we mean $r_c < n$ and $r_c < M$) in the Eq. (4.47) we get the equation to determine the radius (r_c) of the stable circular photon orbit:

$$\begin{aligned}(9 - 4a_M^2)r_{cM}^4 + 4(6n_M^2 - a_M^2)r_{cM}^3 + 2n_M^2(8n_M^2 - 6a_M^2 - 3)r_{cM}^2 \\ +4n_M^2(a_M^2 - 2n_M^2)r_{cM} + n_M^4 = 0 \ ,\end{aligned} \tag{4.49}$$

where the lower index 'M' of a particular parameter represents that the parameter is divided by 'M' (such as, $a_M = \frac{a}{M}$). For $r_c < n$ we get the solution of r_c as

$$\begin{aligned} r_{cM} &= \frac{n_M}{6(a_M^2 - 6n_M^2)}\left[(U - 18Vn_M^2 + 3n_M^2V)^{\frac{1}{3}}\right. \\ &+ \left. W(U - 18Vn_M^2 + 3n_M^2V)^{-\frac{1}{3}} + n_M(8n_M^2 - 6a_M^2 - 3)\right] \ , \end{aligned} \tag{4.50}$$

where the values of U, V, W are given in the footnote [1]. Here, the expression of r_{cM} is the radius of the ISCO as it is the smallest positive real root of the ISCO Eq. (4.49).

Extremal case: We know that in the KTN spacetime, the *horizons* are at

$$r_\pm = M \pm \sqrt{M^2 + n^2 - a^2} \ , \tag{4.51}$$

[1]

$$\begin{aligned} U &= -1584n_M^5a_M^2 + 684n_M^3a_M^4 - 108n_Ma_M^6 - 54n_M^3a_M^2 - 27a_M^4n_M + 1152n_M^7 \\ &+ 540n_M^5 + 512n_M^9 - 1152n_M^7a_M^2 + 864n_M^5a_M^4 - 216n_M^3a_M^6 - 27n_M^3 \ , \\ V &= (-192a_M^8 - 432a_M^8n_M^2 + 1224n_M^2a_M^6 + 1584n_M^4a_M^6 - 2808n_M^4a_M^4 - 351n_M^2a_M^4 \\ &- 1920n_M^6a_M^4 + 1080n_M^4a_M^2 + 1824n_M^6a_M^2 + 768n_M^8a_M^2 - 108n_M^6 - 162n_M^4)^{\frac{1}{2}} \ . \\ W &= (-60n_M^2a_M^2 + 12a_M^4 + 96n_M^4 + 64n_M^6 - 96n_M^4a_M^2 + 36n_M^2a_M^4 + 9n_M^2) \ . \end{aligned}$$

where r_+ and r_- define the event horizon and Cauchy horizon, respectively. In case of the extremal KTN spacetime,

$$\begin{aligned} r_+ &= r_- \ , \\ \text{or,} \quad a^2 &= M^2 + n^2 \ . \end{aligned} \tag{4.52}$$

So, the horizon of the extremal KTN spacetime is at

$$r = M \ . \tag{4.53}$$

Now, we can substitute the value of Eq. (4.43) in Eq. (4.41) (also take $a^2 = M^2 + n^2$) and get the equation for determining the radius (r_c) of the stable circular photon orbit

$$r_c^2(r_c^2-3Mr_c-3n^2)^2-4(M^2+n^2)r_c^2(Mr_c+2n^2)+2Mn^2r_c(r_c^2-3Mr_c-n^2+2M^2)+M^2n^4 = 0 \, . \tag{4.54}$$

Interestingly, the solution of this sixth order *non-trivial* equation is

$$r_c = M \ , \tag{4.55}$$

This is the radius of the ISCO as it is the smallest positive real root of the ISCO Eq. (4.54). It means that the radius of the ISCO (r_c) coincides with the horizon in the extremal KTN spacetime for null geodesics. This is the same thing which happens in the extremal Kerr spacetime also. In the extremal Kerr spacetime, the direct ISCO coincides with the horizon at $r = M$ for null geodesic. Now, we can calculate the critical value of the impact parameter in the extremal KTN spacetime:

$$D_c = M\frac{3M^2 + 5n^2}{M^2 + 3n^2} \ . \tag{4.56}$$

The physical significance of the impact parameter D_c and the ISCO have already discussed in detail. Now, we can give our attention to the Taub-NUT spacetime which is quite interesting.

ISCOs in Taub-NUT spacetimes :

The Taub-NUT spacetime is a stationary and spherically symmetric vacuum solution of Einstein equation [36]. Now, we are discussing a very special case where we set $a = 0$, the angular momentum of the spacetime vanishes. We note that for $a = 0$, the primary metric (Eq. (4.1)) of the KTN spacetime reduce to the Taub-NUT metric in which the constant set as $C = 0$. If we take the Taub-NUT metric in more general form, it would be

$$ds^2 = -f(r)\left[dt - 2n(\cos\theta + C)d\phi\right]^2 + \frac{1}{f(r)}dr^2 + (r^2 + n^2)(d\theta^2 + \sin^2\theta d\phi^2) \ ,$$

where, C is an arbitrary real constant. If we take $C = 0$ for the above metric, the form of the Taub-NUT metric is same as the metric (4.1) of 'KTN spacetimes with $a = 0$'. Physically, $C = 0$ leads to the only possibility for NUT solutions to have a finite total angular momentum [54]. After noting the above points, we write the line element of Taub-NUT spacetimes at the equator as

$$ds_e^2 = -\frac{r^2 - 2Mr - n^2}{r^2 + n^2}dt^2 + \frac{r^2 + n^2}{r^2 - 2Mr - n^2}dr^2 + (r^2 + n^2)d\phi^2 \ . \qquad (4.57)$$

To determine the radius (r_{cn}) of the stable circular photon orbit, we put $a = 0$ in Eq.

(4.54) and get the following

$$r_{cn}^2(r_{cn}^2 - 3Mr_{cn} - 3n^2)^2 \quad + \quad 2Mn^2 r_{cn}(r_{cn}^2 - 3Mr_{cn} - 3n^2) + M^2 n^4 = 0 \ ,$$

or,

$$r_{cn}^3 \quad - \quad 3Mr_{cn}^2 - 3n^2 r_{cn} + Mn^2 = 0 \ . \tag{4.58}$$

Solving the above equation we get,

$$r_{cn} \quad = \quad M + 2(M^2 + n^2)^{1/2} \cos\left[\frac{1}{3}\tan^{-1}\left(\frac{n}{M}\right)\right] \ , \tag{4.59}$$

or,

$$r_{Mcn} \quad = \quad 1 + 2(1 + n_M^2)^{1/2} \cos\left[\frac{1}{3}\tan^{-1}\left(n_M\right)\right] \ . \tag{4.60}$$

This is the radius of the ISCO as it is the smallest positive real root of the ISCO Eq. (4.58). For $n_M = \frac{n}{M} = 0$, we can recover $r_c = 3M$ of Schwarzschild spacetime. We know that the position of *event horizon* in the Taub-NUT spacetime is:

$$r_+ \quad = \quad M + \sqrt{M^2 + n^2} \ , \tag{4.61}$$

or,

$$r_{+M} \quad = \quad 1 + \sqrt{1 + n_M^2} \ . \tag{4.62}$$

It seems that the position of the ISCO (r_{cn}) could be in timelike, nulllike or spacelike surfaces depending on the value of the NUT charge (n_M) in the Taub-NUT spacetime. But, it never happens. We cannot get any solution of n_M for $r_{Mcn} = r_{+M}$. We plot r_{Mcn} (green) and r_{+M} (red) as a function of n_M in Fig. 4.12. We can see that r_{Mcn} and r_{+M} are increasing continuously for $n_M \geq 0$. They cannot intersect each other at any point. So, we can conclude that the ISCO could not be on the horizon for any value of n_M. Thus, the photon orbit is always in timelike region for any real value of n_M in the Taub-NUT

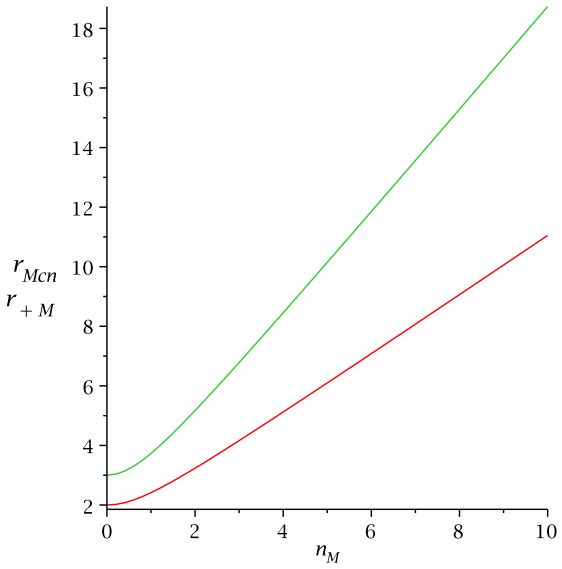

Figure 4.12: *Plot of r_{Mcn} (green) and r_{+M} (red) vs n_M [41].*

spacetime.

ISCOs in massless Taub-NUT spacetimes :

The NUT spacetime, for $M = 0$ is also well defined (see, for example, appendix of Ref. [18]). So, we can also determine the radius (r_{0cn}) of the stable circular photon orbit for massless Taub-NUT spacetimes. This turns out to be

$$r_{0cn} = \sqrt{3}n \ . \tag{4.63}$$

We note that the *horizons* of massless Taub-NUT spacetime are at $r = \pm n$ [28]. So, the ISCO of this spacetime for null geodesic is always outside the *horizon*, i.e. in the timelike surface. Here, it should also be highlighted that in the case of the Taub-NUT spacetime, the *horizons* are at

$$r_{\pm} = M \pm \sqrt{M^2 + n^2} \ , \tag{4.64}$$

as $a = 0$. We can see that one *horizon* is located at $r_+ > 2M$ and the other at $-|n| < r_- < 0$.

Thus there are mainly two important features of the Taub-NUT and massless Taub-NUT spacetime, one is that the second *horizon* is at a *negative* value of the radial Schwarzschild coordinate and another is that the both of the spacetimes possess the quasi-regular singularity [55]. But, the presence of the Kerr parameter (a) leads to the *naked* singularity in the non-extremal KTN spacetime as well as non-extremal Kerr spacetime. In these cases, both the horizons are located at imaginary distances. This means that we can observe the singularity from the infinity. So, this is called as a naked singularity. But, in the Taub-NUT spacetime the absence of Kerr parameter never leads to any of the horizons at imaginary distance. So, there could not be any naked singularity in the Taub-NUT and massless Taub-NUT spacetime. The absence of the Kerr parameter also leads to the non-existence of any *extremal* case for the Taub-NUT spacetime as the *horizons* of the Taub-NUT spacetime cannot act as the *actual* horizons like the horizons of our other well known spacetimes (such as Kerr, Reissner-Nordström geometry). In the extremal KTN spacetime, the horizon is located at $r = M$ which is same as the Kerr spacetime. We note that the NUT charge has no any effect to determine the ISCO in the extremal KTN spacetime as the Kerr parameter takes the highest value $a = \sqrt{M^2 + n^2}$ but the ISCO radius (Eq. (4.50)) in the non-extremal KTN spacetime depends on the NUT charge.

4.5.3 ISCOs for the timelike geodesics in Kerr-Taub-NUT spacetimes

For timelike geodesics, equations (4.26) and (4.27) for $\dot{\phi}$ and $\dot{t}$ remain unchanged; but equation (4.28) is reduced to

$$(r^2+n^2)\dot{r}^2 = 2(L-aE)^2\frac{Mr+n^2}{r^2+n^2} + E^2(r^2+n^2) - (L^2-a^2E^2) - \Delta \ . \tag{4.65}$$

The circular and associated orbits: We now turn to consideration of the radial Eq. (4.65) in general. With the reciprocal radius $u(=\frac{1}{r})$ as the independent variable and substituting $L-aE=x$, the equation takes the form

$$\begin{aligned}(1+n^2u^2)^2 \quad \dot{u}^2u^{-4} &= 2x^2u^3(M+n^2u) + (1+n^2u^2) \\ &\quad [E^2(1+n^2u^2) - (1+a^2u^2-n^2u^2-2Mu) - u^2(x^2+2aEx)] \ . \end{aligned} \tag{4.66}$$

Like the Schwarzschild, Reissner-Nordström and Kerr geometries, the circular orbits play an important role in the classification of the orbits. Besides, they are useful for some special features of the spacetimes, after all; the reason for studying the geodesics. When the values of L and E are completely arbitrary, the quartic polynomial of right hand side of Eq. (4.66) will have a triple root. The conditions for the occurrence of the triple root from the above Eq. (4.66) we get,

$$\begin{aligned} &2x^2u^3(M+n^2u) + (1+n^2u^2). \\ &[E^2(1+n^2u^2) - (1+a^2u^2-n^2u^2-2Mu) - u^2(x^2+2aEx)] = 0 \ , \end{aligned} \tag{4.67}$$

and

$$3Mx^2u^2 + M(1+3n^2u^2) + u(2E^2n^2 - a^2) - u(x^2 + 2aEx) \\ +2n^2u^3(x^2 - 2aEx + E^2n^2 + n^2 - a^2) = 0 \ . \tag{4.68}$$

Equations (4.67) and (4.68)[2] can be combined to give

$$E^2 = 1 - Mu + \frac{Mx^2u^3(1-n^2u^2) + 2x^2n^2u^4}{(1+n^2u^2)^2} \ , \tag{4.69}$$

and

$$2aExu(1+n^2u^2) = [x^2u^2(3M + 3n^2u - Mn^2u^2) - ux^2] \\ - \ (1+n^2u^2)[(a^2 - 2n^2)u - M(1-n^2u^2)] \ . \tag{4.70}$$

By eliminating E between these equations we get the following quadratic equation for x

$$x^4u^2\left[\left(u(3M + 3n^2u - Mn^2u^2) - 1\right)^2 - 4a^2u^3\left(M(1-n^2u^2) + 2n^2u\right)\right] \\ - \ 2x^2u(1+n^2u^2)\left[\left(u(3M + 3n^2u - Mn^2u^2) - 1\right)\left((a^2 - 2n^2)u - M(1-n^2u^2)\right)\right. \\ - \ \left. 2a^2u(1+n^2u^2)(Mu - 1)\right] + (1+n^2u^2)^2\left[(a^2 - 2n^2)u - M(1-n^2u^2)\right]^2 = 0 \ . \tag{4.71}$$

The discriminant "$\frac{1}{4}(b^2 - 4ac)$" of this equation is

$$4a^2u^3(1+n^2u^2)^2[M(1-n^2u^2) + 2n^2u]\Delta_u^2 \ , \tag{4.72}$$

[2]These two equations could also be obtained from the Eqs. (4.93) and (4.94) whose physical significance are discussed in page 95-97.

where,

$$\Delta_u = [1 - 2Mu + (a^2 - n^2)u^2] \ . \tag{4.73}$$

The solution of the Eq. (4.71) is

$$u^2x^2 = (1 + n^2u^2)\frac{Q_\pm\Delta_u - Q_+Q_-}{Q_+Q_-} = \frac{(1 + n^2u^2)}{Q_\mp}(\Delta_u - Q_\mp) \ , \tag{4.74}$$

where,

$$Q_+Q_- = \left[\left(u(3M + 3n^2u - Mn^2u^2) - 1\right)^2 - 4a^2u^3\left(M(1 - n^2u^2) + 2n^2u\right)\right] \ , \tag{4.75}$$

$$Q_\pm = 1 - u(3M + 3n^2u - Mn^2u^2) \pm 2a\sqrt{u^3[M(1 - n^2u^2) + 2n^2u]} \ . \tag{4.76}$$

We verify that,

$$\Delta_u - Q_\mp = u\left[a\sqrt{u} \pm \sqrt{M(1 - n^2u^2) + 2n^2u}\right]^2 \ . \tag{4.77}$$

So, the solution of x takes the simple form,

$$x = -\sqrt{\frac{1 + n^2u^2}{uQ_\mp}}\left[a\sqrt{u} \pm \sqrt{M(1 - n^2u^2) + 2n^2u}\right] \ . \tag{4.78}$$

It will appear presently that the upper sign in the foregoing equation applies to the retrograde orbits, while the lower sign applies to the direct orbits. We adhere to this convention in this whole section. Substituting the value of x in Eq. (4.69), we get

$$E = \frac{1}{\sqrt{(1 + n^2u^2)Q_\mp}}\left[1 - 2Mu - n^2u^2 \mp a\sqrt{u^3[M(1 - n^2u^2) + 2n^2u]}\right] \ , \tag{4.79}$$

and the value of L which is associated with E is

$$L = aE + x = \mp\sqrt{\frac{M(1-n^2u^2)+2n^2u}{u(1+n^2u^2)Q_\mp}}\left[1+(a^2+n^2)u^2 \pm 2a(M+n^2u)\sqrt{\frac{u^3}{M(1-n^2u^2)+2n^2u}}\right] . \quad (4.80)$$

As the manner of derivation makes it explicit, E and L given by Eqs. (4.79) and (4.80) are **Energy** and **Angular momentum** per unit mass, of a particle describing a circular orbit of reciprocal radius u. The angular velocity Ω follows from the equation

$$\Omega = \frac{\dot{\phi}}{\dot{t}} = \frac{d\phi}{dt} = \frac{aP+O\Delta}{BP+aO\Delta} = \frac{a(BE-La)+x\Delta}{B(BE-La)+ax\Delta} . \quad (4.81)$$

Substituting the values of x, L and E in the above equation we get the angular velocity of a chargeless massive test particle which is moving in a particular orbit of radius $R(=\frac{1}{u})$ in the KTN spacetime :

$$\Omega_{KTN} = \frac{\sqrt{u^3[M(1-n^2u^2)+2n^2u]}}{1+n^2u^2 \mp a\sqrt{u^3[M(1-n^2u^2)+2n^2u]}} . \quad (4.82)$$

Generally, Ω_{KTN} is also called as the **Kepler frequency** in the KTN spacetime.

The **Time period** (T) of a massive chargeless test particle which is rotating in a orbit of radius $R(=\frac{1}{u})$ can also be determined from the Kepler frequency by the simple relation between Ω and T:

$$T = \frac{2\pi}{\Omega_{KTN}} . \quad (4.83)$$

For $n = 0$, we can easily get the **Kepler frequency** in the Kerr spacetime:

$$\Omega_K = \frac{\sqrt{Mu^3}}{1 \mp a\sqrt{Mu^3}} = \frac{M^{\frac{1}{2}}}{R^{\frac{3}{2}} \mp aM^{\frac{1}{2}}} . \quad (4.84)$$

It is already noted that the upper sign is applicable for the retrograde orbits and the lower sign is applicable for the direct orbits.

The **Rotational velocity** $v^{(\phi)}$ of a chargeless massive test particle could be determined by the following equation:

$$v^{(\phi)} = e^{\psi-\nu}(\Omega - \omega) \ , \tag{4.85}$$

where, ψ, ν and ω are defined from the general axisymmetric metric [53]

$$ds^2 = -e^{2\nu}(dt)^2 + e^{2\psi}(d\phi - \omega dt)^2 + e^{2\mu_2}(dx^2)^2 + e^{2\mu_3}(dx^3)^2 \ . \tag{4.86}$$

In the above metric ψ, ν, ω, μ_2 and μ_3 are the functions of x^2 and x^3. In our case (for KTN spacetimes),

$$\begin{aligned} e^{2\psi} &= \frac{B^2 - a^2\Delta}{p_e^2} \ , \\ \omega &= \frac{2a(Mr + n^2)}{B^2 - a^2\Delta} \ , \\ e^{2\nu} &= \frac{1}{p_e^2}\left[(r^2 - 2Mr - n^2) + \frac{4a^2(Mr + n^2)^2}{B^2 - a^2\Delta}\right] \ . \end{aligned} \tag{4.87}$$

Now, substituting the above values in the Eq. (4.85), we get the **Rotational velocity** of a chargeless massive test particle which is moving in a particular orbit of radius $R(=\frac{1}{u})$ in the KTN spacetime :

$$\begin{aligned} v^{(\phi)}_{KTN} &= \frac{(B^2 - a^2\Delta)(\Omega - \omega)}{[(r^2 - 2Mr - n^2)(B^2 - a^2\Delta) + 4a^2(Mr + n^2)^2]^{\frac{1}{2}}} \ , \\ &= \frac{(B^2 - a^2\Delta)(\Omega - \omega)}{(r^2 + n^2)\sqrt{\Delta}} \ , \\ &= \frac{\mp\sqrt{u[M(1 - n^2u^2) + 2n^2u]}\,[1 + (a^2 + n^2)u^2] - 2au^2(M + n^2u)}{\sqrt{\Delta_u}\left[1 + n^2u^2 \mp a\sqrt{u^3[M(1 - n^2u^2) + 2n^2u]}\right]} \ . \end{aligned} \tag{4.88}$$

Here, a point, considered as describing a circular orbit (with the proper circumference πe^{ψ}) with an angular velocity Ω (also called the Kepler frequency) in the chosen coordinate frame, will be assigned an angular velocity,

$$e^{\psi-\nu}(\Omega-\omega)\ , \tag{4.89}$$

in the local inertial frame. Accordingly, a point which is considered as at rest in the local inertial frame (i.e., velocity components $u^{(1)}=u^{(2)}=u^{(3)}=0$), will be assigned an angular velocity ω in the coordinate frame. On this account the non-vanishing ω is said to describe as the reason of 'dragging of inertial frame'. In weak gravity regime

$$\omega \sim \frac{2J}{r^3}\ . \tag{4.90}$$

where J is the angular momentum of the spacetime.

We note that the **Effective potential** expression of a massive test particle plays many interesting roles in Gravitational Physics and also in Astrophysics. Here, we need this potential at this moment to determine the radius of the ISCO in the KTN spacetime. We know that

$$\frac{E^2-1}{2}=\frac{1}{2}\dot{r}^2+V_{eff}(r,E,L)\ , \tag{4.91}$$

where the effective potential governing the radial motion is

$$V_{eff}(r,E,L)=\frac{1}{2}\left[(E^2-1)-\frac{P^2-(r^2+n^2+O^2)\Delta}{(r^2+n^2)^2}\right]\ . \tag{4.92}$$

For $n=0$, the effective potential reduces to Eq. (15.20) of Ref. [3]. This is applicable to the Kerr geometry. An important difference is that the potentials are energy and angular momentum dependent in stationary spacetimes, i.e., Kerr, KTN etc. This does not happen in static spacetimes, i.e, Schwarzschild, Reissner-Nordström etc. In static

spacetimes, the Effective potential only depends on radial coordinate r, but not on L and E. This difference has arisen due to the involvement of 'rotational motion' in stationary spacetimes. For example, particles that fall from infinity rotating in the same direction as the spacetime (positive values of L) move in a different effective potential than initially counter-rotating particles (negative values of L). **These differences reflect, in part, the rotational frame dragging of the spinning spacetime and the test particles are dragged by its rotation.**

Many interesting properties of the orbits of particles in the equatorial plane could be explored with the radial equation(4.92) and the equations of the other components (which are already discussed) of the four velocity. We could calculate the radii of circular orbits, the shape of bound orbits etc. These are all different, depending upon whether the particle is rotating with the black hole (corotating) or in the opposite direction (counter-rotating). For instance, in the geometry of an extremal Kerr black hole ($a = M$), there is a corotating stable circular particle orbit at $r = M$ (direct ISCO) and a counterrotating stable circular orbit at $r = 9M$ (retrograde ISCO). However, as we already mentioned, for an introductory discussion it seems appropriate not to discuss on all these interesting properties but rather to focus on the one property which is most important for astrophysics, mainly for Accretion mechanism—-the binding energy of the innermost stable circular particle orbit (**ISCO**).

For a particle to describe a circular orbit at radius $r = R$, its initial radial velocity must vanish. Imposing this condition we get from Eq. (4.91)

$$\frac{E^2 - 1}{2} = V_{eff}(R, E, L) \ . \tag{4.93}$$

To stay in a circular orbit the radial acceleration must also vanish. Thus, differentiating

Eq. (4.91) with respect to r leads to the condition:

$$\frac{\partial V_{eff}(r,E,L)}{\partial r}|_{r=R} = 0 \ . \tag{4.94}$$

Stable orbits are ones for which small radial displacements away from R oscillate about it rather than accelerate away from it. Just as in newtonian mechanics, that is the condition that the effective potential must be a minimum:

$$\frac{\partial^2 V_{eff}(r,E,L)}{\partial r^2}|_{r=R} > 0 \ . \tag{4.95}$$

Eqs. (4.93-4.95) determine the ranges of E, L, R allowed for stable circular orbits in the KTN spacetime. At the ISCO, the one just on the verge of being unstable–(Eq. (4.95)) becomes an equality. The last three equations are solved to obtain the values of E, L, $R = r_{ISCO}$ that characterize the orbit. It should be mentioned here that the Eqs. (4.93) and (4.94) have been used to obtain the Eqs. (4.67) and (4.68), respectively. Now, we obtain the following from Eq. (4.95)

$$\begin{aligned}(r^2 \ &+ \ n^2)[(a^2+2aEx)(3r^2-n^2) - 2Mr^3 + 6Mrn^2 - 6n^2r^2 + 2n^4] \\ &+ \ 3x^2(r^4 - 4Mr^3 - 6r^2n^2 + 4Mrn^2 + n^4) = 0 \ .\end{aligned} \tag{4.96}$$

Substituting the values of Ex and x^2 in terms of $r = R$ in the above equation we get,

$$\begin{aligned}&2M^2R(2n^2R^2 - 3n^4 - 3R^4) + M\left[(R^6 - n^6) - 15R^2n^2(R^2-n^2) + a^2(n^4 + 6n^2R^2 - 3R^4)\right] \\ \mp \ &8a\left[MR(R^2-n^2) + 2n^2R^2\right]^{\frac{3}{2}} - 8n^2R^3(a^2+2n^2) = 0 \ .\end{aligned} \tag{4.97}$$

This is the equation to obtain the radius of the ISCO in the non-extremal KTN spacetime for timelike geodesic. Solving the above equation, we can determine the radius of the *inner-most stable circular orbit* in the non-extremal KTN spacetime. But, this equation

cannot be solved anlytically as it is actually the twelfth order equation. So, we determine the radius of the ISCO in the extremal KTN spacetime. For that we can substitute

$$a^2 = M^2 + n^2, \tag{4.98}$$

in the above equation. Defining

$$R_M = \frac{R}{M} \ , \ \ n_M = \frac{n}{M} \ , \ \ a_M = \frac{a}{M} = \sqrt{1 + n_M^2} \ \ , \tag{4.99}$$

we can rewrite the extremal ISCO equation in the KTN spacetime as

$$\begin{aligned} &2R_M(2n_M^2R_M^2 - 3n_M^4 - 3R_M^4) + \left[(R_M^6 - n_M^6) - 15R_M^2n_M^2(R_M^2 - n_M^2) + (1 + n_M^2).\right. \\ &\left.(n_M^4 + 6n_M^2R_M^2 - 3R_M^4)\right] + 8\sqrt{1 + n_M^2}\left[R_M(R_M^2 - n_M^2) + 2n_M^2R_M^2\right]^{\frac{3}{2}} \\ &-8n_M^2R_M^3(1 + 3n_M^2) = 0 \ . \end{aligned} \tag{4.100}$$

Interestingly, the solution of the above *non-trivial* equation is

$$R_M = 1 \ \text{ or, } \ R = M \ . \tag{4.101}$$

This is the radius of the ISCO as it is the smallest positive real root of the ISCO Eq. (4.100). So, in the extremal KTN spacetime, the direct ISCO radius does not depend on the value of the NUT charge. The ISCO radius is completely determined by the ADM mass of the spacetime. We note that the *horizon* in the extremal KTN spacetime is at $R = M$. So, we can say that at $R = M$, the direct ISCO is on the *horizon* in the extremal KTN spacetime. It is further observed that the timelike circular geodesics and null circular geodesics coalesce into a single zero energy trajectory (both are on the $R = M$)

$$E = 0 \ . \tag{4.102}$$

Thus, the geodesic on the horizon must coincide with the principal null geodesic generator. The existence of a timelike circular orbit turning into the null geodesic generator on the event horizon (nulllike) is a peculiar feature of the extremal KTN spacetime. It is not only that the energy ($E = 0$) vanishes on the ISCO in the KTN spacetime but angular momentum ($L = 0$) also vanishes on that. The same thing also happens in case of the Kerr geometry.

Substituting $n = 0$, we can recover the expressions of Ω, $v^{(\phi)}$ in Kerr spacetimes. These were already described by Chandrasekhar [53] in details. The ISCO equation in the Kerr spacetime is

$$R^2 - 6MR \mp 8a\sqrt{MR} - 3a^2 = 0 \ . \tag{4.103}$$

For the extremal Kerr spacetime we can put $a = M$ in the above equation and solving the above equation we get,

$$\begin{aligned} R_{directISCO} &= M \ , \\ R_{retrogradeISCO} &= 9M \ . \end{aligned} \tag{4.104}$$

ISCOs in Taub-NUT spacetimes :

To get various useful expressions in Taub-NUT spacetimes, we should first take $a = 0$. We don't want to reiterate the whole process for Taub-NUT spacetimes. This is the same as in the previous section in which we have done things in detail for KTN spacetimes. The **Energy** per unit mass (E_{TN}) and the **Angular momentum** per unit mass (L_{TN}) of a chargeless massive test particle which is moving in a particular orbit of radius $r = \frac{1}{u}$

in the Taub-NUT spacetime, are

$$E_{TN} = \frac{(1 - 2Mu - n^2u^2)}{\sqrt{(1 + n^2u^2)Q_{TN}}} \ , \tag{4.105}$$

and

$$L_{TN} = \sqrt{\frac{(1 + n^2u^2)[M(1 - n^2u^2) + 2n^2u]}{uQ_{TN}}} \ , \tag{4.106}$$

where,

$$Q_{TN} = 1 - u(3M + 3n^2u - Mn^2u^2) \ . \tag{4.107}$$

Now, we can find the angular velocity Ω_{TN} of a chargeless massive test particle which is moving in a particular orbit of radius $r = \frac{1}{u}$ at the Taub-NUT spacetime:

$$\Omega_{TN} = \frac{\sqrt{u^3[M(1 - n^2u^2) + 2n^2u]}}{(1 + n^2u^2)} \ . \tag{4.108}$$

For $n = 0$, we can recover the well known *Kepler frequency* for non-rotating star whose geometry is described by Schwarzschild metric. The **Kepler frequency** which is a very useful parameter in relativistic astrophysics, is defined as (substituting $n = 0$ in Eq. (4.108))

$$\Omega^2_{Kep} = Mu^3 = \frac{M}{R^3} \ , \tag{4.109}$$

where, M is the mass of the star, R is the distance of the satellite from the centre of the star and Ω_{Kep} is the uniform angular velocity of the satellite, moving in a circular orbit of radius R around the star.

The **Rotational velocity** $v^{(\phi)}_{TN}$ of a chargeless massive test particle which is moving

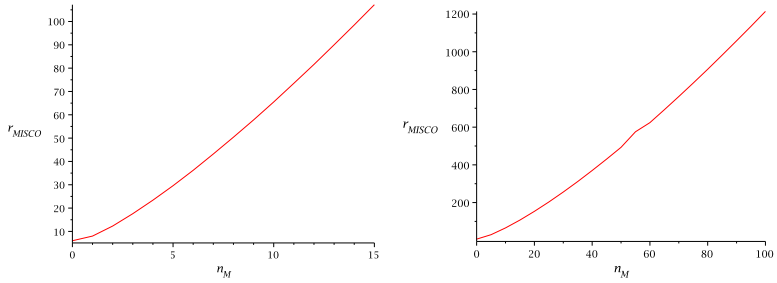

(a) n_M varies from 0 to 15 (b) n_M varies from 0 to 100

Figure 4.13: *Plot of radius of direct ISCO (r_{MISCO}) along y axis vs NUT charge n_M along x axis [41].*

in a particular orbit of radius $r = \frac{1}{u}$ at the Taub-NUT spacetime:

$$v_{TN}^{(\phi)} = \sqrt{\frac{u[M(1-n^2u^2)+2n^2u]}{\Delta_u}} \ . \tag{4.110}$$

Finally, the direct ISCO equation in Taub-NUT spacetimes can be expressed as

$$2r_M(2n_M^2r_M^2 - 3n_M^4 - 3r_M^4) + \left[(r_M^6 - n_M^6) - 15r_M^2n_M^2(r_M^2 - n_M^2)\right] - 16n_M^4r_M^3 = 0 \tag{4.111}$$

It is a sixth order equation which is very difficult to solve analytically. So, we plot the n_M values of r_{MISCO} as a function of n_M in Fig. 4.13. In panel(a) of Fig. 4.13 n_M varies from 0 to 15 whereas it varies from 0 to 100 in panel(b). We can see from the plots (Fig. 4.13) and also from the Table 4.1 that in the Taub-NUT spacetime, the radius of the direct ISCO is increasing with the increasing NUT charge. We do not see this special feature in case of the extremal KTN spacetimes.

Even though we can solve the ISCO equation in Taub-NUT spacetimes with the assumption $r_M > n_M$. In this case, Eq. (4.111) reduces to

$$r_M^3 - 6r_M^2 - 15r_Mn_M^2 - 16n_M^4 = 0 \ . \tag{4.112}$$

NUT charge (n_M)	Radius of horizon (r_{Mhor})	Radius of ISCO (r_{MISCO})	NUT charge (n_M)	Radius of horizon (r_{Mhor})	Radius of ISCO (r_{MISCO})
0	2	6	55	56	558
5	6	29	60	61	624
10	11	65	65	66	693
15	16	107	70	71	763
20	21	153	75	76	834
25	26	203	80	81	907
30	31	256	85	86	982
35	36	312	90	91	1058
40	41	370	95	96	1135
45	46	431	100	101	1214
50	51	493	500	501	10127

Table 4.1: Comparison between the radius of the horizon (r_{Mhor}) and the radius of the ISCO (r_{MISCO}) at Taub-NUT spacetimes [41].

Solving the above equation, we get

$$r_M|_{r>n} = 2 + \frac{1}{\alpha^{\frac{1}{3}}}[\alpha^{\frac{2}{3}} + 5n_M^2 + 4] \ , \tag{4.113}$$

where,

$$\alpha = 8n_M^4 + 15n_M^2 + 8 + n_M^2\sqrt{64n_M^4 + 115n_M^2 + 53} \ . \tag{4.114}$$

The value of r_M determines the radius of the direct ISCO in the Taub-NUT spacetime for timelike geodesic in case of the radius of the Taub-NUT spacetime is much greater than the value of the NUT charge $n_M < r_M$.

For, $n_M = 0$, we can recover $r_M = 6$ as the radius of the ISCO in Schwarzschild spacetime.

We can make an another assumption taking $r < n$ which helps to reduce the Eq. (4.111) as

$$16r_M^3 - 15r_M^2 + 6r_M + n_M^2 = 0 \ . \tag{4.115}$$

Solving this equation we get,

$$r_M|_{r<n} = \frac{5}{16} + \frac{1}{16\beta}[\beta^{\frac{2}{3}} - 7] \ , \tag{4.116}$$

where,

$$\beta = 16\sqrt{64n_M^4 + 115n_M^2 + 53} - 128n_M^2 - 115 \ . \tag{4.117}$$

The value of r_M determines the radius of the direct ISCO in the Taub-NUT spacetime for timelike geodesic when the radius of the Taub-NUT spacetime is much less than the value of the NUT charge $n_M > r_M$.

ISCOs in massless NUT spacetimes :

In massless NUT spacetimes, the **Energy** of a chargeless massive test particle which is moving in a particular orbit of radius $r = \frac{1}{u}$ is

$$E_{0TN} = \frac{(1 - n^2u^2)}{\sqrt{(1 + n^2u^2)(1 - 3n^2u^2)}} \ . \tag{4.118}$$

and, the **Angular momentum** of this particle will be

$$L_{0TN} = \sqrt{\frac{2n^2(1 + n^2u^2)}{(1 - 3n^2u^2)}} \ , \tag{4.119}$$

due to

$$Q_{0TN} = (1 - 3n^2u^2) \ . \tag{4.120}$$

Now, we can find the **Kepler frequency** Ω_{0TN} of a chargeless massive test particle which

is moving in a particular orbit of radius $r = \frac{1}{u}$ at the massless NUT spacetime:

$$\Omega_{0TN} = \frac{\sqrt{2}nu^2}{(1+n^2u^2)} \ , \tag{4.121}$$

and, the **Rotational velocity** $v_{0TN}^{(\phi)}$ of this test particle at the massless NUT spacetime will be

$$v_{0TN}^{(\phi)} = nu\sqrt{\frac{2}{(1-n^2u^2)}} \ . \tag{4.122}$$

The expressions of all astronomical observables are valid for $\frac{1}{u} = r > \sqrt{3}n$ as L and E would be complex for $r < \sqrt{3}n$ and diverges for $r = \sqrt{3}n$. Finally, the direct ISCO equation in massless NUT spacetimes can be expressed as

$$16n^4r^3 = 0 \ . \tag{4.123}$$

As $n \neq 0$, we get

$$r = 0 \ . \tag{4.124}$$

This means that the innermost stable circular orbit is in the centre of the massless NUT spacetime. This is unphysical, because, in the classification of Ellis and Schmidt [55, 56] the singularity of the Taub-NUT spacetime has been termed as quasiregular singularity, since the curvature remains finite (see also Ref. [57, 58]). As $r = n$ has the singularity in the massless Taub-NUT spacetime, all geodesics are terminated at $r = n$ [32] before reaching $r = 0$, which may be regarded as a *spacelike* surface. So, we cannot go beyond $r < n$ to determine the ISCO. Apparently, the curvature of the Taub-NUT spacetime shows that $r = n$ is not a singular surface but in reality, $\theta = 0, \pi$ are the singularities in Taub-NUT spacetimes, as the curvature diverges for $\theta = 0$ and π [47]. Thus, the final

conclusion is that there is no physically reliable innermost stable circular orbit in the massless NUT spacetime for timelike geodesic.

4.6 Summary

We have shown that the LT precession in KTN and Taub-NUT spacetimes are quite different than the LT precession in other spacetimes. Other vacuum solutions of Einstein equation do not show this type of strange feature in the LT precession or frame-dragging effect. It has been discussed that this strangeness in the KTN spacetime is due to only the presence of the NUT parameter or (gravito)magnetic monopoles. Remarkably, it (frame-dragging effect in the KTN spacetime) has an apparent similarity with the frame-dragging effect inside the rotating neutron star. Exact frame-dragging effect inside the rotating neutron star has recently been derived and discussed in detail by Modak, Bandyopadhyay and myself [43] but this is the interior solution of the Einstein equation, not the vacuum solution. In the case of the interior of a pulsar, the LT precession shows the same 'anomaly' like the KTN spacetime but there is also an another basic difference: the anomaly appears in the LT precession rate in the KTN spacetime along the pole but it appears along the equator in the case of a pulsar. The basic features of the plots are same for both the cases. We do not know if there is any connection or not in these two spacetimes. We have already stated that Lynden-Bell and Nouri-Zonoz [29] first highlighted about the observational possibilities for NUT charges or (gravito)magnetic monopoles and they claimed that the signatures of such spacetime might be found in the spectra of supernovae, quasars, or active galactic nuclei. Is there any possibility to find the (gravito)magnetic monopoles inside the rotating neutron star or there are some other reasons for this anomaly? It would be worth investigating the answer to this question.

Side by side, we have calculated the radius of the innermost-stable circular orbit (ISCO) exactly for extremal KTN, Taub-NUT, massless Taub-NUT spacetimes. We have

also calculated some other important astronomical observables (i.e., $L, E, v^{(\phi)}, \Omega_{Kep}$) for KTN (non-extremal and extremal both), Taub-NUT and massless Taub-NUT spacetimes. All the ISCOs of the non-extremal KTN, Taub-NUT and massless Taub-NUT lie on the timelike surface but the ISCOs of the extremal KTN spacetime (both for nulllike and timelike geodesics) lie on the horizons, i.e, on the lightlike surface. We cannot solve the ISCO equation of the non-extremal KTN spacetime analytically. However, one can see intuitively from the ISCO equation that the ISCO must belong to the timelike region, i.e., $r_{ISCO} > r_+$ where $r_+ = M + \sqrt{M^2 + n^2 - a^2}$. The Kerr parameter ($a_k$) of the extremal Kerr metric can take the highest value as $a_K = M$ but it takes $a_{KTN} = \sqrt{M^2 + n^2}$ in case of the extremal KTN spacetime. So, the highest angular momentum of a Kerr spacetime is $J_K = M^2$ but it will be $J_{KTN} = M\sqrt{M^2 + n^2}$ in the case of the extremal KTN spacetime. Thus, the ratio between these two is

$$\frac{J_K}{J_{KTN}} = \frac{a_K}{a_{KTN}} = \frac{M}{\sqrt{M^2 + n^2}} \ . \tag{4.125}$$

But the interesting thing is that the radii of the ISCOs in the extremal KTN spacetime is the same as $R = M$. Thus,

$$\frac{r_{KISCO}}{r_{KTNISCO}} = 1 \ . \tag{4.126}$$

It is quite remarkable that the NUT charge which appears in the expression of maximal angular momentum (J) has no effect for determining the radius of the ISCO in extremal KTN spacetimes. So, the radius of the ISCO is independent of NUT charge n. We know that the radius of the ISCO in extremal Kerr spacetime is M [53] for both null and timelike geodesics. It is expected that if a new parameter appears in the Kerr geometry, the ISCO should be altered away from M. But, this is not happening in the extremal KTN spacetime though the Kerr metric is modified with a new parameter n as KTN spacetime. This non-dependence of ISCO behaviour in the extremal case is somewhat mysterious. The NUT parameter in the extremal KTN spacetime behaves like a *shield*,

so that the ISCO could not go away from the horizon. Another interesting thing is that the geodesic on the horizon coincides with the principal null geodesic generator for both extremal Kerr and extremal KTN spacetimes.

In the very non-extremal spacetime, when the Kerr parameter vanishes, i.e., in case of the Taub-NUT spacetime, the ISCO is shifted to $M + 2(M^2 + n^2)^{1/2} \cos\left[\frac{1}{3}\tan^{-1}\left(\frac{n}{M}\right)\right]$ for null geodesics. For timelike geodesics, the ISCO of the Taub-NUT spacetime is also shifted from null surface (in the case of extremal KTN spacetime) to timelike surface. Another thing is that the massless NUT spacetime does not hold any inner stable circular orbit for timelike geodesics. But, it holds an ISCO at $\sqrt{3}n$ (which is outside the *horizon*) for null geodesics.

There are additional avenues of further work currently being investigated for an understanding of the thin disks accretion mechanism in the KTN spacetime, applicable to some special candidates (like, supernovae, quasars, or active galactic nuclei etc.) which are of astrophysical importance. One could also investigate the exact LT precession rate of a test particle which is rotating on the ISCO in strong gravity regime of extremal KTN spacetimes. This is very important in accretion mechanism as accretion disk is mainly formed near the ISCO which lies in the strong gravity regime. We have derived the exact LT precession rates in the KTN, Taub-NUT and massless Taub-NUT spacetimes but this formula is valid only in the timelike spacetime; it is not valid on the horizon, i.e., null surface. Thus, it is not possible to derive the exact LT precession rate on the ISCO of the extremal KTN spacetime by that formula. Again, we could not also able to solve the ISCO equations of non-extremal Kerr (see Eq. (135) of Ref. [53]), non-extremal KTN (see Eq. 4.97) and Taub-NUT (see Eq. 4.111) spacetimes for *timelike geodesics*, analytically. Thus, we could not get the LT effect on those particular ISCOs and we have to wait for further progression of it. But, it would be quite helpful for accretion mechanism in the future.

Chapter 5

Dragging of inertial frames inside the rotating neutron stars

5.1 Introduction

Compact astrophysical objects such as neutron stars and black holes are the laboratories for the study of Einstein's general relativity in strong gravitational fields. The frame-dragging is one such important general relativistic effect as demonstrated by Lense and Thirring [1]. We have already stated in Chapter 1 that a stationary spacetime with angular momentum shows an effect by which the locally inertial frames are dragged along the rotating spacetime. This makes any test gyroscope in such spacetime precess with a certain frequency called the frame-dragging frequency or the LT precession frequency (Ω_{LT}). The LT frequency is proportional to the angular momentum and compactness of the rotating astrophysical compact object. This effect for a test gyroscope had been calculated and was shown to fall with the inverse cube of the distance of the test gyroscope from the source and vanishes at large enough distances where the curvature effects are small. The precession frequency is thus expected to be larger near the surface of a neutron star and in its interior, rather than at large distance from the star.

The precise mass measurement of PSR J0348+0432 confirmed the existence of a massive neutron star ($> 2M_{\odot}$) [59]. It is also known that some of them are observed to possess very high angular velocities. Hence the spacetime curvature would be much higher in the surroundings of those massive neutron stars and the frame dragging effect also becomes very significant in the strong gravitational fields of those rotating neutron stars. It should be noted that the inertial frames are dragged not only outside but also inside the rotating neutron stars.

The theoretical prescription to determine the rate of the frame-dragging precession inside the rotating neutron star was first given by Hartle [60]. In this formalism, one can estimate the frame-dragging precession rate inside a slowly rotating ($\Omega R << c$, where R is the radius of the pulsar, c is the speed of the light in vacuum) neutron star. The final expression of the frame-dragging precession rate depends solely on r, the distance from the centre of the star, due to the slow rotation approximation, in Hartle's formalism. It was observed that the frame-dragging frequency was higher at the centre of the star than the frame dragging frequency at the surface. The maximum frame dragging frequency at the centre ($r = 0$) would never exceed the frequency of the rotating neutron star. The frame-dragging effect was applied to various astrophysical problems using Hartle's formalism. Hartle studied this effect on the equilibrium structures of rotating neutron stars [61]. The impact of frame dragging on the Kepler frequency was investigated by Glendenning and Weber [62]. It was also demonstrated how this effect might influence the moment of inertia of a rotating neutron star [63]. Furthermore, Morsink and Stella studied the role of frame dragging in explaining the Quasi Periodic Oscillations of accreting neutron stars [64]. Morsink and Stella estimated the precession frequency ν_p of the disk's orbital plane about the star's axis of symmetry as the difference between the frequencies of oscillations of the particle along the longitude and latitude ($2\pi\nu_p = d\phi/dt - d\theta/dt$) observed at infinity. This expression contains the total precession frequency of the disk's orbital plane due to the LT effect as well as the star's oblateness. Their calculation introduced zero angular

momentum observer (ZAMO) and the precession frequency ν_p was observed at infinity. It was found that the LT frequency was proportional to the ZAMO frequency on the equatorial plane in the slow rotation limit. This is similar to Hartle's formalism [60] where the angular velocity ($d\phi/dt$) acquired by an observer who falls freely from infinity to the point (r, θ), is taken as *the rate of rotation of the inertial frame at that point relative to the distant stars.*

In this chapter we derive the exact LT precession frequency (Ω_{LT}) which is measured by a Copernican observer of a gyroscope such as the Gravity Probe B satellite in a realistic orbit [3]. In this case, Ω_{LT} would not only be the function of ω but a complicated function of other metric components also even in the slow rotation limit.

We should note that inside the rapidly rotating stars, one should not a priori expect the similar variation of the precession rates along the equatorial and polar plane. Thus the frame-dragging frequency should depend also on the colatitude (θ) of the position of the test gyroscope. This did not arise in the formalism of Hartle due to the slow-rotation limit. We also note that the LT precession must depend on both the radial distance (r) and the colatitude (θ) (see Eq. (1.23)) in very weak gravitational fields (far away from the surface of the rotating object).

The exact LT precession rate in strongly curved stationary spacetime has been discussed in detail in Chapter 2. Later, this formulation has been applied in various stationary and axisymmetric spacetimes (see Chapter 3). Our main motivation is to compute the exact LT precession rate inside the rotating neutron star. In this case, we avoid all types of approximations and assumptions to obtain the exact LT precession rate inside the rotating neutron stars.

Thus, this chapter is organized as follows. In section 5.2 we present the basic equations of the frame-dragging effect inside the rotating neutron stars. The numerical method, which has been adopted in this chapter, is discussed in section 5.3. We discuss our results in section 5.4. Finally we conclude in section 5.5 with a summary.

5.2 Basic equations of frame-dragging effect inside rotating neutron stars

The rotating equilibrium models considered here are stationary and axisymmetric. Thus we can write the metric inside the rotating neutron star as the following Komatsu-Eriguchi-Hachisu (KEH) [65] form:

$$ds^2 = -e^{\gamma+\sigma}dt^2 + e^{2\alpha}(dr^2 + r^2 d\theta^2) + e^{\gamma-\sigma}r^2\sin^2\theta(d\phi - \omega dt)^2 \ , \tag{5.1}$$

where γ, σ, α, ω are the functions of r and θ only. In the whole thesis we have used the geometrized unit ($G = c = 1$). We assume that the matter source is a perfect fluid with a stress-energy tensor given by

$$T^{\mu\nu} = (\rho_0 + \rho_i + P)u^\mu u^\nu + Pg^{\mu\nu} \ , \tag{5.2}$$

where ρ_0 is the rest energy density, ρ_i is the internal energy density, P is the pressure and u^μ is the matter four velocity. We are further assuming that there is no meridional circulation of the matter so that the four-velocity u^μ is simply a linear combination of time and angular Killing vectors. Now, we have to calculate the frame-dragging rate based on the above metric and this will gives us the exact frame-dragging rate inside a rotating neutron star.

The vector field corresponding to the LT precession co-vector has already been expressed in Eq. (2.30) as

$$\Omega_{LT} = \frac{1}{2}\frac{\epsilon_{ijl}}{\sqrt{-g}}\left[g_{0i,j}\left(\partial_l - \frac{g_{0l}}{g_{00}}\partial_0\right) - \frac{g_{0i}}{g_{00}}g_{00,j}\partial_l\right] \ , \tag{5.3}$$

and for the axisymmetric spacetime and in orthonormal basis (as the only non-vanishing component is $g_{0i} = g_{0\phi}$, $i = \phi$ and $j, l = r, \theta$) with our choice of polar co-ordinates, the

above equation is reduced to (for detailed calculation see section 2.3):

$$\vec{\Omega}_{LT} = \frac{1}{2\sqrt{-g}}\left[\sqrt{g_{rr}}\left(g_{0\phi,\theta} - \frac{g_{0\phi}}{g_{00}}g_{00,\theta}\right)\hat{r} + \sqrt{g_{\theta\theta}}\left(g_{0\phi,r} - \frac{g_{0\phi}}{g_{00}}g_{00,r}\right)\hat{\theta}\right] \ , \tag{5.4}$$

where $\hat{\theta}$ is the unit vector along the direction θ and $\hat{r}$ is the unit vector along the direction r. Again, we note that the above formulation is valid only in the timelike spacetimes, not in the lightlike or spacelike regions.

Now, we can apply the above Eq. (5.4) to determine the exact frame-dragging rate inside the rotating neutron star of which the metric could be determined from the line-element (5.1). The various metric components can be read off from the metric. Likewise,

$$\sqrt{-g} = r^2 e^{2\alpha+\gamma}\sin\theta \ , \tag{5.5}$$

In orthonormal coordinate basis, the exact LT precession rate inside the rotating neutron star is:

$$\begin{aligned}\vec{\Omega}_{LT} &= \frac{e^{-(\alpha+\sigma)}}{2(\omega^2 r^2\sin^2\theta - e^{2\sigma})}.\Big[\sin\theta[r^3\omega^2\omega_{,r}\sin^2\theta + e^{2\sigma}(2\omega + r\omega_{,r} - 2\omega r\sigma_{,r})]\hat{\theta} \\ &+ [r^2\omega^2\omega_{,\theta}\sin^3\theta + e^{2\sigma}(2\omega\cos\theta + \omega_{,\theta}\sin\theta - 2\omega\sigma_{,\theta}\sin\theta)]\hat{r}\Big] \ ,\end{aligned} \tag{5.6}$$

and the modulus of the above LT precession rate is

$$\begin{aligned}\Omega_{LT} &= |\vec{\Omega}_{LT}(r,\theta)| = \frac{e^{-(\alpha+\sigma)}}{2(\omega^2 r^2\sin^2\theta - e^{2\sigma})}.\Big[\sin^2\theta[r^3\omega^2\omega_{,r}\sin^2\theta + e^{2\sigma}(2\omega + r\omega_{,r} - 2\omega r\sigma_{,r})]^2 \\ &+ [r^2\omega^2\omega_{,\theta}\sin^3\theta + e^{2\sigma}(2\omega\cos\theta + \omega_{,\theta}\sin\theta - 2\omega\sigma_{,\theta}\sin\theta)]^2\Big]^{\frac{1}{2}} \ .\end{aligned} \tag{5.7}$$

As a vector quantity the expression of $\vec{\Omega}_{LT}$ (Eq. (5.6)) depends on the coordinate frame (i.e. polar coordinates (r,θ) which is used here) but the modulus of $\vec{\Omega}_{LT}$ or $|\vec{\Omega}_{LT}|$ (Eq. 5.7) must be coordinate frame independent. Here, we use only the modulus of Ω_{LT} in the rest of this chapter.

To calculate the frame-dragging precession frequency at the centre of the neutron star we substitute $r = 0$ in Eq. (5.7) and obtain

$$\Omega_{LT}|_{r=0} = \left[\frac{e^{-(\alpha+\sigma)}}{2}\left[4\omega^2 + (\omega_{,\theta} - 2\omega\sigma_{,\theta})^2 \sin^2\theta + 4\omega\cos\theta\sin\theta(\omega_{,\theta} - 2\omega\sigma_{,\theta})\right]^{\frac{1}{2}}\right]_{|r=0} . \quad (5.8)$$

Solving numerically $\omega_{,\theta}$ and $\sigma_{,\theta}$ at the centre we get the value zero for both of them. Thus, we obtain the frame-dragging precession rate

$$\Omega_{LT}|_{r=0} = \omega e^{-(\alpha+\sigma)}|_{r=0} \ , \quad (5.9)$$

at the center ($r = 0$) of a rotating neutron star.

Following KEH we can write the general relativistic field equations determining σ, γ and ω as

$$\Delta\left[\sigma e^{\frac{\gamma}{2}}\right] = S_\sigma(r,\mu) \ , \quad (5.10)$$

$$\left(\Delta + \frac{1}{r}\partial_r - \frac{\mu}{r^2}\partial_\mu\right)\left[\gamma e^{\frac{\gamma}{2}}\right] = S_\gamma(r,\mu) \ , \quad (5.11)$$

$$\left(\Delta + \frac{2}{r}\partial_r - \frac{2\mu}{r^2}\partial_\mu\right)\left[\omega e^{\frac{\gamma}{2}-\sigma}\right] = S_\omega(r,\mu) \ , \quad (5.12)$$

where

$$\Delta \equiv \partial_r^2 + \frac{2}{r}\partial_r + \frac{1-\mu^2}{r^2}\partial_\mu^2 - \frac{2\mu}{r^2}\partial_\mu + \frac{1}{r^2(1-\mu^2)}\partial_\phi^2 \ , \quad (5.13)$$

is the flat-space spherical coordinate Laplacian, $\mu = \cos\theta$ and $S_\sigma, S_\gamma, S_\omega$ are the effective source terms that include the nonlinear and coupling terms. The effective source terms are given by

$$S_\sigma(r,\mu) = e^{\gamma/2}\left\{8\pi(\rho_0+\rho_i+P)e^{2\alpha}\frac{1+v^2}{1-v^2}+r^2(1-\mu^2)e^{-2\sigma}\left[\omega_{,r}^2+\frac{1-\mu^2}{r^2}\omega_{,\mu}^2\right]+\frac{1}{r}\gamma_{,r}-\frac{\mu}{r^2}\gamma_{,\mu}\right.$$

$$\left.+\frac{\sigma}{2}\left[16\pi Pe^{2\alpha}-\frac{1}{r}\gamma_{,r}+\frac{\mu}{r^2}\gamma_{,\mu}-\frac{1}{2}\gamma_{,r}^2-\frac{1-\mu^2}{2r^2}\gamma_{,\mu}^2\right]\right\}\ , \tag{5.14}$$

$$S_\gamma(r,\mu) = e^{\gamma/2}\left[16\pi e^{2\alpha}P+\frac{\gamma}{2}\left(16\pi e^{2\alpha}P-\frac{1}{2}\gamma_{,r}^2-\frac{1-\mu^2}{2r^2}\gamma_{,\mu}^2\right)\right]\ , \tag{5.15}$$

$$\begin{aligned}S_\omega(r,\mu) &= e^{\gamma/2-\sigma}\left\{-16\pi\frac{(\rho_0+\rho_i+P)(\Omega-\omega)}{1-v^2}e^{2\alpha}+\omega\left[-8\pi\frac{(\rho_0+\rho_i)(1+v^2)+2Pv^2}{1-v^2}e^{2\alpha}\right.\right.\\ &- \frac{1}{r}\left(\frac{1}{2}\gamma_{,r}+2\sigma_{,r}\right)+\frac{\mu}{r^2}\left(\frac{1}{2}\gamma_{,\mu}+2\sigma_{,\mu}\right)+\sigma_{,r}^2-\frac{1}{4}\gamma_{,r}^2+\frac{1-\mu^2}{4r^2}(\gamma_{,\mu}^2+4\sigma_{,\mu}^2)\\ &- \left.\left.r^2(1-\mu^2)e^{-2\sigma}\left(\omega_{,r}^2+\frac{1-\mu^2}{r^2}\omega_{,\mu}^2\right)\right]\right\}\ ,\end{aligned} \tag{5.16}$$

where Ω is the angular velocity of the matter as measured at infinity and v is the proper velocity of the matter with respect to a zero angular momentum observer. The proper velocity of the matter is given by

$$v=(\Omega-\omega)re^{-\sigma}\sin\theta\ , \tag{5.17}$$

and the coordinate components of the four-velocity of the matter can be written as

$$u^\mu=\frac{e^{-(\sigma+\gamma)/2}}{\sqrt{1-v^2}}[1,0,0,\Omega]\ . \tag{5.18}$$

Following Cook, Shapiro, Teukolsky [66] we can write another field equation which

determines α and is given by

$$\alpha_{,\mu} = -\frac{1}{2}(\gamma_{,\mu} + \sigma_{,\mu}) - \left\{(1-\mu^2)(1+r\gamma_{,r})^2 + [\mu - (1-\mu^2)\gamma_{,\mu}]^2\right\}^{-1}$$

$$\left\{\frac{1}{2}\left[r^2(\gamma_{,rr} + \gamma_{,r}^2) - (1-\mu^2)(\gamma_{,\mu}^2 + \gamma_{,\mu\mu})\right][-\mu + (1-\mu^2)\gamma_{,\mu}] + \frac{3}{2}\mu\gamma_{,\mu}[-\mu + (1-\mu^2)\gamma_{,\mu}]\right.$$

$$+\frac{1}{4}[-\mu + (1-\mu^2)\gamma_{,\mu}]\left[r^2(\gamma_{,r} + \sigma_{,r})^2 - (1-\mu^2)(\gamma_{,\mu} + \sigma_{,\mu})^2\right] + r\gamma_{,r}\left[\frac{\mu}{2} + \mu r\gamma_{,r} + \frac{(1-\mu^2)\gamma_{,\mu}}{2}\right]$$

$$-(1-\mu^2)r(1+r\gamma_{,r})\left[\gamma_{,r\mu} + \gamma_{,\mu}\gamma_{,r} + \frac{1}{2}(\gamma_{,\mu} + \sigma_{,\mu})(\gamma_{,r} + \sigma_{,r})\right] + \frac{1}{4}(1-\mu^2)e^{-2\sigma}.$$

$$\left.\left[r^4\mu\omega_{,r}^2 + (1-\mu^2)[2r^3\omega_{,r}\omega_{,\mu} - \mu r^2\omega_{,\mu}^2 + 2r^4\gamma_{,r}\omega_{,r}\omega_{,\mu}] - r^2(1-\mu^2)\gamma_{,\mu}[r^2\omega_{,r}^2 - (1-\mu^2)\omega_{,\mu}^2]\right]\right\} \ . \tag{5.19}$$

5.3 Numerical method

Here we adopt the rotating neutron star (`rns`) code based on the KEH [65] method and written by Stergioulas [67] to obtain the frame-dragging rate inside the rotating neutron stars. The equations for the gravitational and matter fields were solved on a discrete grid using a combination of integral and finite difference techniques. The computational domain of the problem is $0 \leq r \leq \infty$ and $0 \leq \mu \leq 1$. It is easy to deal with finite radius rather than the infinite domain via a coordinate transformation to a new radial coordinate s which covers the infinite radial span in a finite coordinate interval $0 \leq s \leq 1$. This new radial coordinate s is defined by

$$r = r_e.\frac{s}{1-s} \ . \tag{5.20}$$

Thus, $s = \frac{1}{2}$ represents the radius of the equator (r_e) of the pulsar and $s = 1$ represents the infinity.

The three elliptical field equations (5.10)-(5.12) were solved by an integral Green's function approach following the KEH [65]. Taking into account the equatorial and axial symmetry in the configurations we can find the three metric coefficients σ, γ, ω which can be written as [66]

$$\begin{aligned}
\sigma(s,\mu) &= -e^{-\frac{\gamma}{2}} \sum_{n=0}^{\infty} P_{2n}(\mu) \left[\left(\frac{1-s}{s} \right)^{2n+1} \int_0^s \frac{s'^{2n} ds'}{(1-s')^{2n+2}} \int_0^1 d\mu' P_{2n}(\mu') \bar{S}_\sigma(s',\mu') \right. \\
&+ \left. \left(\frac{s}{1-s} \right)^{2n} \int_s^1 \frac{(1-s')^{2n-1} ds'}{s'^{2n+1}} \int_0^1 d\mu' P_{2n}(\mu') \bar{S}_\sigma(s',\mu') \right] , \qquad (5.21) \\
\gamma(s,\mu) &= -\frac{2e^{-\frac{\gamma}{2}}}{\pi} \sum_{n=1}^{\infty} \frac{\sin[(2n-1)\theta]}{(2n-1)\sin\theta} \left[\left(\frac{1-s}{s} \right)^{2n} \int_0^s \frac{s'^{2n-1} ds'}{(1-s')^{2n+1}} \int_0^1 d\mu' \sin[(2n-1)\theta'] \bar{S}_\gamma(s',\mu') \right. \\
&+ \left. \left(\frac{s}{1-s} \right)^{2n-2} \int_s^1 \frac{(1-s')^{2n-3} ds'}{s'^{2n-1}} \int_0^1 d\mu' \sin[(2n-1)\theta'] \bar{S}_\gamma(s',\mu') \right] , \qquad (5.22) \\
\hat{\omega}(s,\mu) &\equiv r_e \omega(s,\mu) = -e^{(\sigma - \frac{\gamma}{2})} \sum_{n=1}^{\infty} \frac{P^1_{2n-1}(\mu)}{2n(2n-1)\sin\theta}. \\
&\left[\left(\frac{1-s}{s} \right)^{2n+1} \int_0^s \frac{s'^{2n} ds'}{(1-s')^{2n+2}} \int_0^1 d\mu' \sin\theta' P^1_{2n-1}(\mu') \bar{S}_{\hat{\omega}}(s',\mu') \right. \\
&+ \left. \left(\frac{s}{1-s} \right)^{2n-2} \int_s^1 \frac{(1-s')^{2n-3} ds'}{s'^{2n-1}} \int_0^1 d\mu' \sin\theta' P^1_{2n-1}(\mu') \bar{S}_{\hat{\omega}}(s',\mu') \right] , \qquad (5.23)
\end{aligned}$$

where $P_n(\mu)$ are the Legendre polynomials and $P_n^m(\mu)$ are the associated Legendre polynomials and $\sin(n\theta)$ is a function of μ through $\theta = \cos^{-1}\mu$. The effective sources could be defined as

$$\bar{S}_\sigma(s,\mu) = r^2 S_\sigma(s,\mu) , \qquad (5.24)$$

$$\bar{S}_\gamma(s,\mu) = r^2 S_\gamma(s,\mu) , \qquad (5.25)$$

$$\bar{S}_{\hat{\omega}}(s,\mu) = r_e r^2 S_\omega(s,\mu) . \qquad (5.26)$$

The advantages of this Green's function approach for solving the elliptic field equations is that the asymptotic conditions on σ, γ, ω are imposed automatically. The numerical integration of Eqs. (5.21)-(5.23) is straightforward. These integrations are solved using the `rns` code and we obtain the value of frame-dragging precession rate inside the rotating neutron star using the equation (5.7).

5.3.1 Equation of state (EoS) of dense matter

Recent observations of PSR J0348+0432 have reported the measurement of a 2.01±0.04 $M_\odot$ neutron star [59]. This is the most accurately measured highest neutron star mass so far. The accurately measured neutron star mass is a direct probe of dense matter in its interior. This measured mass puts the strong constraint on the EoS.

Equations of state of dense matter are used as inputs in the calculation of frame-dragging in neutron star interior. We adopt three equations of state in this calculation. We are considering equations of state of β-equilibrated [68] hadronic matter. The chiral EoS is based on the QCD motivated chiral $SU(3)_L \times SU(3)_R$ model [69] and includes hyperons. We exploit the density dependent (DD) relativistic mean model to construct the DD2 EoS [70]. Here the nucleon-nucleon interaction is mediated by the exchange of mesons and the density dependent nucleon-meson couplings are obtained by fitting properties of finite nuclei. The other EoS is the Akmal, Pandharipande and Ravenhall (APR) EoS calculated in the variational chain summation method using Argonne V_{18} nucleon-nucleon interaction and a fitted three nucleon interaction along with relativistic boost corrections [71].

We calculate the static mass limits of neutron stars using those three equations of state. Maximum masses and the corresponding radii of neutron stars are recorded in Table 5.1. Similarly maximum masses and the corresponding radii of rotating neutron stars at the mass shedding limits are also shown in the tables. These results show that maximum masses in all three cases are above 2 $M_\odot$ and compatible with the benchmark

EoS	P(ms)	$\varepsilon_c(10^{15}$ g/cm$^3)$	$M_G/M_\odot$	R (km)
APR	static	2.78	2.190	9.93
	0.6291	1.50	2.397	14.53
DD2	static	1.94	2.417	11.90
	0.7836	1.00	2.677	17.53
Chiral	static	1.99	2.050	12.14
	0.8778	1.11	2.353	18.17

Table 5.1: Maximum gravitational masses ($M_G/M_\odot$), equatorial radii (R), and their corresponding central energy densities (ε_c) for static ($\Omega = 0$) and Keplerian limit ($P = P_K = 2\pi/\Omega_K$) with different EoS, where P_K is the Kepler period in millisecond [43].

measurement mentioned above.

5.4 Results and Discussion

We divide our results into two parts: in the first part we show the frame-dragging effect in some pulsars which rotate with fixed values of Kepler frequencies Ω_K and central densities ε_c. Next we consider pulsars whose masses and rotational periods are known from observations. Rotational frequencies of observed pulsars are generally much lower than their Kepler frequencies ($\Omega < \Omega_K$).

5.4.1 Pulsars rotating with their Kepler frequencies $\Omega = \Omega_K$

Figure 5.1 displays the frame-dragging frequency (or LT precession frequency) as a function of radial distance for APR EoS. Panel (a) of the figure represents the results along the equator whereas panel (b) implies those along the pole. For both panels of Fig. 5.1, we consider rotating neutron stars with central energy densities 5.2435 $\times 10^{14}$, 6.404 $\times 10^{14}$ and 7.534 $\times 10^{14}$ g/cm^3 and their corresponding Kepler frequencies are 4000 (red), 5000 (green) and 6000 (blue) s^{-1}, respectively whereas masses of the rotating compact stars in three cases range from ~ 0.6 to ~ 1.7 M$_\odot$. The Kepler periods P_K =1.57 ms, 1.26 ms and 1.05 ms correspond to the above Kepler frequencies. Here and throughout the chap-

ter, Ω_{LT} is measured in a Copernican frame. For the cases in panel (a), frame-dragging frequencies decrease initially with increasing distance from the centre and encounters a local minimum at a distance $r_{min} \sim 0.5r_e$ which is well below the surface. It is interesting to note here that the frame-dragging frequencies in all three cases rise again and attain a local maximum at the distance $r_{max} \sim 0.7r_e$ and finally drop to smaller values at the surface. On the other hand, the frame-dragging frequencies along the pole smoothly vary from large values at the centre to smaller values at the surface as evident from panel (b) of Fig. 5.1.

Figure 5.2 shows the frame-dragging frequency along the equator (panel (a)) and along the pole (panel (b)) for the DD2 EoS whereas Figure 5.3 exhibits the frame-dragging frequency along the the equatorial distance (panel (a)) and polar distance (panel (b)) for the Chiral EoS. In both figures, results are shown for Keplerian frequencies $\Omega_K = 4000$, 5000 and 6000 s^{-1}. However, the central energy densities corresponding to the Keplerian frequencies mentioned above are different for three EoSs. The behaviour of frame-dragging frequencies along the equator and pole in Fig. 5.2 and Fig. 5.3 is qualitatively similar to the results of Fig. 5.1. In Figs. 5.1 - 5.3, as the rotation frequency Ω_K and the central energy density ε_c increase, the frame-dragging frequencies increase and also the local maxima and minima shift towards the surface of the neutron star along the equator for all three EoSs. It reveals an important conclusion that *the ratio of the positions of the local maxima and minima to the radius of the neutron star must depend on* Ω *and* ε_c *for a particular pulsar.*

It could be easily seen from Eq. (5.7) that the LT frequency inside a neutron star is a function of both the radial distance r and colatitude θ. The colatitude plays a major role to determine the exact frame-dragging frequency at a particular point inside the rotating neutron star as evident from Figs. 5.1 - 5.3. We obtain the LT frequency at the pole by just plugging-in $\theta = 0$ in Eq. (5.7) and it is given by $\Omega_{LT} = e^{-(\alpha+\sigma)}\omega$. It should be noted here that the LT frequency is connected to ω which appears as the non vanishing

metric component in the metric of the rotating star. According to the theorem by Hartle, the dragging of inertial frames as represented by ω with respect to a distant observer decreases smoothly as a function of r from a large value at the centre of the star to a smaller value at the surface [63] for both equatorial and polar cases. In this formalism the frame-dragging frequency depends solely on r. For a fixed value of r, one gets the same frequency from the equator to the pole inside the rotating neutron star. We obtain the similar behaviour of the LT frequency along the pole in panel (b) of Figs. 5.1 - 5.3 as obtained in Hartle's formalism. However, our results along the equator are quite different from what was obtained using Hartle's formalism [63]. It is evident from Figs. 5.1-5.3 that the plots are smooth along the pole but not along the equator. For the calculation of the LT frequency along the equator, we find that the second term of Eq. (5.7) does not contribute. Further investigation of the first term involving metric components σ, ω and their derivatives reveals that this term is responsible for the local maxima and minima along the equator as reported above. The appearance of local maxima and minima in the LT frequencies along the equator may be attributed to the dependence of Ω_{LT} on r and θ. As a consistency check, we obtain two solutions for local maximum and minimum after extremising the Eq. (5.7) with respect to r and obtain

$$
\begin{aligned}
\frac{d\Omega_{LT}}{dr} &= \Omega_{LT}\left[-(\alpha_{,r}+\sigma_{,r}) - 2\frac{r\omega\sin^2\theta(r\omega_{,r}+\omega)-\sigma_{,r}e^{2\sigma}}{\omega^2r^2\sin^2\theta-e^{2\sigma}}\right] + \frac{1}{\Omega_{LT}}.\frac{e^{-2(\alpha+\sigma)}}{4(\omega^2r^2\sin^2\theta-e^{2\sigma})^2} \\
&. \quad \big\{A\sin^2\theta\left[\omega r^2\sin^2\theta(3\omega\omega_{,r}+2r\omega_{,r}^2+r\omega\omega_{,rr})+2\sigma_{,r}e^{2\sigma}(2\omega+r\omega_{,r}-2\omega r\sigma_{,r})\right. \\
&+ \quad \left. e^{2\sigma}(3\omega_{,r}+r\omega_{,rr}-2r\omega_{,r}\sigma_{,r}-2\omega\sigma_{,r}-2r\omega\sigma_{,rr})\right] + B\left[r\omega\sin^3\theta(2\omega\omega_{,\theta}+2r\omega_{,r}\omega_{,\theta}+r\omega\omega_{,\theta r})\right. \\
&+ \quad 2\sigma_{,r}e^{2\sigma}(2\omega\cos\theta+\omega_{,\theta}\sin\theta-2\omega\sigma_{,\theta}\sin\theta) \\
&+ \quad \left. e^{2\sigma}(2\omega_{,r}\cos\theta+\omega_{,\theta r}\sin\theta-2\sin\theta(\omega\sigma_{,\theta r}+\omega_{,r}\sigma_{,\theta}))\right]\big\} \ ,
\end{aligned}
$$

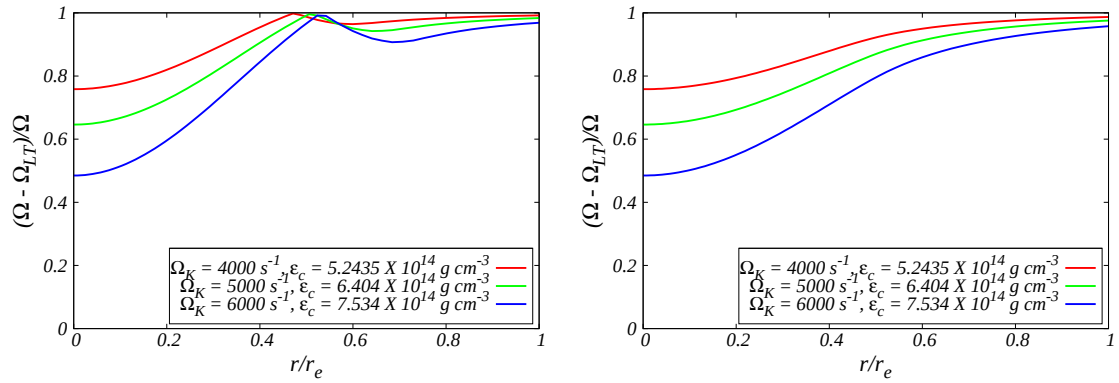

(a) along the equator (b) along the pole

Figure 5.1: *Frame-dragging effect inside the rotating neutron stars from the origin to the surface, calculated for the APR EoS.* Ω_K *and* ε_c *denote the Kepler frequency and the central energy density, respectively. Surface of the neutron star along the pole located around* $0.6r_e$ *but the plot is still valid beyond the surface of the pole as our formalism is applicable for regions outside the pulsar [43].*

where

$$A = r^3\omega^2\omega_{,r}\sin^2\theta + e^{2\sigma}(2\omega + r\omega_{,r} - 2\omega r\sigma_{,r}) ,$$

$$B = r^2\omega^2\omega_{,\theta}\sin^3\theta + e^{2\sigma}(2\omega\cos\theta + \omega_{,\theta}\sin\theta - 2\omega\sigma_{,\theta}\sin\theta) ,$$

and

$$\omega_{,\theta r} \equiv \frac{\partial^2\omega}{\partial\theta\partial r} .$$

Setting $\frac{d\Omega_{LT}}{dr}|_{(r=R_0,\theta=\pi/2)} = 0$ and solving it numerically in the region $0 < R_0 < r_e$, we obtain two positive real roots of r inside the rotating neutron star. One of these is $R_{01} = r_{max}$ and another is $R_{02} = r_{min}$. These are basically the *local maximum* and *local minimum* of the function Ω_{LT} along the equator. These local maximum and local minimum are absent for $\frac{d\Omega_{LT}}{dr}|_{(r=R_0,\theta=0)} = 0$. Thus, we cannot see any such extremum for the plots of Ω_{LT} along the pole.

The normalised angular velocities of the local inertial frame-dragging at the surface ($\tilde{\Omega}_s = \Omega_{LT}^{surface}/\Omega$) and centre ($\tilde{\Omega}_c = \Omega_{LT}^{centre}/\Omega$) of the star models with three EoSs are

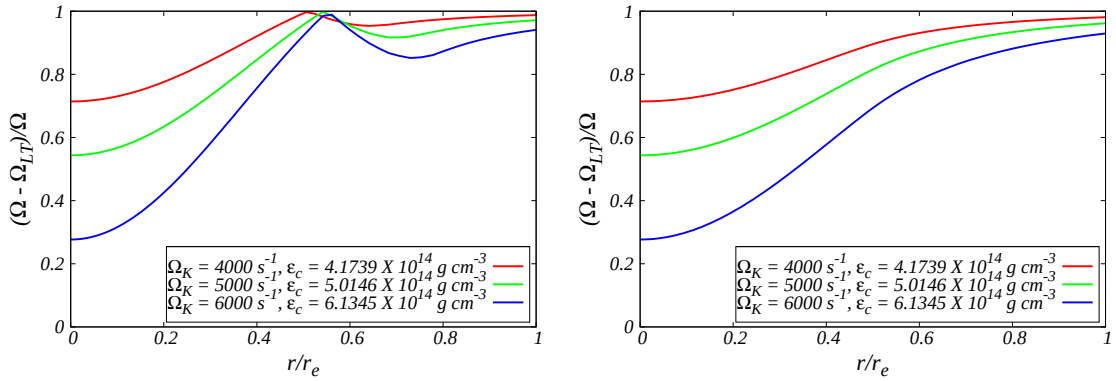

(a) along the equator (b) along the pole

Figure 5.2: *Same as Fig. 5.1, but calculated for the DD2 EoS [43].*

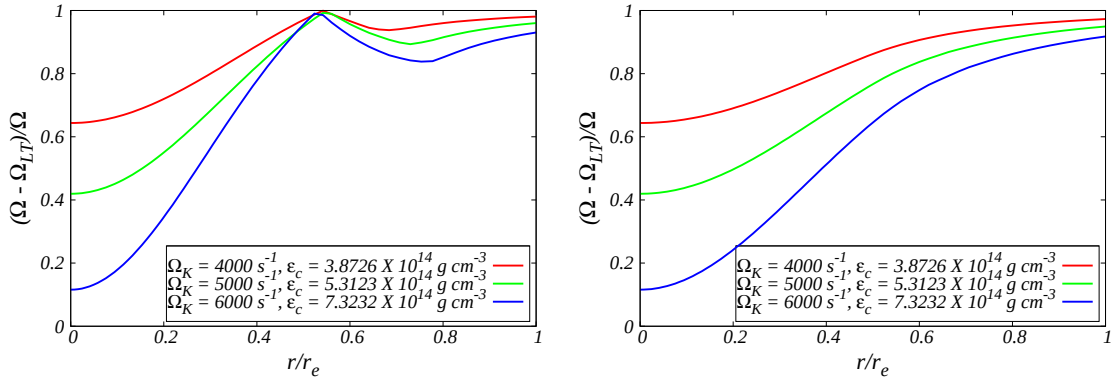

(a) along the equator (b) along the pole

Figure 5.3: *Same as Fig. 5.1, but calculated for the Chiral EoS [43].*

	P_K	Along the equator			Along the pole		
	(ms)	APR	DD2	Chiral	APR	DD2	Chiral
$\tilde{\Omega}_s$	1.57	0.008	0.013	0.019	0.046	0.069	0.099
	1.26	0.016	0.029	0.040	0.087	0.139	0.184
	1.05	0.031	0.059	0.070	0.151	0.252	0.287
$\tilde{\Omega}_c$	1.57	0.242	0.286	0.356	0.242	0.286	0.356
	1.26	0.354	0.457	0.580	0.354	0.457	0.580
	1.05	0.515	0.723	0.884	0.515	0.723	0.884

Table 5.2: Normalised angular velocities of the local inertial frame-dragging at the surface $\tilde{\Omega}_s$ and centre $\tilde{\Omega}_c$ of the neutron stars which are rotating at their respective Kepler periods ($P_K \equiv 2\pi/\Omega_K$) as measured by a distant observer [43].

recorded in Table 5.2. It is noted that the normalised frame-dragging value at the star's center is maximum and falls off on the surfaces of the equator and pole for three EoSs irrespective of whether the compact star is rotating slowly or fast. However, for a particular EoS, the normalised frame-dragging value at the star's centre and surface is higher for a fast rotating star with $P_K = 1.05$ ms than those of a slowly rotating star with $P_K = 1.57$ ms for both cases along the equator and pole. One can see another interesting thing from the Table 5.2 that $\tilde{\Omega}_s$ is always higher at the pole than $\tilde{\Omega}_s$ at the equator for a particular pulsar. It is due to the effect of rotation frequency Ω (of the star) for which pole is nearer to the center than the surface as it is evident from Table 5.2. Thus, the inertial frame-dragging effect is higher at the surface of the neutron star along the pole than that at the surface of the neutron star along the equator.

Now we investigate the dependence of local maxima and minima in Ω_{LT} along the equator on the angle θ. In Figure 5.4, Ω_{LT} is shown as a function of s defined by Eq. (5.20) and $\cos\theta$ for DD2 (panel(a)) and Chiral (panel (b)) EoSs. The local maxima and minima in Ω_{LT} along the equator are clearly visible in both panels of Fig. 5.4. It has been already noted that Ω_{LT} along the pole decreases smoothly from the center to the surface. As the latitude ($\theta' = \pi/2 - \theta$) increases from the equator to the pole, the height between the maximum and minimum of Ω_{LT} diminishes and after a certain 'critical' angle (θ_{cr})

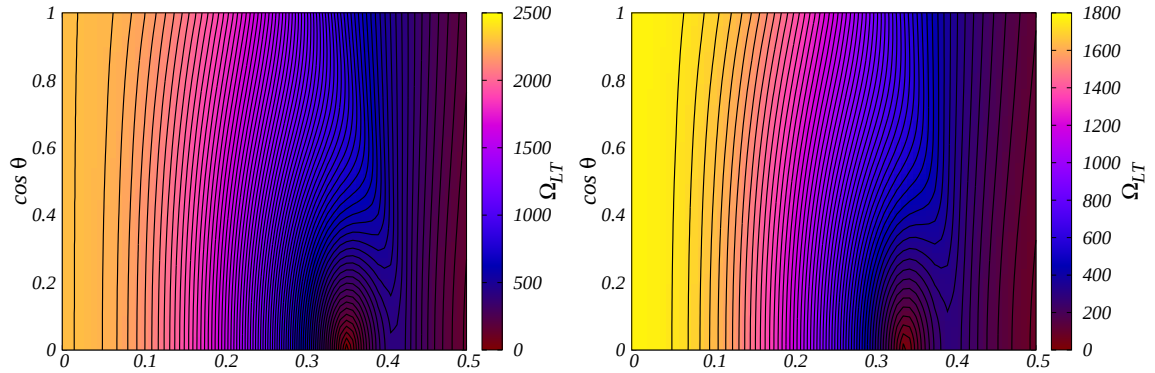

(a) $DD2$ EoS (b) APR EoS

Figure 5.4: *3-D plots of* Ω_{LT} *of the pulsar which is rotating with* $\Omega_K = 5000\,s^{-1}$ as a function of s and $\cos\theta$ for (a) DD2 EoS and (b) APR EoS [43].

both extrema disappear and the plot is smooth like the plot along the pole. The critical angle could be seen from the 3-D plot in Fig. 5.4. This value of the critical angle is $\mu \approx 0.5$ or $\theta'_{cr} = 30^\circ$ where local maximum (r_{max}) and minimum (r_{min}) disappear. So, if we plot Ω_{LT} vs θ at the point r_{max} for a specific Kepler frequency, (namely $\Omega_K = 5000\,\mathrm{s}^{-1}$), we could find that the frame-dragging frequency increases from the equator to the pole for the specific r_{max} as it is exhibited by Fig. 5.4.

5.4.2 Pulsars rotating with their frequencies $\Omega < \Omega_K$

Now we apply our exact formula of Ω_{LT} to three known pulsars. Three pulsars chosen for this purpose are J1807-2500B, J0737-3039A and B1257+12. Periods of those pulsars are given by Table 5.3. Masses of those pulsars are also known and range from 1.337 to 1.5 $\mathrm{M}_\odot$. Furthermore, we adopt the same EoSs in this calculation as considered in the previous sub-section. Though periods of these pulsars are larger than the Keplerian periods, the calculation of Ω_{LT} inside these real pulsars are equally important like the cases with Kepler frequencies demonstrated already.

We calculate the normalised angular velocity at the centre and surface of these pulsars with APR, DD2 and Chiral EoSs. It is noted from Table 5.3 that the behaviour of the

	Name of the Pulsar	P (ms)	Along the equator			Along the pole		
			APR	DD2	Chiral	APR	DD2	Chiral
$\tilde{\Omega}_s$	J1807-2500B	4.19	0.099	0.075	0.064	0.156	0.120	0.105
	J0737-3039A	22.70	0.095	0.073	0.062	0.154	0.122	0.106
	B1257+12	6.22	0.122	0.091	0.077	0.188	0.145	0.126
$\tilde{\Omega}_c$	J1807-2500B	4.19	0.707	0.548	0.516	0.707	0.548	0.516
	J0737-3039A	22.70	0.685	0.538	0.502	0.685	0.538	0.502
	B1257+12	6.22	0.825	0.632	0.601	0.825	0.632	0.601

Table 5.3: Normalised angular velocities of the local inertial frame-dragging at the surface $\tilde{\Omega}_s$ and centre $\tilde{\Omega}_c$ of some known rotating neutron stars [43].

normalised angular velocity from the centre to the surface or along the pole and equator is qualitatively same as shown in Table 5.2.

We also plot the frame-dragging frequency (Ω_{LT}) as a function of radial distance along the equator (panel (a)) and pole (panel (b)) for three EoSs in Figures 5.5 - 5.7. The frame-dragging frequency behaves smoothly along the pole from the centre to the surface as shown by panel (b) of these figures. Results of panel (a) of the figures show similar features of local maxima and minima along the equator as found in Figs. 5.1-5.3. We note that all the local minima of Ω_{LT} are located around $r_{min} \sim 0.7r_e$ and the local maxima are located around $r_{max} \sim 0.9r_e$ in Figs. 5.5 - 5.7.

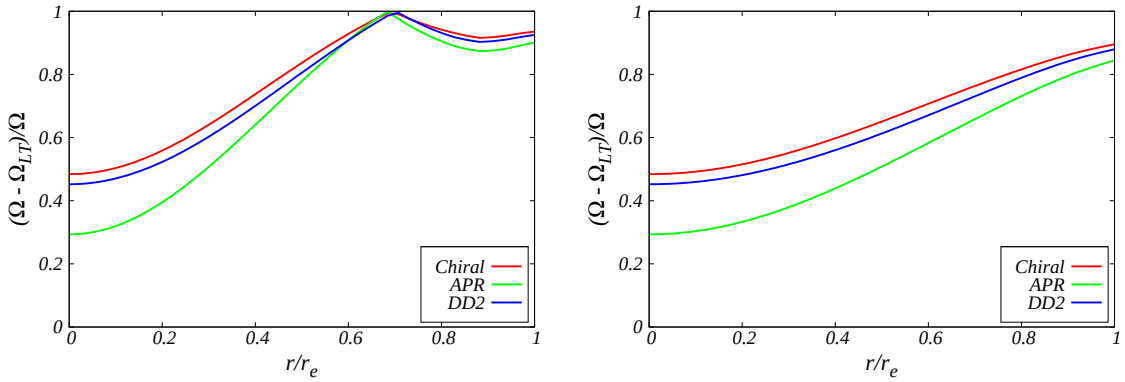

(a) along the equator (b) along the pole

Figure 5.5: *Frame-dragging effect inside the rotating neutron star from the origin to the surface, calculated for J1807-2500B* ($M = 1.366M_\odot, \Omega = 1500.935\, s^{-1}$) *[43].*

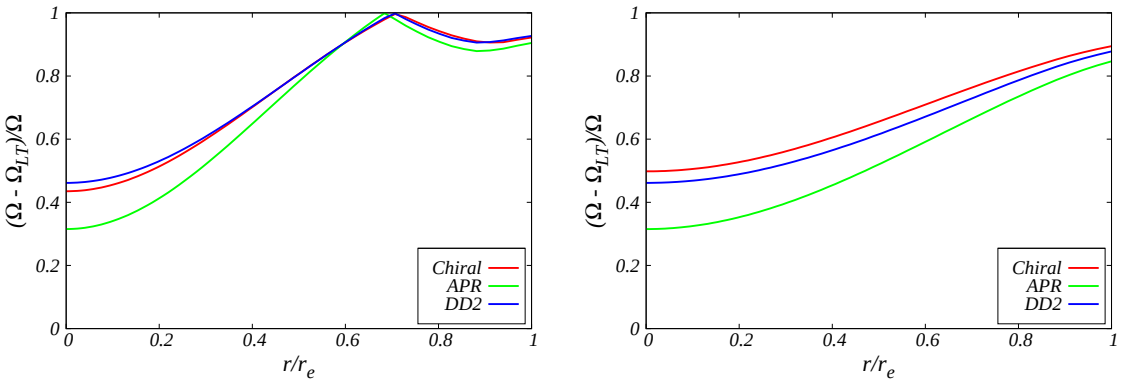

(a) along the equator (b) along the pole

Figure 5.6: *Frame-dragging effect inside the rotating neutron star from the origin to the surface, calculated for J0737-3039A* ($M = 1.337 M_{\odot}, \Omega = 276.8\ s^{-1}$) *[43].*

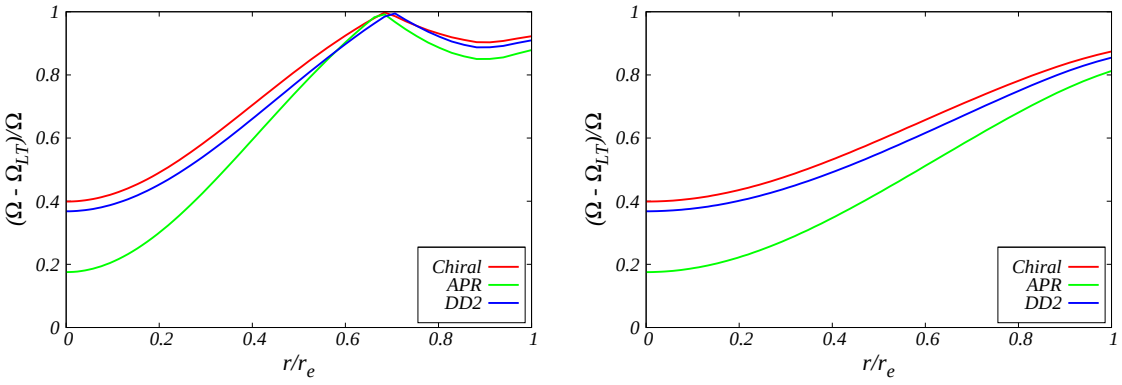

(a) along the equator (b) along the pole

Figure 5.7: *Frame-dragging effect inside the rotating neutron star from the origin to the surface, calculated for B1257+12* ($M = 1.5 M_{\odot}, \Omega = 1010.321\ s^{-1}$) *[43].*

We also plot the Ω_{LT} of pulsar J0737-3039A as a function of s and $\cos\theta$ for DD2 (panel (a)) and APR (panel (b)) EoSs in Figure 5.8. It is noted from Fig. 5.8 that the value of θ_{cr} is around 30° for the pulsar J0737-3039A for DD2 and APR EoSs.

5.5 Summary

We have derived the exact frame dragging frequency inside the rotating neutron star without making any assumption on the metric components and energy-momentum tensor.

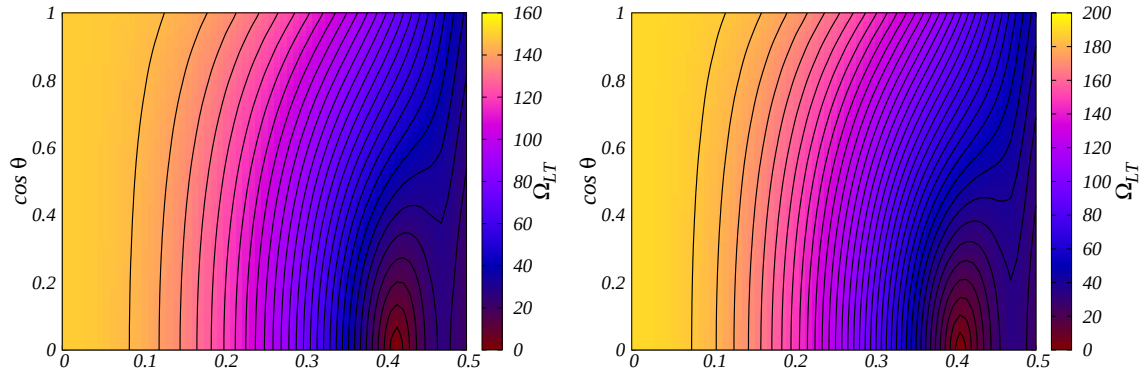

(a) *DD*2 EoS (b) APR EoS

Figure 5.8: *3-D plots of* Ω_{LT} *of the pulsar J0737-3039A as a function of* s *and* $\cos\theta$ *for DD2 (panel (a)) and APR (panel (b)) EoSs [43].*

We show that the frequency must depend both on r and θ. It may be recalled that the frame-dragging frequency depends only on r in Hartle's formalism because of the slow rotation approximation. We predict the exact frame-dragging frequencies for some known pulsars as well as neutron stars rotating at their Keplerian frequencies. We have also estimated LT precession frequencies at the centers of these pulsars without imposing any boundary conditions on them. We have found local maxima and minima along the equator due to the dependence of Ω_{LT} on the colatitude (θ) inside pulsars. The positions of local maximum and minimum depend on the frequency Ω and the central density ε_c of the particular pulsar. Furthermore, it is observed that local maximum and minimum in Ω_{LT} along the equator disappear at a critical angle θ_{cr}.

Quasi periodic oscillations (QPOs) in magnetars were studied by various groups. These studies in several cases were carried by considering spherical and non-rotating relativistic stars having dipolar magnetic field configuration [72]. It would be worth investigating the effect of our exact frame-dragging formulation on the magnetic field distribution in rotating neutron stars and its implications on QPOs.

Chapter 6

Conclusion & Outlook

In contrast to most calculations of the LT precession rate in the literature, which focus on the weak-field approximation, this thesis has discussed in some detail the problem of the exact LT precession formula in any stationary spacetime and derived the exact LT precession formula for full Kerr, KTN, Plebański-Demiański and other spacetimes. The weak-field approximation for the Kerr spacetime by Hartle (Eq. (2.43)) has been then shown to emerge straightforwardly from our general formulation. Interestingly, we have shown that in the *non-rotating* and *spherically symmetric* Taub-NUT spacetime the LT precession does not vanish. Applying the general LT formula we have also obtained the exact frame-dragging rate inside the rotating neutron stars. We have also studied causal geodesics in the equatorial plane of the extremal KTN spacetime, focusing on the ISCO, and compared its behaviour with extant results for the ISCO in the extremal Kerr spacetime. This work is important due to its future applications mainly for the accretion disk theory in the KTN spacetime.

Accretion disk theory and the related astrophysical phenomena have been investigated using Newtonian or post-Newtonian Gravity. The strong gravity LT effect has not been considered in those calculations. Recently, Banerjee and Mukhopadhyay [73] have claimed to have established a relation between the Mass and the Spin of Stellar-Mass Black Holes

within a theoretical analysis involving Post-Newtonian approximations. However, in this work the strong gravity frame-dragging effect has not been taken into account. As the accretion disks extend to the vicinity of black hole horizons associated with the very strong gravity regime, the effect of the frame-dragging may have to be taken into account. It will be interesting to investigate the changes to the standard accretion disc theory that this inclusion might entail.

The exact frame-dragging rates have already been derived inside and outside of the rotating neutron stars by us. Now, it would be worth to study the quasi-periodic-oscillations (QPOs) in the case of accreting neutron stars. The broad peaks at frequencies $\sim$ 20-40 Hz in the power spectra of three sources 4U 1728-34, 4U 0614+091 and KS 1731-260 and their variations with the higher kHz QPO frequency have been matched by the LT precession of the material in the innermost disk region by Stella and Vietri [74]. But surprisingly, the preliminary LT precession rate equation which has been used here is only $\Omega_{LT} = J/r^3$. This is equivalent to the LT precession frequency (Eq. (2.43)) at equatorial plane $\theta = \pi/2$ in the weak gravity regime. The strong gravity LT frequency formula is not used here. The rotating neutron star also leads to a stellar oblateness; thus a quadrupole term arises in the formulation. Török et. al [75] implied the mass-angular momentum $(M - j)$ relations by models of twin peak QPOs. They also proposed for the correction in the LT precession model as they considered the Kerr geometry approximation in their case and the influence of quadrupole momentum on Ω_{LT} had not been taken into account to determine the $(M - j)$ relations. In our formulation we do not introduce any approximation to calculate the frame-dragging effect inside and outside of the neutron star. Thus, the prescription of Stella and Vietri and also the $(M - j)$ relations in the light of our strong gravity LT precession formulation could be investigated.

In the theoretical explanation of QPOs and jets from accreting neutron stars and black holes, the strong gravity frame-dragging effect might play an important role. It was first suggested by Stella and Vietri [74] that QPOs were connected to the LT precession

frequency. They predicted that the peaks observed in the power spectra of several low mass X-ray binaries (LMXRBs) at a frequency of tens of Hz were due to the precession of the innermost disk region and it was dominated by the LT effect. Veledina et. al [76] also suggested that QPOs in black hole binaries were produced by the LT precession of the hot accretion flow whose outer parts radiate in optical wavelengths. They investigate the QPO harmonic content and find that the amplitudes have a variability which might originate from the LT precession. In another recent paper, Stefanov [77] discusses the various models for high-frequency QPOs with the LT precession. These papers do not provide a detailed theoretical explanation of QPOs and jets by taking into consideration strong gravity frame-dragging effects. Stone and Loeb [13] also discuss jets which are observed in many accreting black hole systems but they do not consider the strong gravity LT effect in their calculation.

There are four primary accretion disk models: Polish doughnuts (thick disks), Shakura-Sunyaev (thin) disks, slim disks and advection-dominated accretion flows (ADAFs). Among these Shakura-Sunyaev model is quite successful. The general relativistic version of the Shakura-Sunyaev disk model has been worked out by Novikov and Thorne [78]. It would be very interesting to investigate the Novikov-Thorne version of Shakura-Sunyaev disk model and consider modifying the disk equations by using the strong gravity LT precession rate formula.

Another important topic in this entire area is that of the ISCO. The ISCO plays an important role in the accretion disk theory as well as QPOs. More precisely, circular geodesic motion in the equatorial plane ($\theta = \pi/2$) is of fundamental importance in the black hole accretion disk theory [78]. That fact is important for spectral analysis of X-ray sources. The strong gravity LT effect will also modify the variability pattern and quality factor. Variability amplitudes are strongly related to QPOs.

Though the analytic disk solutions are stable against finite perturbations, these perturbations often excite oscillatory behaviour. Oscillation is a common dynamical response

in many fluid bodies. It would be interesting to explore the nature of oscillations in the accretion disks. This topic is important to understand physical mechanisms of QPOs. QPOs have been discussed in the literature vis-a-vis the frame-dragging effect only for slow rotation approximation. It would be worth investigating this problem for rapidly rotating astrophysical objects. QPOs have frequencies of a few hundred Hz for Galactic black hole and neutron star sources. The frequency range 100-1000 Hz formally corresponds to orbital frequencies of a few gravitational radii away from the stellar-mass object. The focus on orbital frequencies is further motivated by the stability of observed QPO frequencies over very long periods of time. The oscillation frequencies do not depend on magnetic field, density, temperature and accretion rate rather it depends only on mass and spin of the black hole. Thus, one of the most important frequencies which are connected only to these two parameters (mass & spin) is the LT precession frequency.

Among models proposed to understand QPOs in accretion phenomena, the mathematical resonance model by Rebusco and Horák [79] is significant. However, it does not explain the non-linear resonance of two "modes" (pendulum mode & spring mode) of oscillation. What these modes are, how they are excited and many other questions are unresolved until now. Without answering these questions the QPO puzzle will not be resolved. The investigation of this fundamental issue is important so that it can solve the QPO puzzle properly by the exact LT precession formula.

In another recent related paper, Nowak and Lehr [80] attempt to explain that the 67 Hz QPO feature seen in GRS 1915+105 was due to the LT effect but the LT frequency has been taken as $\Omega_{LT} = 2J/r^3 = 2aM/r^3$ (a is the Kerr parameter and M is the mass) which is generally considered for the weak gravity regime. In the theoretical models of disk oscillations, a new class of modes (c-modes) has been identified and Nowak and Lehr show that the fundamental c-mode eigenfrequency was approximately the LT frequency for $M = 1$ and $|a/r^{1/2}| << 1$. Physically, the mode resembles a tilted inner disk which precesses slowly around the spin axis of the black hole. C-mode may produce very little

intrinsic luminosity modulation due to the little temperature or pressure fluctuation in the disk. Cui, Zhang and Chen [81] have chosen the QPO frequency as the LT frequency at the radius at which the accretion disc effective temperature is maximum and derived $a \sim 1$ for both GRS 1915+105 and GRO J1655-40, but this is a debatable issue. However, the tilted angle of the accretion disk can easily be determined by our basic formula of the LT effect as well as the whole thing could be strongly modified and no approximation is required for that. This can also help us for more accurate calculation as well as the future observation. The conclusion of Cui et. al. [81] may also be reconsidered by the strong gravity LT precession formula.

There is a strong observational connection between accreting black holes QPOs and relativistic jets. The theoretical understanding of accretion disks and relativistic jets has proceeded separately and the physical link between the two things still remains uncertain. Veledina et.al [76] proposed that Optical and IR (OIR) wavelengths QPOs might originate from the jet if it is entirely driven by the accretion flow and in this case the LT effect may be the cause of jet precession. According to the strong gravity LT formula, relativistic jets will be affected very much by the strong gravity LT precession as it forms along the pole. A possible connection between the black hole spin and jet power was predicted by the Blandford-Znajek mechanisms which could be modified by the strong gravity LT precession to get the possible connection between the jet and OIR QPOs.

Bibliography

[1] J. Lense, H. Thirring, *Phys. Z.* **19**, 156-163 (1918) 16, 22, 45, 111

[2] L. I. Schiff, *American Journal of Physics* **28**, 340(1960) 16

[3] J. B. Hartle, *Gravity:An introduction to Einstein's General relativity*, Pearson (2009) 16, 20, 21, 36, 69, 80, 98, 113

[4] L. Iorio, *Astrophys Space Sci*, **331**: 351395 (2011) 21

[5] C. W. F. Everitt et. al., *Phys. Rev. Lett.* **106**, 221101 (2011) 22, 23

[6] R. Kannan, P. Saha, *The Astrophysical Journal*, **690**, 1553 (2009) 23

[7] E. Hackmann, C. Lämmerzahl, *Phys. Rev.D*,**85**, 044049 (2012) 23, 45, 46, 50, 51, 52, 54

[8] G. V. Kraniotis, *Class. Quantum Grav.*, **21**, 4743-4769 (2004) 23

[9] G. V. Kraniotis, *Class. Quantum Grav.*, **24**, 17751808 (2007) 23

[10] I. Ciufolini, E. C. Pavlis, *Nature* **431**, 958 (2004) 23

[11] S. Bhattacharya, Lecture at Conference on *Advances in Astroparticle Physics and Cosmology*, Darjeeling (March 2012) 23

[12] L. Stella, A. Possenti, *Space Sci. Rev.* **148**, 105 (2009) 23

[13] N. Stone, A. Loeb, *Phys. Rev. Lett.*, **108**, 061302 (2012) 24, 133

[14] N. Straumann, *General Relativity with applications to Astrophysics*, Springer (2009) 10, 24, 29, 31, 32, 45, 52

[15] A. P. Lightman, W. H. Press, R. H. Price, S. A. Teukolsky, *Problem book in Relativity and Gravitation*, Princeton university press (1979) 24, 32

[16] C. W. Misner, K. S. Thorne, J. A. Wheeler, *Gravitation*, W. H. Freeman & Company (1973) 24, 41

[17] R. M. Wald, *General Relativity*, Chicago (1984) 28, 64

[18] S. Ramaswamy, A. Sen, *J. Math. Phys. (N.Y.)* **22**, 2612 (1981) 33, 45, 51, 64, 79, 91

[19] M. Bejger, P. Haensel, *Astronomy and Astrophysics* **396**, 917-921 (2002) 36

[20] N. Stergioulas, *Living Rev. Relativity* **6**, 3 (2003) 42

[21] G. L. Comer, *Phys. Rev.* **D69**, 123009 (2004) 42

[22] E. Berti, N. Stergioulas, *MNRAS* **350**, 1416-1430 (2004) 42

[23] M. C. Miller, F. K. Lamb, *ApJ* **470**, 1033 (1996) 43

[24] C. Chakraborty, P. Pradhan, *Eur. Phys. J.* **C73**, 2536 (2013) 43, 65, 83

[25] R. P. Kerr, *Phys. Rev. Lett.* **11**, 237-238, (1963) 44

[26] J. Plebański, M. Demiański, *Ann. Phys.* (N.Y.) **98**, (1976) 44

[27] S. W. Hawking, S. F. Ross, *Phys. Rev. Lett.* **75**, 3382 (1995) 45

[28] C. Chakraborty, P. Majumdar, *Class. Quantum Grav.* **31**, 075006 (2014) 10, 38, 45, 47, 49, 51, 57, 66, 69, 74, 75, 78, 82, 91

[29] D. Lynden-Bell, M. Nouri-Zonoz, *Rev. Mod. Phys.* **70**, 427445 (1998) 51, 52, 63, 76, 108

[30] S. Ramaswamy, A. Sen, *Phys. Rev. Lett.* **57**, 8 (1986) 51, 63

[31] M. Mueller, M. J. Perry, *Class. Quantum Grav.* **3**, 65-69 (1986) 51

[32] V. Kagramanova, J. Kunz, E. Hackmann, C. Lämmerzahl, *Phys. Rev.* **D81**, 124044 (2010) 51, 52, 63, 67, 79, 81, 82, 107

[33] S. Drasco, S. A. Hughes, *Phys. Rev.* **D69**, 044015 (2004) 51

[34] R. Fujita, W. Hikida, *Class. Quantum Grav.* **26**, 135002 (2009) 51

[35] V. Kagramanova, in private communication 52

[36] C. W. Misner, *J. Math. Phys.*, **4**, 924 (1963) 53, 76, 89

[37] A. H. Taub, *Ann. Maths.* **53**, 3 (1951) 53, 81

[38] E. Newman, L. Tamburino, T. Unti, *J. Math. Phys.*,**4**, 7 (1963) 53, 81

[39] Y. Li, J. Yang, Y-L. Li, S-W Wei, Y-X Liu, *Class. Quantum Grav.* **28**, 225006 (2011) 54, 60

[40] P. Pradhan, P. Majumdar, *Eur. Phys. J. C* **73**, 2470 (2013) 58, 61, 81

[41] C. Chakraborty, *Eur. Phys. J.* **C74**, 2759 (2014) 10, 12, 63, 67, 91, 104, 105

[42] C. Liu, S. Chen, C. Ding, J. Jing, *Phys. Letts* **B 701**, 285 (2011) 63, 81

[43] C. Chakraborty, K. P. Modak, D. Bandyopadhyay, *ApJ* **790**, 2 (2014) 10, 11, 12, 64, 108, 121, 124, 125, 126, 127, 128, 129, 130

[44] J. G. Miller, *J. Math. Phys.* **14**, 486 (1973) 65, 81

[45] C. Chakraborty, arXiv:1407.6294v2 [gr-qc] (2014) 10, 66, 67, 69, 70, 71, 72, 73, 74

[46] C. Bunster, M. Henneaux, *PNAS* **104**, 12243 (2007) 68

[47] J. G. Miller, M. D. Kruskal, B. B. Godfrey, *Phys. Rev.* **D4**, 2945 (1971) 78, 107

[48] M. A. Abramowicz, P. C. Fragile, *Living Rev. Rel.* **16**, 1 (2013) 80

[49] J. F. Steiner, J. E. McClintock, R. A. Remillard, L. Gou, S. Yamada, R. Narayan, *Astrophys. J. Lett.* **718**, L117-L121 (2010) 80

[50] D. Barret, J.-F. Olive, M. C. Miller, *Mon. Not. R. Astron. Soc.*, **361**, 855860 (2005) 80

[51] D. Barret, J.-F. Olive, M. C. Miller, *Mon. Not. R. Astron. Soc.*, **376**, 11391144 (2007) 80

[52] A. Abdujabbarov, F. Atamurotov, Y. Kucukakca, B. Ahmedov, U. Camci, *Astrophys. and Space Science* **344**, 2, 429-435 (2013) 81

[53] S. Chandrasekhar, *The Mathematical Theory of Black Holes*, Oxford (1992) 81, 82, 86, 97, 102, 109, 110

[54] V. S. Manko, E. Ruiz, *Class. Quantum Grav.* **22**, 3555-3560 (2005) 89

[55] G. F. R. Ellis, B.G. Schmidt, *Gen. Rel. Grav.* **8**, 915 (1977) 92, 107

[56] B. G. Schmidt, *Gen. Rel. Grav.* **1**, 269 (1971) 107

[57] R. Geroch, *J. Math. Phys. (N.Y.)* **9**, 450 (1968) 107

[58] W. Israel, *Phys. Rev.* **D15**, 935 (1977) 107

[59] J. Antoniadis et al., *Science* **340**, 1233232 (2013) 112, 120

[60] J. B. Hartle, *ApJ* **150**, 1005 (1967) 112, 113

[61] J. B. Hartle, *ApJ* **153**, 807 (1968) 112

[62] N. K. Glendenning, F. Weber, *Phys. Rev.* **D50**, 3836 (1994) 112

[63] F. Weber, *Pulsars as Astrophysical laboratories for Nuclear and Particle Physics*, IOP (1999) 112, 123

[64] S. M. Morsink, L. Stella, *ApJ* **513**, 827 (1999) 112

[65] H. Komatsu, Y. Eriguchi, I. Hachisu, *MNRAS* **237**, 355 (KEH) (1989) 114, 118, 119

[66] G. B. Cook, S. L. Shapiro, S. A. Teukolsky, *ApJ* **398**, 203 (1992) 117, 119

[67] N. Stergioulas, J. L. Friedman, *ApJ* **444**, 306 (1995) 118

[68] S. Banik, H. Matthias, D. Bandyopadhyay, W. Greiner, *Phys. Rev.* **D 70**, 123004 (2004) 120

[69] M. Hanauske, D. Zschiesche, S. Pal, S. Schramm, H. Stöcker, W. Greiner, *Astrophys. J.***537**, 958 (2000) 120

[70] S. Typel, G. Röpke, T. Klähn, D. Blaschke, H. H. Wolter, *Phys. Rev.* **C 81**, 015803 (2010) 120

[71] A. Akmal, V. R. Pandharipande, D. G. Ravenhall, *Phys. Rev.* **C 58**, 1804 (1998) 120

[72] H. Sotani, K. D. Kokkotas, N. Stergioulas, *MNRAS* **375**, 261 (2007) 130

[73] I. Banerjee, B. Mukhopadhyay, *Phys. Rev. Lett.* **111**, 061101 (2013) 131

[74] L. Stella, M. Vietri, *ApJ*, **492**, L59 (1998) 132

[75] G. Török et. al, *ApJ* **760**, 138 (2012) 132

[76] A. Veledina, J. Poutanen, A. Ingram, *ApJ* **778**, 165 (2013) 133, 135

[77] I. Z. Stefanov, arXiv:1403.4136v1 [astro-ph.HE] (2014) 133

[78] M. A. Abramowicz, P. C. Fragile, *Living Rev. Relativity*, **16**, 1 (2013) 133

[79] P. Rebusco, *Publ. Astron. Soc. Japan* **56**, 553-557 (2004), J. Horák et. al, *Astron. Astrophys.* **499**, 535-540 (2009) 134

[80] M. A. Nowak, D. E. Lehr, arXiv:9812004v1 [astro-ph] (1998) 134

[81] W. Cui, S. N. Zhang, W. Chen, *ApJ* **492**, L53-57 (1998) 135

“শেষ নাহি যে,

শেষ কথা কে বলবে ?”

There is no End,

What would our last whisper be?...

— Rabindranath Tagore